Department of Chemistry

Influence of Monoethylene Glycol (MEG) on the Corrosion Inhibition of Wet-Gas Flow Lines

Hoda Ehsani

This thesis is presented for the Degree of
Master of Philosophy
of
Curtin University

September 2013

Declaration

To the best of my knowledge and belief this thesis contains no material previously published by any other person except where due acknowledgment has been made.

This thesis contains no material which has been accepted for the award of any other degree or diploma in any university.

Signature: 

Date: …...23/09/2013.....

Abstract

In gas producing fields, there is a risk of gas hydrate formation inside flowlines, when certain conditions are met. Gas hydrates are solids, which will be formed if condensed water and hydrocarbon gas and/or carbon dioxide combine, at high pressures and temperatures below the hydrate formation point. Hydrate formation needs to be avoided because it can plug pipelines that may cause operational problems and disturb production, and in the worst case, may lead to rupture of the flowlines. To prevent gas hydrate formation, liquid monoethylene glycol (MEG) is injected at the inlet in order to bind the water.

This study is conducted to characterize the influence of monoethylene glycol on the CO_2 corrosion behaviour of carbon steel, the commonly used pipeline material. The effect of MEG concentration, acetic acid concentration, temperature, and immersion time on the corrosion rates of mild steel in CO_2 environments have been characterised by electrochemical measurements and surface analysis.

The results demonstrate a decrease in corrosion rates with increasing MEG concentrations. Both the anodic and cathodic reactions are retarded in the presence of MEG. It has been demonstrated that the inhibition efficiency of MEG decreases with increasing temperature. The temperature effect is more pronounced at low MEG concentrations and diminishes with concentrations similar to lean MEG (20% or less water content).

MEG, in the presence of acetic acid in concentrations between 100 and 500 ppm, is found to have no influence on the anodic reaction (iron dissolution) but reduces the cathodic reaction (hydrogen evolution), which is demonstrated by decreased corrosion current densities measured in the presence of MEG.

Since subsea pipelines are surrounded by cold seawater, the water vapour originating from the gas reservoir condenses on the internal wall of the pipe and collects at the bottom of the pipe. This condensation is very corrosive, due to the presence of CO_2 in the gas phase, which dissolves in the condensed water and forms carbonic acid (H_2CO_3). Carbonic acid is a weak acid and causes a decrease in pH and attacks both the top and bottom of the line. Furthermore, the low ionic strength of the condensed water favours the dissolution of the protective iron carbonate film

at the top of the line, as the condensed water runs off before it reaches saturation of iron and carbonate ions that would allow a protective scale to form.

The condensation rate is the main factor influencing the corrosion rate at the top of the line and control of the water condensation is the most reasonable way to control the internal corrosion rate of wet gas pipelines. In this study the effect of the presence of MEG in the liquid phase (bottom of the line) on the condensation rate and the possibility of transporting glycol from the liquid phase to the gas phase and its co-condensation with the water are investigated. The measurement of MEG content in the condensing liquid is based on the analysing condensing liquid using Fourier transform infrared spectroscopy (FTIR) to obtain quantitative data on the mass transport of MEG from the liquid water/MEG phase to the condensing liquid on the sample surface.

The results indicate that MEG effectively reduces the condensation rate with increasing MEG concentration in the aqueous phase. Furthermore, it has been demonstrated that significant amounts of MEG are present in the condensing liquid at higher temperatures, which could effectively control top of the line corrosion.

Table of Contents

List of Figures

List of Tables

Acknowledgement

I would like to thank Dr. Katerina Lepkova for co-supervising this Master project. I really appreciated her patience. I would also like to say thanks to Prof. Rolf Gubner for giving me the chance to carry out this project in his group, for his confidence in me and for being my supervisor. I would also like to thank Woodside Energy Limited, Mike Brameld and Neil Kavanagh, for the financial support that enabled me to perform this study.

All the people in the Corrosion Centre for Education, Research and Technology (CORR-CERT) are sincerely thanked for their scientific and personal support. I learned a lot from each of them.

Last but not least I would like to thank my family, my husband (Raja) and my gorgeous little girl (Termeh). Without their support and patience, I would not have come so far! I appreciate all the time they gave me to write this thesis, which I could not spend with them.

CHAPTER 1. Introduction

Carbon dioxide (CO_2) corrosion is one of the major problems in oil and gas production and transportation facilities. Despite considerable research efforts, there are still many open questions and arguments on how different parameters influence it. Moreover, most of the studies contain insufficient information to take into account all the parameters in deep sea pipeline environments. Dissolved CO_2 in aqueous solutions causes severe corrosion problems of pipeline carbon steel and process equipment used in the extraction, production and transportation of oil and gas in the petroleum industry. Due to complexity of the environment in oil and gas reservoirs, CO_2 corrosion depends on many variables such as: CO_2 partial pressure, temperature, pH, flow conditions, corrosion scale,[1] liquid compositions, concentration of corrosion inhibitors, and hydrate inhibitors.[2] Determination of the corrosion rate and understanding of the corrosion behaviour of steel under these conditions are the key factors contributing to providing an accurate risk assessment of the internal corrosion.[3]

Transportation of multiphase gas mixtures (oil/gas/water) requires having a reliable pipeline. Carbon steel is often selected as a base material for construction of pipelines because of its mechanical characteristics and economic feasibility compared to corrosion resistance alloys.[4] However, this material has limitations in its corrosion resistance.[5]

1.1 Theory of Uniform CO_2 Corrosion of Carbon Steel in Aqueous Solution

Natural gas from sweet fields primarily consists of carbon dioxide (CO_2) and hydrogen sulphide (H_2S) gases in addition of a hydrocarbon gas mixture.[6] Corrosion mechanisms of carbon dioxide and its effects on carbon steel under different experimental conditions such as CO_2 pressure, pH and temperature has been investigated by many authors and is well described in corrosion text books, such as Uhlig's Corrosion Handbook.[7] It is known that gaseous carbon dioxide is not corrosive unless it dissolves into aqueous solution:

$$CO_2(g) \overset{k_H}{\leftrightarrow} CO_2\,(aq) \tag{1.1}$$

Based on Henry's law, the equilibrium constant of this reaction is a function of temperature (T)[8,9]:

$$\log K_H = \frac{3482.89}{T} + 19.1271 \log T - 2.790 \times 10^{-4} T - 60.3994 \tag{1.2}$$

Where K_H for a given temperature is Henry's constant.

There are a number of chemical, electrochemical, and transportation processes that occur simultaneously during uniform CO_2 corrosion process.[10] Aqueous CO_2 corrosion of carbon steel is particularly an electrochemical reaction[5] as the metal corrosion often occurs through electrochemical reactions at the interface between the metal surface and the aqueous solution.[3] The summary of the available information in literature is given in following section.

In de-aerated carbon dioxide brine solution, the possible cathodic reactions may be either reduction of water or hydration of dissolved CO_2 by water and the formation of carbonic acid (H_2CO_3) which then partially dissociates in two steps to produce bicarbonate (HCO_3^-) and carbonate (CO_3^{-2}) ions[8,10]:

$$CO_2\,(g) + H_2O \leftrightarrow H_2CO_3 \tag{1.3}$$

$$H_2CO_3 \leftrightarrow HCO_3^- + H^+ \tag{1.4}$$

$$HCO_3^- \leftrightarrow {CO_3}^{2-} + H^+ \tag{1.5}$$

This is followed by hydrogen evolution reaction through direct reduction of water:

$$H_2O + e^- \rightarrow OH^- + H^+ \tag{1.6}$$

$$H^+ + e^- \rightarrow H \tag{1.7}$$

Hydrogen gas evolution results as a reaction product released from both reduction reactions:

$$2H \rightarrow H_2 \tag{1.8}$$

Additionally, there is the possibility of the direct reduction of H_2CO_3, which can increase the corrosion rate further[10]:

$$2H_2CO_3 + 2e^- \rightarrow 2HCO_3^- + H_2 \quad (1.9)$$

As suggested by de Waard and Milliams[11] the undissociated carbonic acid (H_2CO_3) reduces after it is absorbed on the metal surface, and this is the rate determining step of the corrosion process. Thus, the corrosion rate of the carbon steel is directly related to the concentration of the undissociated carbonic acid in the solution.
At the same time, during the corrosion process of mild steel, the anodic reaction of iron dissolution is most likely accelerated by the CO_2 concentration[8]:

$$Fe \rightarrow Fe^{2+} + 2e^- \quad (1.10)$$

Thus, the overall reaction is[7,12]:

$$Fe + CO_2 + H_2O \rightarrow Fe^{2+} + CO_3^{2-} + H_2 \quad (1.11)$$

For this reaction to occur, the two electrons produced must be consumed in a cathodic reduction reaction[12]. When the concentration of ferrous and carbonate ions in the solution on the steel surface are large enough to exceed the solubility product, iron carbonate precipitation forms on the steel surface[8]:

$$Fe^{2+} + CO_3^{2-} \leftrightarrow FeCO_3 \quad (1.12)$$

This process is affected by some variables such as: pH, temperature, and chemical composition of the aqueous phase, which influence the supersaturation of iron carbonate and formation of the corrosion scale. For instance, depending on the chemistry of the solution, the corrosion product precipitation in a CO_2 environment can result in formation of a protective film, for example iron carbonate ($FeCO_3$) film which limits the corrosion rate by making a barrier against the transportation of the

species involved in the corrosion reaction and by blocking or covering parts of the metal surface.[10]

1.2 Influence of MEG on CO_2 Corrosion

In wet-gas pipelines (the pipelines between the wells and the gas processing facility), there is a risk of hydrate formation which forms if there is condensed water or water droplets in the hydrocarbon gas/CO_2 phase, at sufficient pressure and temperatures below the hydrate formation point. Hydrate formation needs to be avoided because it can plug pipelines that may cause operational problems and interrupt production.[4] One way to prevent gas hydrates formation is for liquid monoethylene glycol (MEG) to be injected at the inlet or wellhead. MEG captures the water and makes it unavailable for hydrate formation.

Typically 80–95 wt% (lean MEG) is injected in the inlet and it decreases to typically 30–60 wt% (rich MEG) in the outlet as a result of dilution by the condensed water.[13,14] During the wet-gas dehydration process, the glycol absorbs water and dissolves gas molecules including carbon dioxide (CO_2), hydrogen sulphide (H_2S), and some heavy hydrocarbons.[15] Each of these contaminants, as well as the water itself, affects the performance of the glycol as a dehydration fluid. Besides prevention of hydrate formation, glycols have an inhibiting effect on CO_2 corrosion.[7,16,17] Other commonly used glycols in hydrate prevention are diethylene glycol (DEG), and triethylene glycol (TEG).[15]

Many wet-gas carbon steel pipelines use the addition of glycols for hydrate prevention and the pH-stabilization technique for corrosion control.[18,19,20] The basis of pH-stabilization is the addition of alkaline chemicals (e.g. sodium hydroxide (NaOH) or N-methyl-diethanolamine (MDEA)) in order to increase the pH of the glycol/water mixture and thus facilitate the formation of their corrosion films and improve the protective properties.[14] This has proven to be an efficient technique to deal with corrosion in pipelines and problems related to corrosion products in process systems, however, the scaling might become an issue.[13]

In addition to its function as a hydrate inhibitor, it has been shown that a reduction of the carbon dioxide (CO_2) corrosion rate of carbon steel occurs when glycol is present in the aqueous mixture.[4,13,16,21]

Some understanding of the inhibition role of glycols, especially MEG (which is the most commonly used glycol), can be learned from field experiences related to pH stabilization and top of the line corrosion control methods.[17,18,19,20,22] Glycols have been reported to exhibit an inhibiting effect on CO_2 corrosion without pH stabilization, but only a few studies have been specifically focused on the effect of MEG (without pH stabilizer) on the corrosion reactions and its inhibiting effect and there has been increasing attention to the beneficial effect of MEG as a corrosion inhibitor. There are several oil and gas transportation pipelines, especially wet gas pipelines, which utilize glycol for corrosion control.[2,10,23] According to one field experience using diethylene glycol (DEG) in the pipeline as the main corrosion preventer, binding the water with 80% DEG reduces the corrosion rate in the bottom of the line by 90%, while 50% MEG is shown to reduce the corrosion rate by 70%.[23]

Gulbrandsen and Morard[16] report a decrease in the corrosion rate in the presence of 30 and 70 vol% MEG at low CO_2 pressure, room temperature and pH buffered solutions. They show that both anodic and cathodic reactions of CO_2 corrosion are depressed in the presence of MEG. The reduced cathodic reaction in the presence of MEG is known to be related to the absorbance of glycol on the steel surface which keeps CO_2 and water away from the metal surface. However, their results do not clarify the details of the anodic reaction in MEG solutions.
More importantly, it is shown that the presence of MEG influences the process of protective film formation on the steel surface. The reason provided by Dugstad et al.[14] is that increasing MEG concentration decreases the iron carbonate solubility and, therefore, facilitates the formation of the protective film.

It is well known that the presence of MEG changes the physio-chemical properties of water-glycol solutions mainly by decreasing the CO_2 solubility with increasing MEG content up to 60%. However, above 60% MEG concentration CO_2 solubility increases again.[14,16,24] This is further supported by data presented by Oyevaar et al.[24] These data confirm that the solubility of CO_2 has a minimum value at around 60 mass percentage of glycol after which it increases rapidly. Moreover, diffusivity of CO_2 decreases with increasing MEG concentration and the solution viscosity increases strongly.[16] Suppressed diffusivity is followed by a raising of the Fe^{2+}, HCO_3^- and CO_3^{2-} concentrations close to the steel surface, and therefore, $FeCO_3$

supersaturation is much faster achieved,[7] leading to the formation of the protective film. Furthermore, the solution polarity decreases with increasing MEG concentration[16] and the dielectric constant of water decreases from 78 to 56 in 70% MEG[25] which affects the chemical potentials of the ionic species in the solution and changes the equilibrium constants.[16]

More recent studies confirm the inhibition effect of MEG on non-carbon steel alloys by adsorption of MEG on the metal surface and formation of a film, which acts as a barrier between the metal surface and corrosive species. Song and StJohn[26] report the adsorption of MEG on the metal surface that covers the surface more completely in concentrated ethylene glycol solution and effectively protects the surface from the water corrosion. The authors also observe that the corrosion rate of magnesium based alloys in brine/ethylene glycol solution depends on the ethylene glycol concentration. They find that the solution resistance has a significant effect on the corrosion rate of magnesium since the solution resistance increases with increasing ethylene glycol concentration. It is also reported[27] that at room temperature, the resistance and the relative thickness of the surface film on the sample increases as the concentration of ethylene glycol in the solution increases.

In summary, the main proposed approaches in the literature to explain the inhibition effect of MEG on metal are:

1. Presence of MEG changes the physio-chemical properties of water-glycol solutions.
2. Adsorption of MEG on the metal surfaces and formation of a protective film on an active metallic surface influences the kinetics or mechanism of the anodic and/or cathodic reactions.

1.3 Influence of Acetic Acid on CO_2 Corrosion of Carbon Steel

Many hydrocarbon reservoirs contain organic acids. Acetic acid (HAc) is the most prevalent low molecular weight organic acid found in the oil and gas environment.[28] It is acknowledged that the general[29] and localized[30] corrosion of carbon steel

accelerates due to decreased pH when organic acids are present in CO_2 containing environments.

The effect of acetic acid on general and localized CO_2 corrosion of carbon steel has been studied by several authors,[28,31] but it is not still well understood. In 1983, Crolet and Bonis[32] reported that the corrosion rate of carbon steel in the brine solution increases significantly in the presence of HAc. It was believed that acetic acid could influence both the electrochemical corrosion reactions (the cathodic and anodic reactions) and the corrosion products' film protectiveness.

HAc influences the electrochemical reactions of CO_2 corrosion by accelerating the cathodic reaction[30] by either a direct reduction of HAc on the steel surface and producing hydrogen gas, or dissociating to acetate (Ac^-) and hydrogen (H^+) ions and acting as an extra source of hydrogen ion.[31,33] HAc is a weak acid that also acidifies the solution. HAc (pKa = 4.67) is a stronger acid than carbonic acid (pKa = 6.35), at 25°C and it is the main source of acidity (H^+) at the same concentration of two acids.[34] George et al.[35] assume that HAc dissociates in the aqueous media and acts as a main source of hydrogen ions which contributes to the corrosion rate of carbon steel in acidic media.

A study of the effect of acetate buffer ions on the corrosion rate of carbon steel in the absence of CO_2 at 60°C, reveals a new cathodic HAc reduction reaction in addition to the one that corresponds to the reduction of hydrogen ions (free proton).[36] This additional reaction in the presence of HAc is attributed to the direct reduction of HAc into hydrogen and acetate ions:

$$HAc + e^- \leftrightarrow H^+ + Ac^- \qquad (1.13)$$

At the corrosion film free surface, the cathodic process on the surface does not distinguish between the reduction of hydrogen ions (free protons) and the direct reduction of HAc as the dissociation reaction of HAc occurs very fast.

Veloz and Gonzalez[37] published a study on the corrosion behaviour of carbon steel in buffered HAc/Ac^- solutions at 25°C and in absence of CO_2, using impedance techniques. Analysis of their results does not show the formation of a corrosion product film, since the characteristics of the impedance spectra exhibit a significant

corrosion of steel in the acid solution. It is demonstrated in their study that the corrosion process is controlled by the adsorbed complex of HAc and acetate in the solution, which prevents the formation of a passive film.

HAc also influences the anodic reaction part of the CO_2 corrosion although the mechanistic effect of HAc on the reaction is still not conclusive. Some researchers report an inhibited anodic reaction relating the role of HAc to an associated inversion of the acetate/bicarbonate ratio,[32] and the others report the accelerated or unaffected anodic dissolution reaction[37].

De Marco et al.[38] postulate an inhibited anodic corrosion mechanism in the presence of HAc. The authors demonstrate that the inhibition of the anodic dissolution of iron in the presence of HAc is related to the ability of acetate to facilitate the formation of a thin and porous passive film on the corroding mild steel electrode by altering the crystallization habit of the corrosion products formed during CO_2 corrosion. In another study the mild inhibition of the anodic reaction in buffered acetate solutions, compared to brine solutions, is found to be related to the adsorption of acetate onto the corrosion products and the formation of a barrier between the steel surface and the corrosive species in the aqueous phase.[39] It should be noted that the inhibitive behaviour of HAc on the anodic reaction of the corrosion process is mostly observed at lower temperatures (20–40°C).[32] However, other authors, who observed unaffected or accelerated anodic dissolution of iron in CO_2 corrosion environments in the presence of HAc, argue that the reported retardation of the anodic portion of the potentiodynamic polarization curve in the presence of HAc is overshadowed by the large increase in the cathodic reaction, which results in a large change of the corrosion potential.[40]

Moreover, addition of HAc reduces the protectiveness of the corrosion product layer on the steel surface by decreasing the iron carbonate ($FeCO_3$) supersaturation, which results in the enhancement of the corrosion rate.[41] As mentioned above, at the same pH and CO_2 pressure, HAc is the main reactant for the cathodic reaction, as it is a stronger acid than carbonic acid. HAc dissociates and forms acetate ions (Equation 1.13). The acetate ions then react with iron to form iron acetate:

$$Fe + 2HAc \rightarrow Fe(Ac)_2 + H_2 \qquad (1.14)$$

Iron acetate is highly soluble in aqueous solutions, whilst iron carbonate is poorly soluble.[42] Therefore, the Ac^- ion can solubilise the iron ions (Fe^{2+}) as they are formed, transporting them away from the steel surface. Without a stable protective film forming on the steel surface, the corrosion rate remains at high levels.[42,43]

In particular, the detrimental effect of HAc is accelerated with increasing temperature and concentration.[44] As temperature increases the corrosivity of the HAc containing solution increases. For instance, adding 100 ppm HAc increases the corrosion rate about 30% at 22°C, whilst increasing the temperature to 60°C, the same concentration of HAc doubles the corrosion rate.[40] It has also been confirmed that with increasing temperature both anodic and cathodic current densities increase and that the corrosion rate is under mass transfer limiting current (cathodic reaction) control.[40] This is confirmed by Zhu et al.[9] that in the presence of HAc, the influence of temperature on the anodic and cathodic reactions of corrosion is more pronounced compared to that in the absence of HAc.

In summary, when HAc is present in the system, it accelerates the cathodic reaction due to the direct reduction of undissociated HAc. Regarding the effect of HAc on the anodic current, there are no conclusive results in the literature. Some authors report retardation of the anodic reaction in the presence of HAc and the others report an unaffected anodic reaction. Addition of HAc also reduces the protectiveness of corrosion product films due to its effect on $FeCO_3$ formation.

1.4 Concurrent Effect of MEG/HAc

There are several offshore wet-gas pipelines that transport unprocessed (wet) gas over large distances, under hydrate forming conditions with various concentrations of acidic gases.[21] The gas may contain CO_2, acetic acid, MEG and condensate as well as hydrocarbons. Film forming corrosion inhibitors and/or pH stabilized MEG are used to control the corrosion rates in these pipelines.[45] However, the effect of HAc in combination with MEG at the bottom of the line is not completely understood. Some understanding of the role of MEG in acid CO_2 corrosion is gained

from field experiences, often related to top of the line corrosion (TLC),[46] and from experiences with pH-stabilization. It is important to have a good knowledge of the combined effect of MEG and HAc, in order to be able to select the most efficient internal corrosion control method/combination of methods for wet-gas pipelines.

The enhancement of MEG/water corrosivity in the presence of acetic acid in CO_2 saturated solutions has been discussed in a few field studies.[20,29,46] In pH stabilized MEG/water systems, the acetic acid dissociates in solution (depending on the pH). The remaining HAc (free HAc) accelerates the corrosion rate by direct reduction at the surface of the metal.[47]

In the experiments conducted by Mendez et al.[29] a liquid phase of 50% glycol in water was used to demonstrate that the general corrosion rate at the bottom of the line is one-third greater compared with the corrosion rates in the absence of MEG and HAc at the same pH value. However, the authors postulate that glycol does not react with acetic acid chemically. According to a field experience,[44] MEG regeneration leads to an accumulation of acetate ions and increases in free HAc concentration, which results in increases in the iron solubility and, therefore, increased corrosion rates.[44] However, comparatively little experimental data are available in the literature for the synergistic effect of MEG and HAc.

1.5 The Effect of Temperature on CO_2 Corrosion in the Presence of MEG

Temperature has a significant influence on the electrochemical corrosion rate of metals.[48] At low pH (<4), when protective film formation does not occur, temperature accelerates all the electrochemical, chemical and transport processes involved in the corrosion process, which results in increased corrosion rates.[40] In deoxygenated CO_2 solutions increasing the temperature has an increasing effect on the CO_2 mass transport for the cathodic reaction or charge transfer rates; however, on the other side it decreases CO_2 solubility in the aqueous phase. From laboratory experiments it is known that the uniform corrosion rate increases initially up to 60–80°C[49] depending on water chemistry and flow conditions. Above these temperatures, the corrosion rate decreases with increasing temperature due to the faster kinetics in protective scale formation, which is attributed to the decrease in iron carbonate solubility.[47] In the case of corrosion in acidic solutions, the corrosion

rate increases significantly with increasing temperature due to the hydrogen evolution overpotential decrease (depolarization of hydrogen).[46] The correlation between corrosion current and temperature is described by the Arrhenius equation which provides the determination of the activation energy of the corrosion process[50]:

$$i_{corr} = \lambda \exp(-E_a / RT) \quad (1.15)$$

where i_{corr} is the corrosion current density in A/cm

λ is the pre-exponential factor

E_a is the activation energy of the corrosion process in kJ/mol

R is the molar gas constant in J/mol K

T is the absolute temperature in K.

The temperature dependence of the corrosion inhibitor efficiency (IE) and the comparison of the activation energy (E_a) values of the corrosion process provide information about the inhibition mechanism. Increasing the temperature leads to a decrease in IE which results in variation of the E_a values. In general, higher activation energy in the presence of a corrosion inhibitor compared to the inhibitor's absence demonstrates the formation of an adsorptive film of a physical or electrostatic character. Lower activation energy in the inhibitor's presence is often interpreted as an indication of a chemisorptive bond between the metal surface and the organic molecules.[48]

1.6 Top of the Line Corrosion

The temperature in gas reservoirs is much higher compared with seabed temperatures. It is not uncommon nowadays to reach wellhead temperatures of 80°C to 120°C. As discussed above, these reservoirs contain varying amounts of formation water, thus the produced gas contains varying amounts of water vapour. The unprocessed gas is often transferred in large multiphase pipelines over long distances to process facilities, or several wet-gas streams from a number of wells are collected into one flowline and transported to a processing facility many kilometres away from the wellheads. Additionally, the gas phase contains corrosive species,

such as carbon dioxide (CO_2) and acetic acid (HAc).[51] Since the seabed temperature can be as low as 4°C (deep sea), the temperature difference between the inside of the pipeline and the surrounding environment is large. Therefore, if the flow line is not sufficiently insulated, gas phase hydrocarbons (condensate) and water vapour cool down quickly and condense on the internal wall of the pipe. This condensation, given the right conditions, is very corrosive, especially at the top of the line (10 o'clock to 2 o'clock position) due to the presence of CO_2 in the gas phase. The CO_2 dissolves in the condensed water, forms carbonic acid (H_2CO_3), which causes a decrease in pH and attacks both top and bottom of the line.[52] Furthermore, the low ionic strength of the condensed water favours the dissolution of the protective iron carbonate film.[49]

The following factors are believed to influence top of the line corrosion. The water condensation rate is the first and main factor influencing the corrosion rate [46,53]. The condensation rate varies with differences in temperatures between the inside of the pipeline and the temperatures on the outside of the flow lines.[54,55] Based on the literature, prevention and control of the water condensation are reasonable ways to control the internal corrosion rate of wet-gas pipelines.[51] Water condensation rates lower than 0.15–0.25 mL/m^{2}s result in low corrosion rate at the top of the line, since the formation of protective iron carbonate scales is favoured because the condensed water quickly saturates with iron and carbonate (supersaturation).[56] The second factor is the composition and distribution of the chemical components in the water condensate which influences its corrosivity.[55] As the third factor, the corrosion process influences the water condensate chemistry by formation of corrosion products (ferrous ions) and changing (increasing) the pH and pH-dependent equilibriums.[57]

From bottom of the line (BOL) investigations, it is known that there is a reduction in CO_2 corrosion of carbon steel when glycol represents part of the aqueous mixture.[21] MEG has been used as a combined hydrate and corrosion inhibitor in a number of wet-gas transportation pipelines[19] and there has been increasing attention to the beneficial effect of MEG as a corrosion inhibitor at the top of the line.[14,29]

According to Nyborg et al.[55] MEG can inhibit the corrosion rate at the top of the line by reducing the water condensation rate due to its ability to bind water (dehydration), which reduces the partial pressure of the water vapour by absorbing it

from the gas phase, which in turn results in a lower dew point of the gas. It has been shown that the addition of 50% glycol in the liquid phase decreases the corrosion rate at the top of the line by approximately 70% compared with a pure water phase.[14] It can be argued[29] that the inhibition effect of MEG with and without a pH stabilizer is applicable at the bottom of the line where the liquid is flowing but not at the top of the line. This was investigated[14] by the likelihood of the transportation of glycol from the liquid water/glycol phase in the bottom of the pipe to the gas phase in the form of droplets and attaching the wall. In this case, the iron carbonate solubility is reduced and corrosion films with good protective properties can develop. Dugstad et al.[14] perform a series of flow loop experiments to study entrainment of glycol to the aqueous film on the upper wall by droplets in the gas phase. The authors demonstrate that the top of the line corrosion rate will be substantially reduced even if only a very small amount of glycol droplets are transported to the top of the line. However, co-condensation of MEG at the top of the line has to date not been considered in the literature as a viable transport mechanism.

Singer et al.[58] found that the increasing corrosive behaviour of condensed water is also related to the ability of volatile acidic species to decrease the pH and therefore, increase the solubility of iron ions.

Andersen et al.[46] explain that the condensation rate can affect formation of corrosion products, iron carbonate ($FeCO_3$), on the metal surface, which form a protective layer and reduce the corrosion rate. But, a high condensation rate results in more water available and, hence, more iron ions needed to saturate the condensed water before iron carbonate can form on the steel surface. In addition, a high condensation rate results in an increased run-off of the condensed liquid before saturation is reached, which might result in the dissolution of any iron carbonate previously formed.

In summary, at a constant CO_2 partial pressure, top of the line corrosion is governed by the condensation rate, which in turn depends on the temperature difference between the inside the pipe and the wall temperature of the flow line. Thus, prevention and control of water condensation may be seen as the most reasonable way to control internal the corrosion rate of wet-gas pipelines.[57,59]

It is difficult to draw clear conclusions from the limited data in the literature on the inhibition effect of MEG. The effect of MEG on the corrosion reactions of carbon

steel at variable temperatures and concentrations of MEG has not been described in detail to date. A full understanding of the corrosion behaviour of carbon steel in MEG solutions is essential prior to identifying the right mitigation methods.

1.7 Research Objectives

The main objective of this research was to study the influence of MEG on CO_2 corrosion behaviour of carbon steel at both bottom and top of the pipeline. The following objectives have been achieved:

- Determination of the optimal amount of MEG required for the best corrosion mitigation efficiency (Chapter 3.1 and 3.2).
- Investigation of the influence of MEG on the CO_2 corrosion process (Chapter 3.3)
- Study of the effect of acetic acid on the corrosion behaviour of carbon steel in presence of MEG (Chapter 4.1).
- Study of the effect of MEG concentration on CO_2 corrosion in the presence of acetic acid (Chapter 4.2).
- Study of the effect of temperature on the inhibition efficiency of MEG (Chapter 5.1).
- Study of the effect of immersion time on the inhibition efficiency of MEG (Chapter 5.2).
- Investigation of the effect of MEG on the water condensation rate at variable temperature range (Chapter 6.1).
- Investigation of the condensate composition to determine its corrosiveness and the amount of MEG transported from bottom of the line (Chapter 6.2).

CHAPTER 2. Electrochemical Techniques and Methodology

Corrosion in an aqueous environment is known to be a natural electrochemical process including metal oxidation and the concurrent reduction of corrosive species in the solution. Thus, the corrosion rate corresponds to the rate of charge transfer between the corroding metal surface and an aqueous oxidant. Electrochemical techniques are useful to monitor the corrosion process occurring *in-situ*. There are many electrochemical tests developed for corrosion monitoring. The most extensively used techniques are linear polarization resistance (LPR), Tafel polarization and electrochemical impedance spectroscopy (EIS). The fundamental aspect of all the electrochemical techniques is an electron transfer reaction between molecules at the metal surface and the electrolyte solution.[60]

2.1 Electrochemical Techniques

The application of electrochemical techniques in corrosion science makes it possible to measure the corrosion process parameters. Besides direct determination of the corrosion rate, electrochemical techniques provide more detailed aspects of the electrokinetic and corrosion reaction mechanisms.[61] The electrochemical tests applied in this study are introduced in the following sections.

2.1.1 Linear Polarization Resistance (LPR)

Linear polarization resistance (LPR) is the most commonly used corrosion monitoring technique in the area of CO_2 corrosion of carbon steels. This technique is based on the calculation of the corrosion rate by monitoring the linear relationship between the applied potential and the resulting generated current.[62] LPR monitoring has been widely used by industry for nearly 50 years.[62] A major advantage of LPR measurement is a fast response of changes in the corrosion rate which is particularly useful in measuring the effectiveness of inhibition processes. LPR measurements can also provide information on the corrosion behaviour of metals, for example when the surface changes from a passive to an active state, which indicates

increased susceptibility to corrosion. As it continuously monitors the corrosion rate, interpretation of the measurements is easy and straightforward. However, this technique is based on the uniform corrosion principals only and it is not applicable to the investigation of localized corrosion[63].

Electrical conductivity (corresponding to solution resistance) of a fluid can be used to determine its corrosiveness. However, monitoring corrosion with LPR technique in high resistivity media (as in a MEG system) is a challenge. The resistance measured with LPR is a combined resistance of the solution resistance and the polarization resistance. In the case of high solution resistivity (low conductivity) there is a risk of underestimation of the corrosion rate. However if the polarization resistance value is large compared to the solution resistance, then the error will be small.[64]

A three electrode probe (electrically isolated from each other) is for this purpose inserted into the corrosive environment. A linear polarization experiment is carried out by applying a small potential range from approximately +20 mV to -20 mV from the open circuit potential (OCP)[65] (which minimises disruption of the natural corrosion process) between the electrodes. The resulting current is then measured. For this small deviation from the OCP, the response current is assumed to be linear. The ratio of the applied potential to the produced current density ($\Delta E/\Delta i$) at free corrosion potential is known as the polarization resistance (R_p) (based on Ohm's law: E = IR). R_p is defined as the resistance of the metal specimen to oxidation by an external potential. The resistance to current flow also contains the resistance of the solution between the electrodes (R_s). The error produced by solution resistance can be substantial, especially in low conductivity solutions in the presence of MEG as mentioned above.

The polarization resistance data are then graphed as a plot of potential vs. current as displayed in Figure 2.1. The R_p value is the slope of the straight line fit to the linear polarization data. To calculate the corrosion rate from the polarization resistance (R_p) the corrosion current density (i_{corr}) should be calculated first by the following equation:

$$i_{corr} = \frac{B}{R_p} \qquad (2.1)$$

where R_p is polarization resistance of the corroding electrode in ohm.cm^2

i_{corr} is corrosion current density in A/cm^2

B is the Stern-Geary coefficient or empirical polarization resistance constant with the unit voltage (V).

It can be derived from the slope of the anodic (b_a) and cathodic (b_c) Tafel reactions. The B value depends on the system and can be obtained from the literature or determined by a separate experiment with the help of following equation:

$$B = \frac{ba\ bc}{2.303\ (ba+bc)} \tag{2.2}$$

For the LPR measurements in this work the same B value has been considered in all experiments (B = 26; b_a and b_c = 120 mV/dec). The validity of the corrosion rate values using constant Tafel slopes (used in LPR measurements) are checked against the corrosion rate values using Tafel slopes gained from the potentiodynamic measurements. The error of recalculated corrosion rates is always below the acceptable error of factor of 2.[66]

The corrosion current density is then used to calculate the corrosion rate[65]:

$$CR = K_1 \frac{icorr}{\rho} EW \tag{2.3}$$

where CR is corrosion rate in mm/y and i_{corr} in μA/cm^2

K_1 is a constant with the value of 3.27×10^{-3} in mm.g/μA.cm.yr

ρ is density in g/cm^3

EW is the equivalent weight defined as the mass of metal (dimensionless).

LPR measurements in this study are conducted using a Gill ACM instrument potentiostat with a multiplexer according to ASTM Standard G 59-97, Standard Test Method for conducting potentiodynamic polarization resistance measurement.[67] The potential is scanned at a rate of 0.1667 mV/s at -10 to +10 mV vs. open circuit potential (OCP). Continuous LPR measurements are carried out for a period of 24 hours.

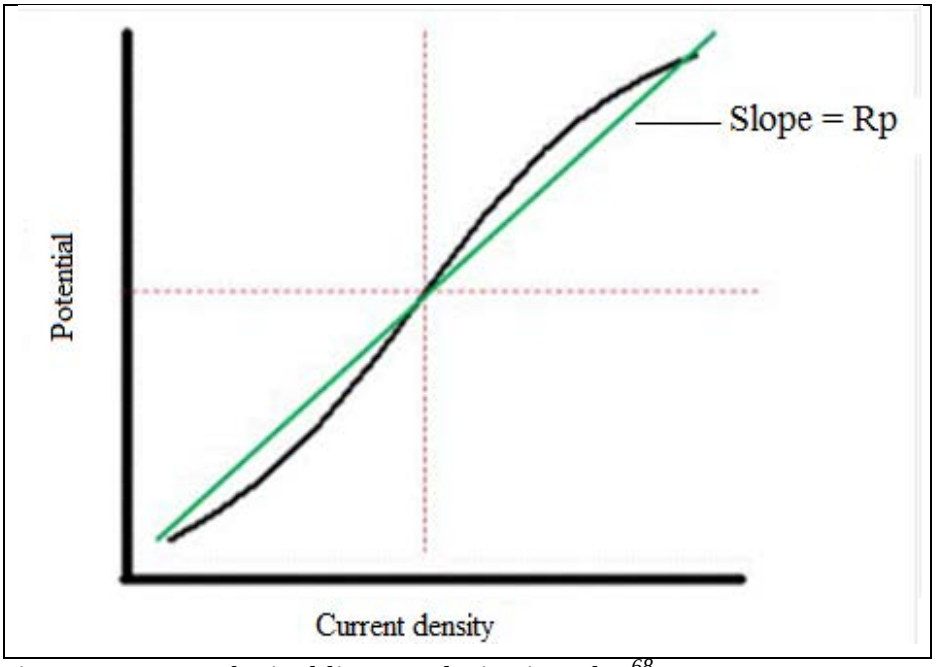

Figure 2.1: Hypothetical linear polarization plot.[68]

2.1.2 Potentiodynamic Polarization (Tafel Extrapolation)

Potentiodynamic polarization (Tafel extrapolation) is an electrochemical technique based on the linear relationship between the logarithm of the current density and the over potential discovered by Julius Tafel in 1905.[69] This technique is based on the data obtained from cathodic and anodic polarization measurements by applying potentials of about 300 mV vs. the OCP in both positive and negative (potential) directions and monitoring the produced current through the electrolyte.[60,61] For anodic polarization, the potential of the working electrode becomes more positive, causing the working electrode to become the anode and the electron transfer to the solution during the oxidation process. For cathodic polarization, the potential of the working electrode is changed in the cathodic direction causing the working electrode to become more negative. The reduction of species occurs in the environment during the cathodic polarization, such as the water reduction reaction. Tafel data are then graphed as a plot of the logarithm of the measured current (log i) vs. the applied potential. When the Tafel scan is complete, extrapolating the resulting linear current lines to the two Tafel regions provides values for the corrosion potential (E_{corr}) and the corrosion current (i_{corr}) at the point where the two lines cross. The corrosion current (i_{corr}) is utilized to calculate the corrosion rate (Equation 2.3). Another

important information that can be abstracted from the Tafel plot is the slope of the straight line fitted to the linear regions of the anodic and cathodic Tafel plots that correspond to the anodic and cathodic Tafel slopes (b_a and b_c),[70] respectively. In this work, the anodic and cathodic Tafel slopes are determined for each potentiodynamic polarization scan. The anodic and cathodic Tafel slopes determined by this technique are close to the Tafel constants ($b_a = b_c = 120$) which were used in the LPR measurement.

Figure 2.2a shows the set-up for a typical electrochemical three electrode cell, which is used for the electrochemical measurements and Figure 2.2b shows a hypothetical curve demonstrating the anodic and cathodic polarization curves corresponding to hydrogen evolution and metal dissolution. The corrosion current density (i_{corr}) then can be used to calculate the corrosion rate in desired units by using Faraday's law.

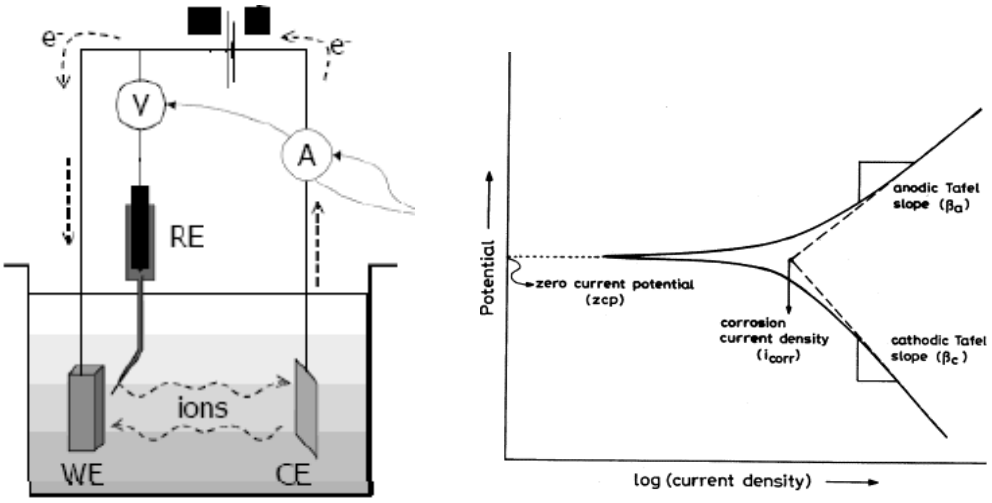

(a) (b)

Figure 2.2: Tafel analysis: (a) Three electrode electrochemical cell set-up reference electrode (RE), working electrode (WE) and counter electrode (CE), and (b) A hypothetical Tafel Plot.[71]

Potentiodynamic polarization measurements are carried out using a Gill ACM instrument potentiostat with a multiplexer. The potentiodynamic polarization scans are run immediately after 24 hours linear polarization resistance tests within the potential range of -250 to +250 mV vs. OCP at a sweep rate of 0.1667 mV/s. Analysis of the resulting Tafel scans and the determination of anodic and cathodic

Tafel slopes are carried out using the commercial software of Corrview (CView Version: 2.70, Scriber Associates, Inc.). These anodic and cathodic Tafel slopes are used to calculate the B value (Equation 2.2).

2.1.3 Electrochemical Impedance Spectroscopy

The concept of electrical impedance was first introduced by Oliver Heaviside in the 1880s and later on developed in terms of vector diagrams and complex representation by Kennelly and especially Steinmetz.[72,73] It has been proven that EIS is a powerful and accurate method to measure corrosion rate.[63] Electrochemical impedance spectroscopy (EIS) is an alternating current (AC) electrochemical technique, which can quantify distinct analogous electrical components such as resistance, capacitance, inductance, etc. produced from the physical and chemical features of an electrochemical process.

The advantage of the EIS technique is that it clearly separates the charge transfer resistance (R_{ct}) and the solution resistance (R_s),[74] while most of the available standard DC techniques basically merge the R_{ct} and R_s into one resistance, commonly called polarization resistance (R_p), which is explained earlier. The frequency dependence of the EIS spectra can be used to analyse the mechanisms and kinetics of a specific reaction on the electrode surface. Therefore, EIS is a useful technique to investigate the corrosion process in a low conductivity environment.[75]

An electrical double layer forms at the metal/solution interface, due to the electrochemical potential difference between the metal surface and the solution. Upon applying an electrical signal for example, an amplitude sinusoidal potential (V_o) to the surface, (the cell has been shown in Figure 2.2a) over a range of distinct frequencies (ω) of 10^{-3} Hz to 10^5 Hz, the response signal (e.g., a varying current) exhibits a capacitive character.

$$V_{(t)}=V_o\sin(\omega t) \tag{2.4}$$

$$\omega = 2\pi f \tag{2.5}$$

where $V_{(t)}$ is the frequency dependent potential (volt) at time t

V_0 is the amplitude of the signal

t is the time in second

ω is the radial frequency in radians/second

f is the signal frequency in Hz.

At each individual frequency in the frequency range the corresponding phase shift (θ) and magnitude (i_0) of the produced sinusoidal current ($i_{(t)}$) are then measured (Figure 2.3).[76]

$$i_{(t)}=i_o\sin(\omega t + \theta) \qquad (2.6)$$

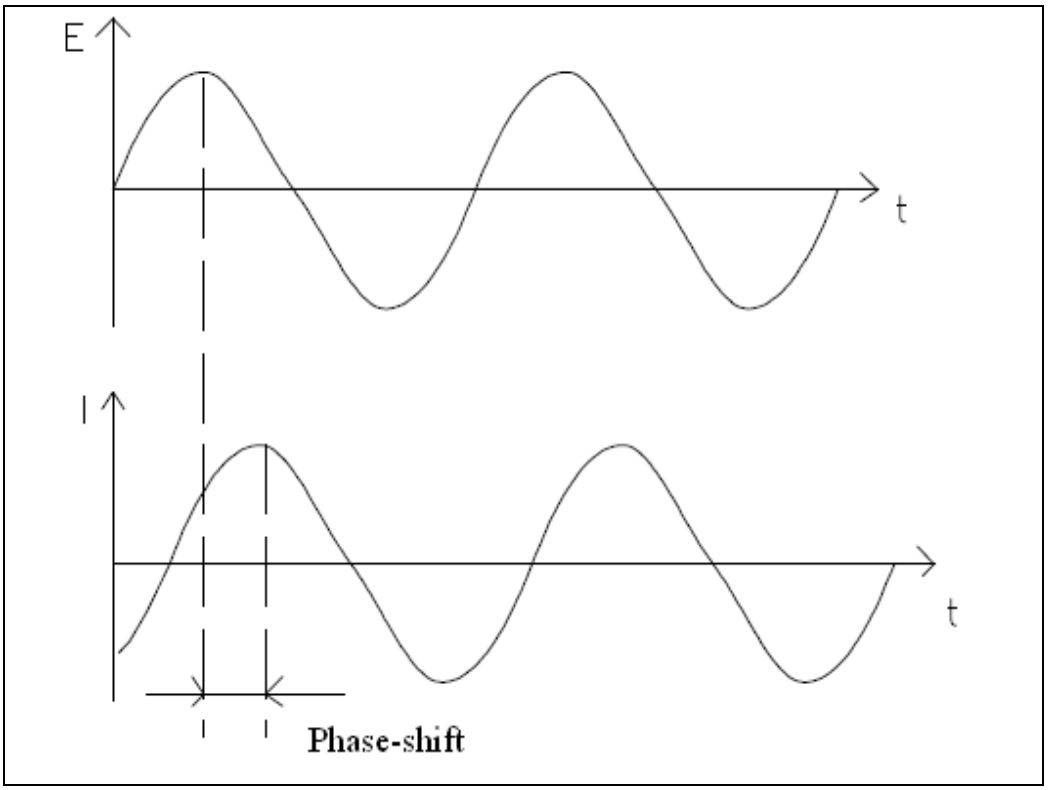

Figure 2.3: Sinusoidal current responses to the applied AC potential in a linear system.[76]

The relationship between the applied potential and the corresponded current is analogous to that of resistance.[76] For an altering current (AC) signal this resistance is nominated as the impedance ($Z_{(t)}$), which has the unit dimensions of ohms (**Ω**). The

measured impedance may be defined as a vector comprising both magnitude (impedance (Z)) and direction (phase angle (θ)). The impedance can be expressed according to Ohm's law in the form of the following equation[75]:

$$Z_{(t)} = \frac{V_{(t)}}{i_{(t)}} = \frac{V_0 \sin(\omega t)}{i_0 \sin(\omega t+\theta)} = Z_0 \frac{\sin(\omega t)}{\sin(\omega t+\theta)} \quad (2.7)$$

Where Z_0, V_0, i_0 are frequency dependent impedance (**Ω**), potential (volt) and current (amp), respectively;
θ is the phase shift between potential and produced current in degrees; $\theta = 0$ for purely resistive behaviour. ω is $2\pi f$ in radians/second.

Consequently, the impedance ($Z_{(t)}$) can be expressed in terms of a magnitude (Z_0) and phase shift (θ).

The impedance results can be presented in a graphical format. There are two commonly used such formats, which are used to report the electrochemical impedance data, namely the Nyquist and Bode plots.[76]

The Nyquist plot is a graphical representation of the impedance in the form of a semicircle with an in-phase (real $Z_{(t)}$) and out-of-phase (imaginary $j\,Z_{(t)}$) component (Figure 2.4). The real component of impedance is plotted on the abscissa (x axis) and the negative of the imaginary component is plotted on the ordinate (y axis). Positive values of the real component of impedance are plotted to the right of the origin parallel to the x axis representing the resistive element (R). Negative values of the imaginary component of impedance are plotted vertically from the origin parallel to the y axis representing the capacitance of the system.[76]

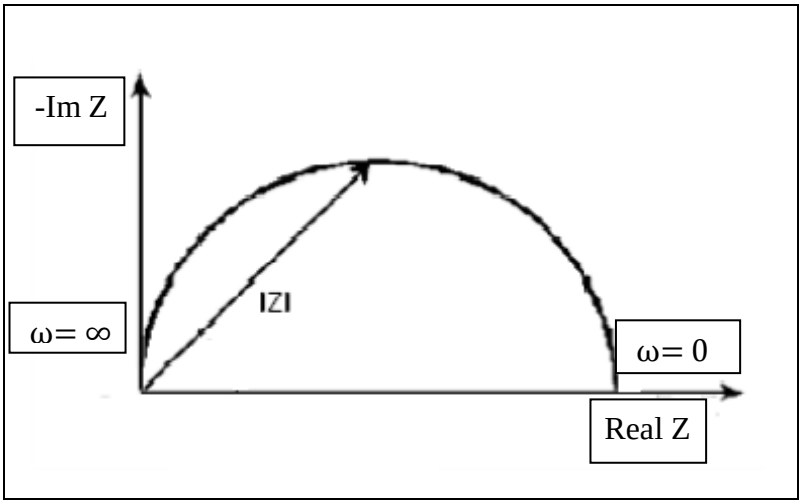

Figure 2.4: Schematic illustration of the real and imaginary components of a simple Nyquist plot.[76]

The frequency dependence of data is better represented in the form of Bode plots compare to the Nyquist plot. The Bode plots report the corresponding phase angle and impedance magnitude vs. the frequency of the applied signal. These plots are named Bode Phase and Bode Magnitude plots[77] and are shown in Figure 2.5 (a) and (b) respectively.

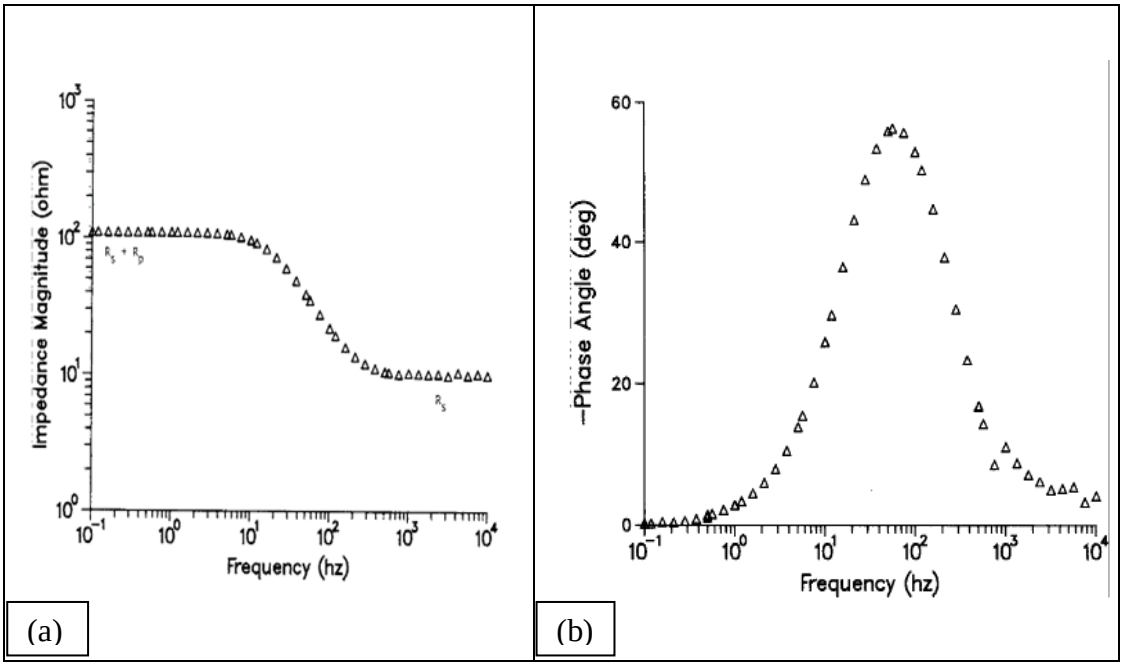

Figure 2.5: (a) Bode Magnitude plot and (b) Bode Phase plot from a corroding mild steel electrode.[77]

In order to interpret EIS spectra in detail, it is important to highlight some general points:

- In Nyquist curves, the magnitude of the impedance loop is equal to the capacitive behaviour of the electrode. A capacitive behaviour of the loop originates from the time constant of the electric double layer and charge transfer resistance. A depressed capacitive loop with the centre below the real axis indicates a frequency dispersion of the capacitive properties of the solid metal electrodes.
- Conversely, an inductive loop is attributed to the adsorption of an intermediate product of the corrosion process.[78] The high frequency intercept on the real axis represents the solution resistance, R_s, and the diameter of the semi-circle of the impedance loop corresponds to the charge transfer resistance (R_{ct}) which is the same as the polarization resistance (R_p), resulting from the charge separation across the solid interface to the outside edge of the double layer. The stability of this resistance can be associated with the passive layer or corrosion products formation on the surface[79].
- Additionally, the Bode plots (frequency vs. phase angle plot) provide information about changes on the surface[80] and are used to verify the time constant proportional to the formation of protective films on the surfaces. The quality and stability of the film formed on the surface can be evaluated from the frequency vs. log |Z| mode of the Bode curve; the smaller the changes in the slope, the more stable is the film on the surface.[69]

To determine the charge transfer resistance (R_{ct}) or solution resistance (R_s), which are proportional to the rate of the corrosion, it is necessary to define an electronic equivalent circuit model of the interface. With the help of computer software, the best frequency response of a given EIS spectrum and the best fitting parameters can be determined. How well the fitting curve overlaps the original one is an indication of the quality of the fitting.[76] The circuit model facilitates understanding of the EIS results and leads to more detailed information of the corrosion behaviour and/or mechanism. The equivalent circuit that describes a bare electrode surface undergoing a simple kinetically controlled redox process is presented in Figure 2.6 and this model is used to analyse the EIS spectra obtained in this study. The chosen

equivalent circuit is commonly referred to as a Randles circuit and represents a general starting point for more complex models.[81] This simulation provides a reasonably good fit to the measured impedance data in this work. In all cases, the equivalent circuit consists of a parallel resistor (charge transfer resistance, R_{ct}) and a double layer capacitance (C_{dl}) in series with another resistor (solution resistance, R_s) between the specimen and the reference electrode. The values of the charge transfer resistance (R_{ct}) are calculated from the difference in impedance at lower and higher frequencies. A Constant-Phase Element (CPE) is introduced instead of a C_{dl} capacitor to give a more accurate fit, because the impedance results in the Nyquist plots are depressed due to surface roughness, heterogeneity and adsorption effect or other effects that cause non-uniform current distributions on the electrode surface.[27,82]

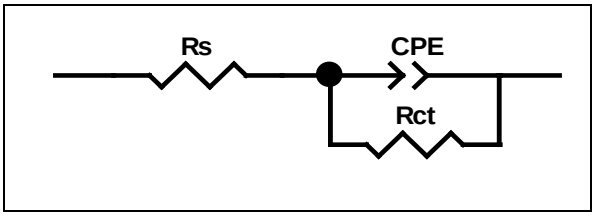

Figure 2.6: Randles equivalent circuit model used to interpret impedance spectra.

Regarding the impedance data of the Nyquist plot, the distance from the origin to the first (high frequency) intercept with the x-axis corresponds to R_s. The distance between the first intercept and the second (low frequency) intercept with the abscissa corresponds to R_p.[76]

In the case that there is no inductive loop at low frequency in the Nyquist plots, the R_{ct} value can be approximated as equal to the R_p value and, therefore the R_p value is inversely proportional to the corrosion rate.[79] According to Equation 2.8, an increase in R_p reflects the decrease in corrosion current/rate. Therefore, the R_{ct} values are used to calculate the corrosion current with different concentrations and temperatures using the following equations:

$$R_p = \frac{B}{i_{corr}} = \frac{(\Delta E)}{(\Delta i)_{\Delta E \to 0}} \tag{2.8}$$

$$i_{corr} = \frac{B}{R_p} \tag{2.9}$$

Where R_p is the polarization resistance in $\Omega.cm^2$

i_{corr} is corrosion current density in $\mu A/cm^2$

B is the Stern-Geary coefficient or empirical polarization resistance constant with the unit voltage (V) that has been considered as 26 in all EIS experiments (B = 26).

and IE% of MEG is calculated from the following equation:

$$IE\%=[(R_{ct}-R^{\circ}_{ct})/R_{ct}]x100 \qquad (2.10)$$

R°_{ct} and R_{ct} are the charge transfer resistances for the solutions without and with MEG, respectively.

Once the impedance data have been defined, computer software is used to fit them to an appropriate equivalent circuit. This equivalent circuit then compares the experimentally measured impedance as a function of the frequency with the theoretically calculated impedance for a particular mechanism in terms of rate constants and other kinetic parameters.

In this study, the results of EIS measurements are fitted and analysed by using the commercial software ZView (ZView Version: 3.0a, Scribner Associates, Inc.).

2.2 Rotating Cylinder Electrodes (RCE's)

Rotating cylinder electrode (RCE) is the most widely used technique in the measurement of kinetic parameters for electrochemical reactions and simulation of flow in turbulent piping systems.

In RCE testing a cylindrical metal sample is rotated in the solution at speeds from 100-5000 rpm. RCE is used to simplify fluid dynamics equations so that corrosion rate can be correlated with mass transfer, which in turn can be related to the velocity effects in pipeline. The same electrochemical techniques used on static samples are applicable to the rotating cylinder electrodes[68].

2.3 Methodology

To achieve the objectives of the study stated in Section 1.7, two sets of laboratory based experiments were developed, which are introduced in the following sections:

2.3.1 Bottom of the Line (Set 1)

In the first set of experiments, in order to examine the corrosion behaviour at the bottom of the line, electrochemical experiments and surface examination are performed using rotating cylinder electrodes (RCE's) in glass cells. The following test matrix is performed to address the objectives of Section 1.7 relating to the bottom of the line (Set 1):

Table 2.1: Test matrix of the research project for bottom of the line (set 1).

Parameter	Set 1
Solution	3% NaCl in DI-water
De-oxygenated gas	CO_2, N_2
Oxygen concentration	<20 ppb
MEG concentration (vol%)	0–80
HAc concentration (ppmv)	0–5000
Temperature (°C)	24, 40, 60
Rotation velocity (rpm)	1000
Measurement techniques	LPR, Potentiodynamic polarization, EIS, SEM

2.3.1.1 Material and Media Preparation

Two types of carbon steels are used to investigate the corrosion at the bottom of the line. Electrochemical experiments are conducted using 1030 grade carbon steel. The working electrode cylindrical specimen is machined from the parent rod material with an area of approximately 3.14 cm^2. Chemical composition of the steel is presented in Table 2.2. Prior to each experiment, the steel surfaces are

polished using silicon carbide (SiC) abrasive paper in a sequence of 120-, 320-, and 600-grit. The test samples are degreased in ethanol, sonicated in acetone for two minutes and dried under nitrogen. Both diameter and length of the cylinder are measured using a digital calliper (Mitutoyo Absolute Digimatic CD-6 CSX) to calculate the surface area (SA) using the following equation:

$$SA = 2\pi \frac{D}{2} \times L \quad (2.11)$$

Where D is the diameter and L is the length of the cylinder in cm.

Immersion experiments are conducted using 1020 grade carbon steel. The coupons are cut from parent carbon steel sheet into 2 cm x 2 cm x 3 mm coupons. Chemical composition of the steels is presented in Table 2.3. Prior to immersion, all the coupons are polished using silicon carbide (SiC) abrasive paper in a sequence of 120-, 320-, and 600-grit. After polishing, the test samples are degreased in ethanol, sonicated in acetone for two minutes and dried under nitrogen. Chemical composition of the steel used in the immersion tests is presented in Table 2.3.

Table 2.2: Chemical composition of the 1030 carbon steel used for the electrochemical tests (wt%).

C	P	Mn	Si	S	Ni	Cr
0.330	0.014	0.710	0.261	0.040	0.012	0.029
Sn	N	Fe				
0.004	0.012	98.588				

Table 2.3: Chemical composition of the 1020 carbon steel used for the immersion tests (wt%).

C	P	Mn	Si	S	Ni	Cr
0.200	0.017	0.730	0.010	0.016	0.014	0.020
Sn	Mo	Al	N	Fe		
0.005	0.003	0.035	0.005	98.940		

The brine solution used in this research is made up from ultra-pure water (Mili-Q system, resistivity 18.2 MΩ. cm) and 3 wt% sodium chloride (NaCl; Ajax Finechem, analytical reagent, 99.9%). All the solutions are prepared by volume using a

standard volumetric flask. Different volume concentrations of monoethylene glycol (MEG; Ethanediol; Chem-supply, analytical reagent) is added to the brine solution by mixing MEG and brine in the required ratio (vol%).

2.3.1.2 Experimental Setup

The experiments are performed in 1 litre glass cells. The glass cell is filled with the test solution (500 mL). CO_2 or N_2 gas (high purity of 99.9992%, BOC Gas Supply, Australia) is purged at atmospheric pressure for at least two hours prior to starting the measurements to saturate the test solution and remove the oxygen. After two hours, the dissolved oxygen level is measured using a DO probe (Orion, 5 star series, A07825) to ensure the oxygen level <20 ppb. The solution is sparged throughout the experiments to keep the system deaerated.

The test temperature is controlled using electronic hot plates with thermocouples (IKA, RET control 3364100) inserted into the test solution and is maintained within ± 1°C for all experiments. Acetic acid (HAc Glacial; Chem-Supply, analytical reagent) is added to the test solution 10 minutes before sample immersion for some experiments. The sample and experimental setup are shown in Figure 2.7 (a) and (b). All experiments are performed using a three-electrode system: A carbon steel rotating cylinder electrode (RCE) is used as the working electrode (WE), prepared as described in Section 2.2.1.1. The test sample is then mounted on the specimen holder (Figure 2.7a) and immersed in the test solution (Figure 2.7b). A platinum mesh electrode is used as a counter electrode (CE) and a saturated silver-silver chloride electrode (Ag/AgCl) was used as a reference electrode (RE).

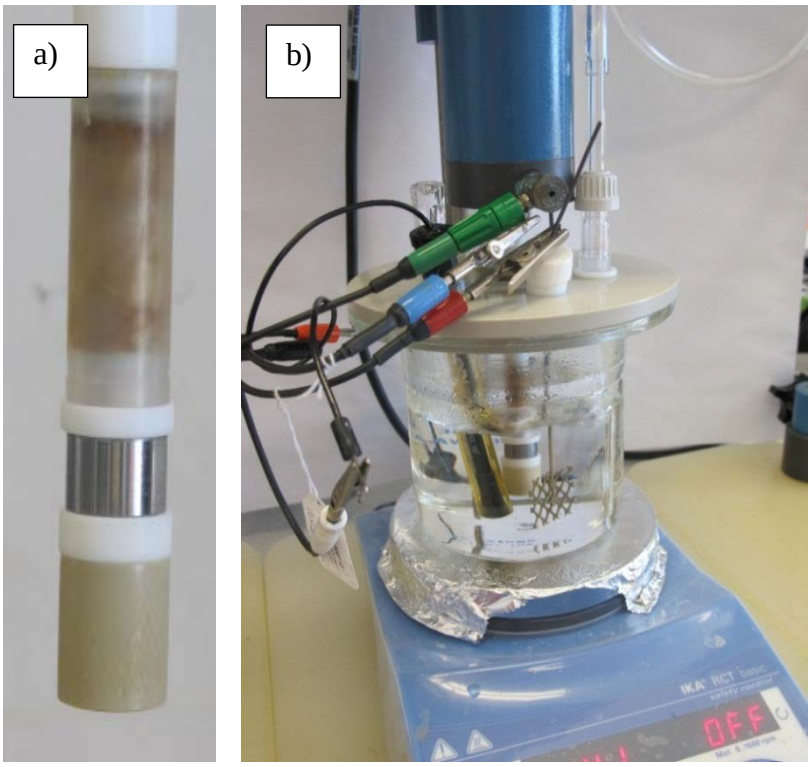

Figure 2.7: (a) Test sample mounted on the specimen holder (b) Three-electrode experimental setup.

The rotation speed of the WE is adjusted to 1000 rpm using a control box. After the initial deaeration of the test solution with CO_2 or N_2 (high purity of 99.9992%), the pH is measured using a pH electrode probe (Orion, 5 star series, A07825). The pH glass probe is calibrated before each test to ensure reliability. The pH meter is also calibrated in MEG solutions. The pH calibration method and measurement correction in MEG solutions are given in Section 2.2.1.4.

The WE is immersed in the test solution, the potentiostat electrical connections are attached and the measurements started. At the end of the experiments, the samples are removed from the cell, rinsed with DI water, dried using high purity N_2 and stored in a moisture-free desiccator for SEM analysis.

2.3.1.3 Electrochemical Measurements

All electrochemical experiments are conducted as outlined in Section 2.1.

Each experiment is run multiple times to give reproducible results.

2.3.1.4 pH Measurement in MEG Solutions

The presence of MEG in the test solution has an influence on the pH. Therefore, there is a need for accurate pH measurements in the MEG mixtures. If an electrode calibrated in aqueous pH standards is used to measure pH the result will be in error due to the large change in solvent properties.[83] The calibration procedure reported by Sandengen et al.[84] is used to calculate the error between the measured and the actual pH of MEG/water mixtures (ΔpH_{MEG}). The term ΔpH_{MEG} describes the difference between actual and measured pH values. ΔpH_{MEG} is found by measuring pH_{meas} in potassium hydrogen phthalate (KHPh; Ajax Finechem, analytical reagent, 99.9%) standard solutions (buffer solutions of 0.05 m KHPh). Buffer solutions of 0.05 m KHPh have been extensively studied and are designated as the reference value pH standard (RVS).[84] ΔpH_{MEG} is calculated by the following equation:

$$\Delta pH_{MEG} = pH_{Rvs} - pH_{meas} \quad (2.12)$$

Where pH_{Rvs} is given by Equation 2.13:

$$pH_{Rvs} = 4.00249 + 1.0907\ w_G + 0.9679\ w_G^2 + 0.3430\ z + 0.03166\ w_G\ z - 0.8978\ w_G^2 z + 7.7821\{\ln(T/\theta)-z\} + 9.8795\ w_G^3\ \{\ln(T/\theta)-z\} \quad (2.13)$$

Where $z = T - \theta/T$, $\theta = 298.15$, θ and T are temperature in K and °C

w_G is the weight fraction of ethylene glycol.

To determine the pH_{meas} value, the pH electrode is first calibrated with standard aqueous solutions (pH~ 4, 7 and 10). Buffer solutions of 0.05 m KHPh were prepared as follows: six calibration mixtures of MEG/water solutions of different ratios (0–90 wt% MEG) are prepared. A known amount of KHPh is added to the MEG/water mixtures to prepare buffer solutions of 0.05 M KHPh. The solutions are magnetically stirred. Then, the pH is measured for each MEG/water mixture. The results are plotted in Figure 2.8.

The final pH of the MEG/water mixtures reported in this work (pH_{act}) is therefore, the sum of the measured pH of the test MEG/water mixture and ΔpH_{MEG} at different weight fractions of MEG:

$$pH_{act} = pH_{meas} + \Delta pH_{MEG} \quad (2.14)$$

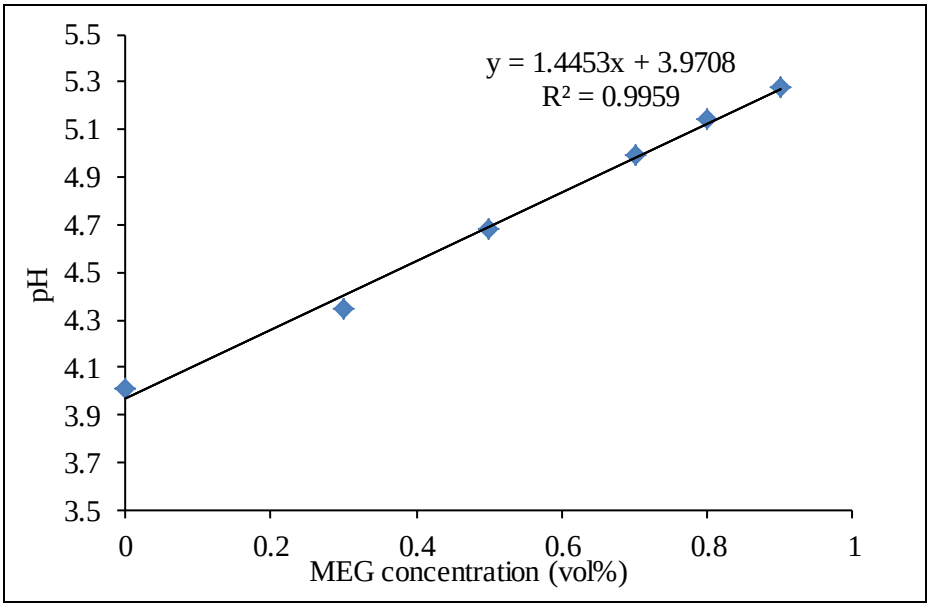

Figure 2.8: pH calibration plot of different MEG/water mixtures at 24°C.

2.3.1.5 Morphology Observation

The corrosion morphologies after experiments are characterized using scanning electron microscopy (Zeiss Evo 40XVP). The elemental analysis of the steel surface is conducted using electron dispersive x-ray spectroscopy (EDS) (Zeiss Evo 40XVP). The data obtained from the EDS are analysed using Inca computer software version 4.11 (Oxford Instrument Analytical Ltd).

2.3.2 Top of the Line (Set 2)

In the second experimental setup, in order to determine the effect of MEG on the condensation rate at the top of the line, high pressure and high temperature

autoclaves (Parr instrument, series 4520 bench top reactor) are used to simulate the condensing water corrosion.

The following test matrix is performed to address the above objectives related to the top of the line (Set 2).

Table 2.4: Test matrix of the research project for Top of the line (Set 2).

Parameter	Set 2		
Solution	DI-Water		
De-oxygenated gas	CO_2		
CO_2 partial pressure (bar)	20		
MEG concentration (vol%)	0, 50, 90		
Bulk solution temperature T_a (°C)	60	90	120
Cooling temperature T_c (°C)	10, 20, 30, 40	20, 30, 40, 50, 60	40, 50, 60, 70, 80

2.3.2.1 Material and Media Preparation

Test samples are carbon steel tubes of a ¼-inch tube diameter. All samples are made according to the ASTM standard A 179/A 179M-90a[85] to ensure comparable and reproducible results during the whole testing procedure. Chemical composition of the U-tube steel is presented in Table 2.5. The U-tube sample is cut from the parent carbon steel tube with a length of 130 mm, bent to the U-shape with a surface area of 2073.5 mm^2. Prior to each test, the U-tube specimen is sandblasted, cleaned in acetone using an ultrasonic bath, further rinsed in isopropanol and then mounted into the autoclave.

Table 2.5: Chemical composition of the carbon steel used for top of the line tests (wt%).

C	P	Mn	Si	S	Fe
0.079	0.014	0.429	0.204	0.007	99.263

The aqueous phase is prepared from ultra-pure water (Milli-Q, Resistivity 18.2 MΩ.cm) and monoethylene glycol (MEG; Ethanediol; Chem-supply, analytical reagent). Two water/MEG mixture concentrations are used: a mixture of 50:50 and 90:10 v/v MEG/water. The autoclave is filled with ~ 650 mL of the water/MEG mixture.

2.3.2.2 Experimental Setup

Experiments are performed in a static, high pressure, high temperature autoclave (Parr Instrument, 4520 bench top reactor) based test system with a cooled U-tube on which the condensation takes place. The U-tube is connected to the cooling coil ports of the autoclave head and a custom-made beaker is placed under the sample to collect the condensate (Figure 2.9a).

After the U-tube sample is mounted, the autoclave's head is closed. Then the autoclave is transferred to the pressurisation manifold. It is then pressurised and depressurised with CO_2 gas (high purity of 99.9992%) four times to decrease the oxygen level to less than 20 ppb. On the fifth pressurisation cycle the vessel is allowed to equilibrate over a 20 minute period. The efficiency of this oxygen removal process is checked by measuring the oxygen level using an Orbisphere (Hach Orbisphere 3655). In all the experiments the pressure is set to 20 bar. Once the vessel is pressurised, it is transferred into the heater assembly (Figure 2.9b). The temperature probe is inserted. The proposed test bulk liquid temperature is set at the autoclave controller (Figure 2.9c). After the system reaches the proposed temperature, inhibited cooling water solution is pumped through the U-tube sample for a period of 18 hours. The cooling water solution is inhibited using a nitrate-based corrosion inhibitor mixed with tap water at a ratio of 30 mL in 1000 mL water. The temperature difference between the autoclave and the cooling water (ΔT) varies between 20°C to 60°C.

(a)

(b)

Vessel temperature

Set point temperature

Pressure in the vessel (psi)

(*c)*

Figure 2.9: (a) Custom-made beaker placed under the sample to collect the condensate and (b) Autoclave experimental set-up and (c) Digital display box used to set the temperature and pressure.

2.3.2.3 Condensation Rate Measurements

The volume of the condensate collected in the beaker is measured using a standard measuring cylinder after the test and the condensation rate is calculated using Equation 2.15. The effect of re-evaporation in the beaker is very low and is neglected in this work. The condensate from the test is analysed using an FT-IR spectrometer (Perkin Elmer Spectrum 100) to estimate possible MEG transportation from the liquid water/MEG phase via the gas phase into the condensate. The procedure is been described in Section 2.2.2.4.

The condensation rate is calculated from the following equation:

$$CR = \frac{V_{CR}}{SA \times t} \tag{2.15}$$

where CR is the condensation rate in mL/m^2s

V_{CR} is the condensation volume in mL

SA is the surface area in m^2

t is the time in seconds.

2.3.2.4 MEG Content in the Condensate

The measurement of MEG content in the condensing liquid is based on analysing the condensing liquid using Fourier transform infrared spectroscopy (FTIR) to obtain quantitative data on the mass transport of MEG from the bulk liquid to the gas phase, and its following condensation on the sample surface.

The first step is the assignment of the absorption bands in the infrared spectra and selection of the absorption band further used for the quantitative analysis. The infrared spectra of pure MEG (a) and the MEG/water mixture (b) are shown in Figure 2.10. The broad band at 3310 cm^{-1} and the band at around 1647 cm^{-1} can be assigned to both symmetric and asymmetric stretching and the H−O−H bending vibrations of water molecules. While the bands between 3000 and 2800 cm^{-1} and also the ones around 1100–1000 cm^{-1} are assigned to various vibrations of MEG molecule ($HO-CH_2-H_2C-OH$). The peak at 2937 cm^{-1} is due to asymmetric

stretching vibration of C−H and the one at 2876 cm^{-1} is due to C−H symmetric stretching vibration. The peak at 1031 cm^{-1} is assigned to C−O vibrations of the MEG molecule. The assignment of the absorption bands is presented in Table 2.6.[86] The absorption band at around 1028 cm^{-1} is selected for further quantitative analysis of the bulk and condensing liquids.

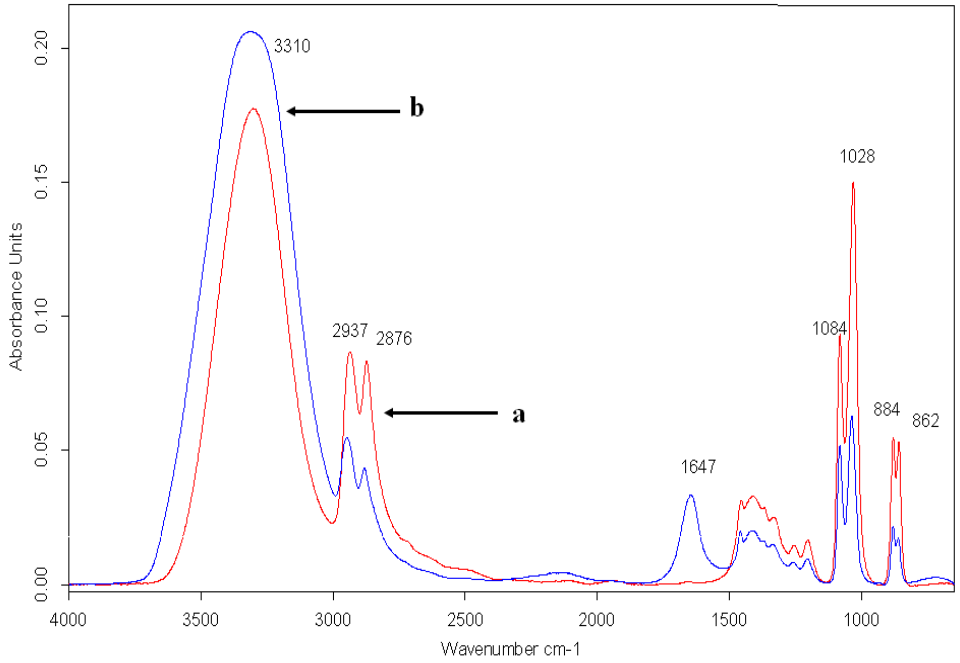

Figure 2.10: Representative FTIR spectra of the (a) pure MEG and (b) MEG/water mixture.

Table 2.6: Tentative assignment of the absorption bands.[86] Spectra are shown in Figure 2.10.

Wavenumber (cm^{-1})	3291	2930	1642	1031	883
Bond assignment	O−H	C−H	H−O−H	C−O	C−H

To estimate the concentrations of MEG from the selected absorption band, nine calibration mixtures of water/MEG solutions (0–100 vol% MEG) are prepared and analysed with the FTIR. The calibration plot is shown in Figure 2.11. The calibration plot is then used to determine the concentration of MEG in the condensing liquid.

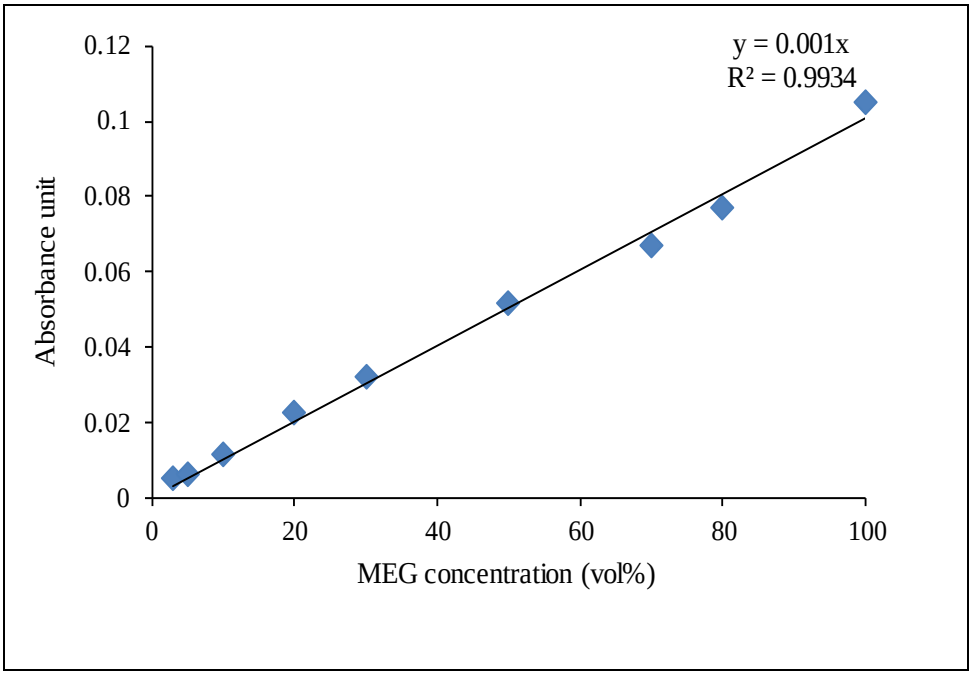

Figure 2.11: Absorbance calibration plot of the standard MEG/water mixtures analysed with the FTIR.

CHAPTER 3. Effect of MEG Concentration on CO_2 Corrosion

In this chapter the effect of the MEG concentration on CO_2 corrosion of carbon steel is evaluated. MEG was used in concentrations of 10% to 80% in 3% NaCl solution at 24°C and 60°C. The test without MEG is used as a reference. The experimental set-up is described in detail in Section 2.2.1. To clarify the role of CO_2 in the corrosion behaviour of carbon steel in the presence of MEG, a series of experiments are performed in solutions de-oxygenated using N_2.

3.1 Evaluation of Corrosion Rate at 24°C

In order to clarify the effect of the MEG concentration on the general rate of CO_2 corrosion of carbon steel, LPR measurements are conducted with different concentrations of MEG for a period of 24 hours. The results at 24°C are shown in Figure 3.1 and the corrosion rates after the 24 hours are summarized in Table 3.1.

It is seen that an increase in the MEG concentration results in a decrease in the corrosion rate at all concentrations tested. In the absence of MEG the corrosion rate increased with time and the value recorded after 24 hours was 1.1 mm/y. The corrosion rates recorded in the presence of 10% and 33% MEG were almost the same during the 24 hours experimental duration. It can be seen that at MEG concentrations below 50% the corrosion rate does not stabilise and follows an increasing trend. In 50% and 80% MEG solutions the corrosion rates are very close to each other with values of ≤0.1 mm/y. The corrosion rates stabilised approximately an hour after immersion in the solution containing 50% MEG and less than an hour after immersion to the solution with 80% MEG. A similar non-linear decreasing trend in corrosion rates with increasing MEG concentration has been elsewhere reported for carbon steel in 10% to 70% MEG solutions[16] and for a Mg/ethylene glycol solutions interface[26] both at 25°C.

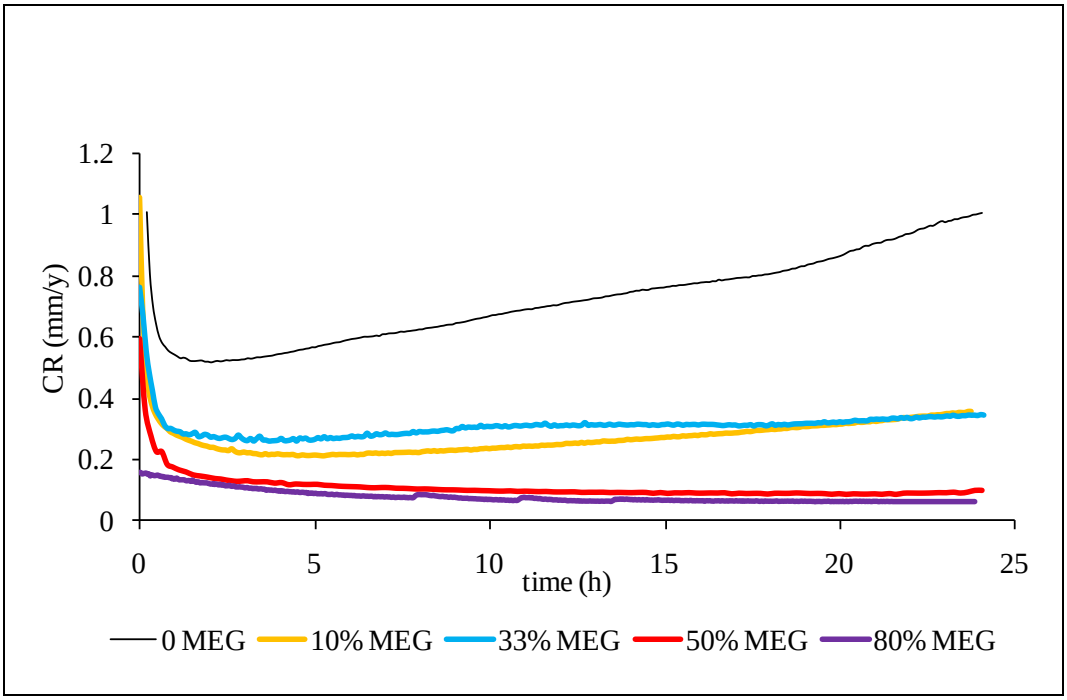

Figure 3.1: Corrosion rates of carbon steel in CO_2 saturated 3% NaCl solution containing various concentrations of MEG at 24°C.

Table 3.1: Corrosion rate values at various MEG concentrations after 24 hours immersion at 24°C. Data from LPR measurements shown in Figure 3.1.

C_{MEG} (vol%)	0	10	33	50	80
CR (mm/y)	1.10±0.1	0.36±0.04	0.34±0.05	0.10±0.02	0.06±0.01

Gulbrandsen and Morard[16] suggest that the inhibition effect of MEG on CO_2 corrosion can be related to changes in the properties of the solution. The addition of MEG increases the viscosity of the solution and decreases the diffusivity of carbon dioxide. The corrosion rate trends in the presence of 50% and 80% MEG suggest that at high enough concentration, in a short time after immersion of the sample, MEG can adsorb on the metal surface and keep water and CO_2 molecules away from the surface.[16,17,26]

3.2 Evaluation of Corrosion Rate at 60°C

As temperature has a great influence on the CO_2 saturated solution properties (such as viscosity, conductivity and CO_2 solubility) in the presence of MEG[87] and the corrosion rates in general, the inhibition efficiency of various concentrations of MEG are studied at an elevated temperature of 60°C. The experimental results are

shown in Figure 3.2 and the corrosion rate values after 24 hours are summarized in Table 3.2.

As in the LPR experiments carried out at 24°C (Chapter 3.1), the corrosion rate follows a decreasing trend as the concentration of MEG is increased. In the absence of MEG the corrosion rate stabilized after approximately 3 hours at 4.37 mm/y and each concentration of MEG provided a specific corrosion protection to the carbon steel. The general corrosion rate reached the minimum value of 0.14 mm/y with 80% of MEG after 24 hours. The results from LPR measurements at 60°C show an exponential decrease in the rate of corrosion with increasing MEG concentration. The corrosion rates listed in Table 3.2 show that none of the MEG concentrations used provide adequate protection to the steel samples at 60°C to reduce the corrosion rates to less than 0.1 mm/y.

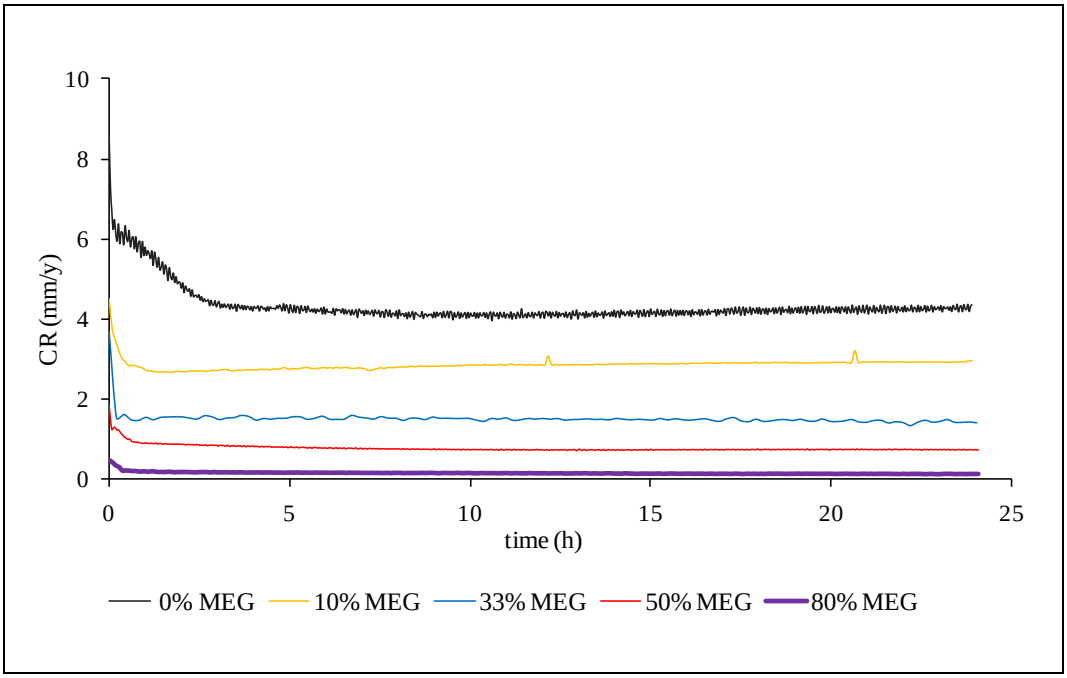

Figure 3.2: Corrosion rates of carbon steel in CO_2 saturated 3% NaCl solution containing various concentrations of MEG at 60°C.

Table 3.2: Corrosion rate values at various MEG concentrations after 24 hours immersion at 60°C. Data from LPR measurements shown in Figure 3.2.

C_{MEG} (vol%)	0	10	33	50	80
CR (mm/y)	4.37±0.26	3.00±0.2	1.50±0.18	0.73±0.09	0.14±0.008

Summarising the results obtained at 24°C (Figure 3.1) and 60°C (Figure 3.2) it is apparent that the corrosion rates decrease with increasing concentration of MEG at both temperatures. The general corrosion rates are found to increase with increasing temperature at all MEG concentrations. At 24°C, corrosion rates lower than 3.1 mm/y are recorded at MEG concentrations ≥50%. It is also worth noting the significant differences in the corrosion rates from the solutions with 33% and 50% MEG at 24°C and 60°C. Stable corrosion rates are established after 24 hours at 60°C in all cases compared to the measurements at 24°C, but no corrosion rate values below 0.1 mm/y are recorded.

3.3 Consideration of the Possible CO_2 Corrosion Mechanism

It is demonstrated in Sections 3.1 and 3.2 that the concentration of MEG influences the general corrosion rate of the carbon steel. In order to further investigate the effect of MEG on the anodic and cathodic reactions of the corrosion process, potentiodynamic polarization measurements are conducted immediately after the 24 hours linear polarization resistance test.

The potentiodynamic polarization measurements recorded at 24°C are presented in Figure 3.3.

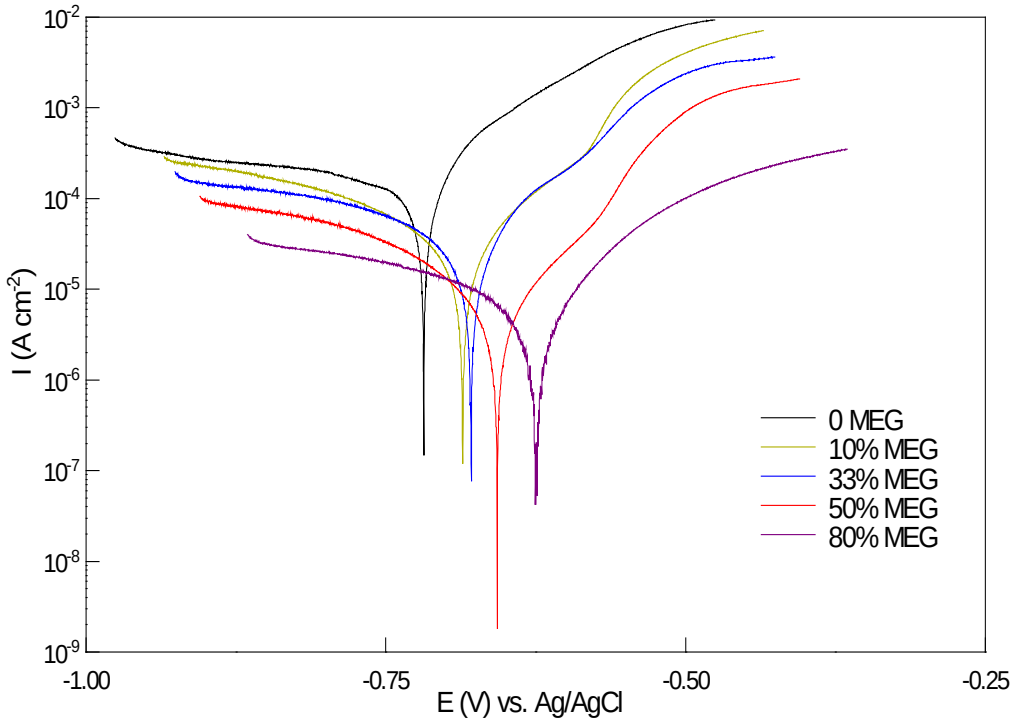

Figure 3.3: Representative potentiodynamic polarization plots of carbon steel in CO_2 saturated 3% NaCl solution containing various concentrations of MEG after 24 hours immersion at 24°C.

It can be seen that with increasing MEG concentration the corrosion potential shifts to more positive potentials. Both anodic and cathodic currents decrease with respect to that of the blank solution (0% MEG). However, the reduction of the anodic currents is more significant than that of the cathodic currents. The positive shift in corrosion potential combined with the large decrease in anodic current density indicates that MEG inhibits the anodic reaction to a large extent.

The potentiodynamic measurements at 60°C are shown in Figure 3.4. The same trend as in experiments at 24°C (Figure 3.3) is observed, where both anodic and cathodic current densities decrease with increasing MEG concentration and the corrosion potential shifts in the positive direction. The effect of MEG is more pronounced on the anodic reaction.

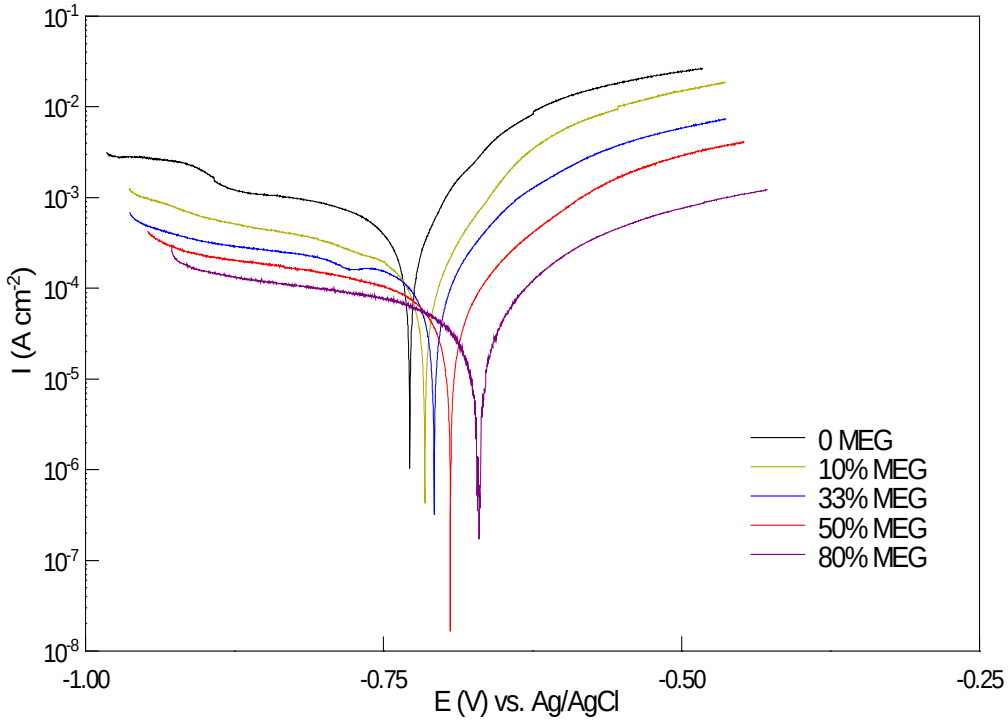

Figure 3.4: Representative potentiodynamic polarization plots of carbon steel in CO_2 saturated 3% NaCl solution containing various concentrations of MEG after 24 hours immersion at 60°C.

The electrochemical parameters obtained from the potentiodynamic polarization measurements are summarized in Table 3.3 and Table 3.4 for experiments carried out at 24°C and 60°C, respectively. Lower corrosion current densities and higher inhibition efficiencies are associated with the higher MEG concentrations and lower E_{corr} values at both temperatures investigated. Further inspection of Table 3.3 and Table 3.4 reveals that at both 24°C and 60°C, anodic and cathodic Tafel slopes (b_a and b_c) decrease with the addition of MEG into the blank solution (0% MEG), but do not change significantly with the change of MEG concentration.

The results show that MEG acts as an inhibitor in the CO_2 corrosion process. The positive shift in corrosion potential in addition to the inhibition of both anodic and cathodic reactions indicates that the inhibitor is affecting the corrosion process by blocking the active sites of the surface.[77] It is assumed that in the absence of MEG, the active sites on the metal surface are the same for both anodic and cathodic reactions. In the presence of MEG, on the other hand, adsorption of the inhibitor changes those active sites and, therefore, reduces the anodic and cathodic reactions rate.[88]

There is no appreciable difference in Tafel slopes observed with increasing MEG concentration and temperature, suggesting that the type of inhibition activity is similar in all the conditions studied.

Table 3.3: Electrochemical parameters of carbon steel in CO_2 saturated 3% NaCl solution containing various concentrations of MEG after 24 hours immersion at 24°C.

C_{MEG} (vol %)	E_{corr} (mV)	i_{corr} ($\mu A/cm^2$)	b_a (mV)	$-b_c$ (mV)	IE (%)	CR (mm/y)
0	-739	120	110	185	-	1.38±0.15
10	-685	18	75	115	80	0.20±0.01
33	-679	17	73	110	81	0.19±0.03
50	-645	6.5	70	110	94	0.07±0.00
80	-620	4.5	70	110	95	0.05±0.00

Table 3.4: Electrochemical parameters of carbon steel in CO_2 saturated 3% NaCl solution containing various concentrations of MEG after 24 hours immersion at 60°C.

C_{MEG} (vol%)	E_{corr} (mV)	i_{corr} ($\mu A/cm^2$)	b_a (mV)	$-b_c$ (mV)	IE (%)	CR (mm/y)
0	-726	250	85	225	-	2.87±0.30
10	-711	92	45	130	63	1.05±0.18
33	-702	68	48	120	72	0.78±0.12
50	-690	38	60	118	84	0.43±0.43
80	-634	24	70	116	90	0.27±0.00

The reduction of the cathodic current with increasing MEG concentration is, most probably, associated with the fact that upon addition of MEG, the hydrogen diffusion and the CO_2 solubility are retarded. The decrease in the solubility and diffusivity of CO_2 with increasing MEG concentration is due to the increase in the solution viscosity.[16] This proposed effect of MEG is further investigated and discussed in more detail in Section 3.3.1.

It was shown that like many other organic molecules, MEG can be adsorbed on an electrode surface to effectively cover and protect the surface from CO_2 corrosion attack.[26] When the concentration of MEG increases, the steel surface is more completely covered by MEG molecules, which inhibits the anodic reaction more effectively.

In view of the discussion above, and the presented potentiodyamic polarization results, additional experiments are carried out in order to describe the effect of MEG on the cathodic and anodic reactions in respect to the reaction time.

Figure 3.5 shows the potentiodynamic polarization curves measured in the absence and the presence of MEG immediately after immersion of the steel to the corrosive media and compares these with the measurements recorded 24 hours after the immersion at 60°C (data from Figure 3.4). The results indicate that MEG inhibits the anodic current density immediately after immersion, but the cathodic current density is unaffected by the presence of MEG. Furthermore, the corrosion rate decreases immediately upon immersion from 2.07 mm/y in the absence of MEG to 1.50 mm/y in the presence of 50% MEG. In contrast, after 24 hours of immersion both anodic and cathodic currents decreased in the presence of MEG compared to the solution without MEG and the resulting corrosion rates decreased from 2.87 mm/y in the absence of MEG to 0.43 mm/y in the 50% MEG solution. These results confirm the fast inhibition effect of MEG on the anodic reaction. The decrease in the anodic current from the start of the immersion in the presence of MEG may be related to the development of a surface layer over the corroding metal due to adsorption of MEG on the surface. The increase in the inhibition effect of MEG on the anodic reaction and also inhibition of the cathodic reaction with increasing time suggests the development of a protective MEG layer on the surface. The effect of immersion time and the development of a surface film are discussed further in Section 5.3.

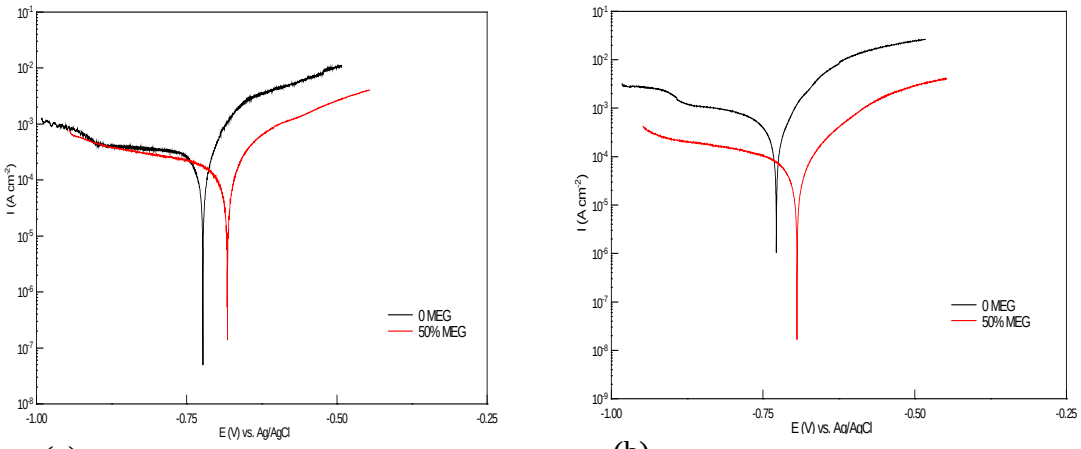

Figure 3.5: Representative potentiodynamic polarization plots of carbon steel in CO_2 saturated 3% NaCl solution in absence and presence of 50% MEG at 60°C, the scans were performed (a) immediately after immersion and (b) 24 hours after immersion.

In order to obtain more information about the inhibition effect of various concentrations of MEG on CO_2 corrosion of carbon steel, EIS measurements are performed. The experimental setup is described in Section 2.2.1.

EIS measurements are performed after the sample is immersed in the test solution for a period of 24 hours. Figure 3.6 shows a set of Nyquist plots for mild steel in 3% NaCl solutions saturated with CO_2 at 24°C in the absence and in the presence of 50% and 80% MEG. A single depressed capacitive semicircle equivalent to charge transfer resistance (R_{ct}) is observed in both high and low frequency regions in the absence and the presence of MEG. This capacitive loop is related to the time constant of the charge transfer reaction in the electric double layer capacitance in both high and low frequency regions[78] indicating that the corrosion reactions, both without and with MEG, are charge transfer controlled. It is also shown that the magnitude and the diameter of the capacitive loop increase with increasing MEG concentration and compared to the blank solution, which indicates a reduction in the corrosion rates. Increasing both the impedance magnitude and impedance diameter with increasing MEG concentration confirms the above proposed formation of a surface film on the metal surface, which acts as a barrier against the charge transfer of the species in the solution. This result is consistent with the potentiodynamic polarization results, which show an active site blocking effect of MEG on the cathodic and anodic corrosion reactions possibly due to adsorption of MEG on the steel surface (Section 3.3). The results are consistent with a previous study, where the solution resistance and polarization resistance of the magnesium alloy after 10 days immersion in various concentrations of ethylene glycol in water solutions at 25°C is measured.[26]

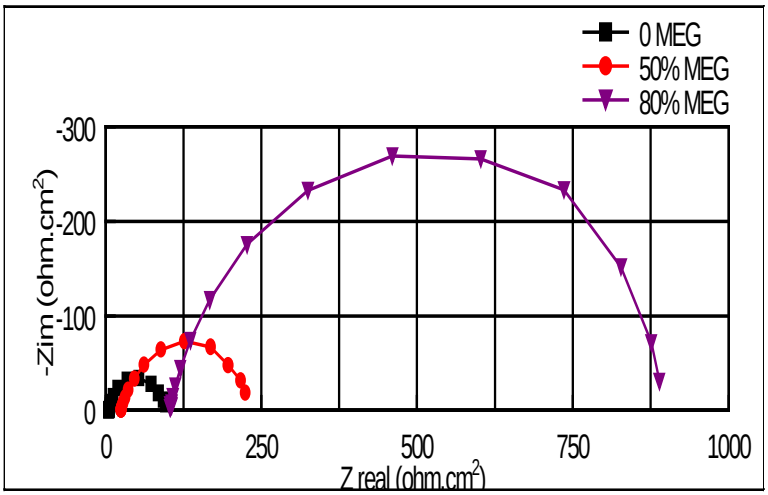

Figure 3.6: Representative Nyquist plots of carbon steel in CO_2 saturated 3% NaCl solution containing various concentrations of MEG after 24 hours immersion at 24°C.

The Nyquist plots of carbon steel electrodes in absence and presence of 10% to 80% MEG solutions at 60°C (Figure 3.7) shows a single semicircle at all frequencies, which is consistent with the results obtained at 24°C indicating that the corrosion reactions are charge transfer controlled both without and with MEG. Both the impedance magnitude and the diameter increase with increasing MEG concentration, which indicates increasing inhibition efficiency with increasing amount of MEG. As for the 24°C experiments, the impedance loop is shifted along the real Z axis with increasing MEG concentration. This shift is less pronounced between 10% and 50% MEG solutions at 60°C and increases considerably for the 80% MEG solution. The shift indicates increase in the solution resistance and formation of a film at the steel surface.

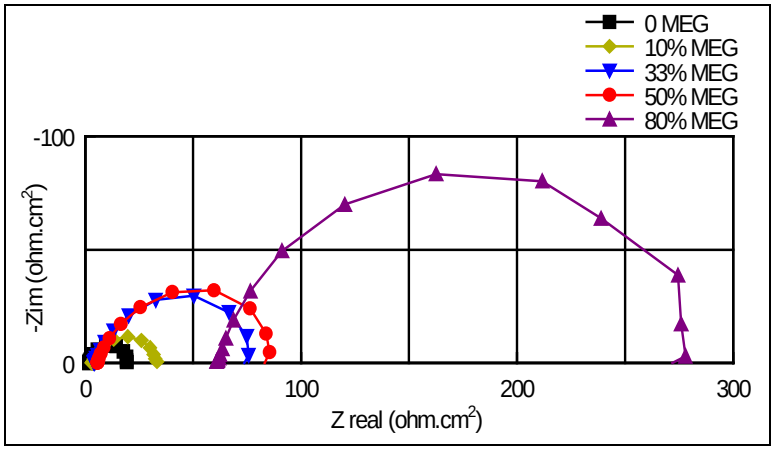

Figure 3.7: Representative Nyquist plots of carbon steel in CO_2 saturated 3% NaCl solution containing various concentrations of MEG after 24 hours immersion at 60°C.

The equivalent circuit shown in Figure 2.6 represents the best fit to the obtained result and is used to analyse the EIS spectra and the resulting data is presented in Table 3.5 and Table 3.6, for 24°C and 60°C, respectively. This is a circuit for the corrosion system under charge transfer control, where no mass transport is detected[79] and indicates that the inhibition action of MEG is controlled by a charge transfer process, which is most likely a layer of MEG forming a barrier on the metal surface.

Table 3.5: Comparative analysis of the value of equivalent circuit parameters obtained from measurements in solutions with different concentrations of MEG at 24°C.

C_{MEG} (vol%)	R_s (Ω cm²)	R_{ct} (Ω cm²)	C (F cm²)	i_{corr} (μA/cm²)	CR (mm/y)	IE%
0	5.3	91.5	0.82	130	1.5±0.18	-
50	25	212.5	0.75	35	0.4±1.05	56
80	120	810	0.74	10	0.11±0.55	87

Table 3.6: Comparative analysis of the value of equivalent circuit parameters obtained from measurements in solutions with different concentrations of MEG at 60°C.

C_{MEG} (vol%)	R_s (Ω cm²)	R_{ct} (Ω cm²)	C (F cm²)	i_{corr} (μA/cm²)	CR (mm/y)	IE%
0	3	25.5	0.85	480	5.57±0.34	-
10	3.5	31.0	0.80	190	2.20±0.10	40
33	4.1	73.6	0.79	180	0.95±0.14	74
50	9.1	78.1	0.78	88	1.00±0.63	76
80	61.2	225	0.77	33	0.35±0.05	91

Data presented in Table 3.5 and Table 3.6 show that the solution resistance, R_s, increases with increasing MEG concentration at both temperatures. The values of solution resistance reduce with increasing temperatures for all MEG concentrations. The value of charge transfer resistance (R_{ct}) represented by the size of the semicircle, increases when higher MEG concentrations are present in the solution. It is also demonstrated that in the presence of MEG the capacitance decreases to lower values.

The increase in solution resistance (R_s) is related to the decrease in the conductivity of the solution in the presence of MEG.[89] The conductivity of the test solutions is measured and the results are summarized in Table 3.7. It can be seen that the conductivity reduces continuously from 53 mS/cm for the brine solution to 1.1 mS/cm and from 55.5 mS/cm to 1.9 mS/cm in 80% MEG solution at 24°C and 60°C, respectively. The dilution by water may tend to facilitate the hydrolysis of the hydroxyl groups of MEG and decrease the viscosity of the solution which leads to increase in electrical conductivity.[26,27] The conductivity decreases (solution resistance decreases) with increasing MEG concentration due to the decreasing ionic strength. Temperature increase leads to a further increase in conductivity and thus a reduction of solution resistance.

Table 3.7: Conductivity of the MEG solutions in different concentrations at 24°C and 60°C.

C_{MEG} (vol%)		0	10	50	80
Conductivity (mS/cm)	24°C	53	33.9	7.1	1.1
	60°C	55.5	33.9	9.3	1.9

An increase in R_{ct} and a decrease in overall capacitance correspond to a strong adsorption.[26] The R_{ct} value is very close to R_p values as there is no sign of an inductive loop at low frequency in the Nyquist plots (Figure 3.6 and Figure 3.7) and the R_p value is inversely proportional to the corrosion rate; according to Equation 2.9, an increase in R_p reflects the decrease in corrosion current. The corrosion currents then are used to calculate the corrosion rates using Equation 2.3. Thus, the increasing values of R_{ct} (Table 3.5 and Table 3.6) results in a decreasing trend in the corrosion rate, which indicates the inhibition effect of MEG with its increasing concentration.

The sum of solution resistance (R_s) and charge transfer resistance (R_{ct}) is the total resistance (R_T). The total resistance (R_T) and capacitance (C) are the general characteristics that simultaneously determine the surface film protectiveness. These values are presented in Table 3.5 and Table 3.6. The effect of the MEG concentration on the relative capacitance (C), which is inversely proportional (1/C) to the thickness of the surface film and/or adsorption of MEG on the surface,[26,89] indicate that the total resistance value (R_T) increases, while the capacitance value decreases (thickness of the surface film (1/C) increases). The decreasing interface capacitance can be a result of water molecules being replaced by MEG's larger molecules on the steel surface.[26,89] With increasing MEG concentration more MEG may be adsorbed on the surface resulting in further decrease of the capacitance. The results indicate that MEG molecules physically adsorb on the electrode and cover the surface effectively to make a barrier between the water and surface.

3.3.1 Evaluation of the MEG Effect on the Corrosion Reactions in the Absence of CO_2 (N_2 Saturated solutions)

In order to define the contribution of CO_2 on the inhibition effect of MEG additional experiments are performed in a nitrogen saturated system. Initially the corrosion rate of carbon steel is determined by LPR in 3% NaCl solutions and different concentrations of MEG (in a range of 0 to 80% MEG solutions) saturated with high purity nitrogen (N_2) for a period of 24 hours. Then the potentiodynamic polarization measurements are conducted to further evaluate the inhibition effect of MEG and the role of CO_2 in both the cathodic and anodic reactions of the corrosion process. The experimental setup is described in Section 2.2.1; and the only difference is that N_2 is used to saturate the test solution instead of CO_2.

The corrosion rate measurement results are shown in Figure 3.8 and corrosion rate values after 24 h are summarized in Table 3.8. The results show that the presence of MEG reduces the corrosion rate of carbon steel except for the lowest concentration of 10% MEG solution, which does not seem to have an effect. The corrosion rate of carbon steel in nitrogen saturated brine solution was low even in the absence of MEG (about 0.035 mm/y). The corrosion rate values oscillate in a narrow range

during the 24 hours of LPR measurement for the blank and 10% MEG solutions. With increasing the concentration of MEG to 50% and 80% the corrosion rate of carbon steel are suppressed to the very low values of 0.017 and 0.005 mm/y. These results confirm the inhibition effect of MEG on the general corrosion rate of carbon steel in brine solution, except for the lowest concentration (10%) of MEG.

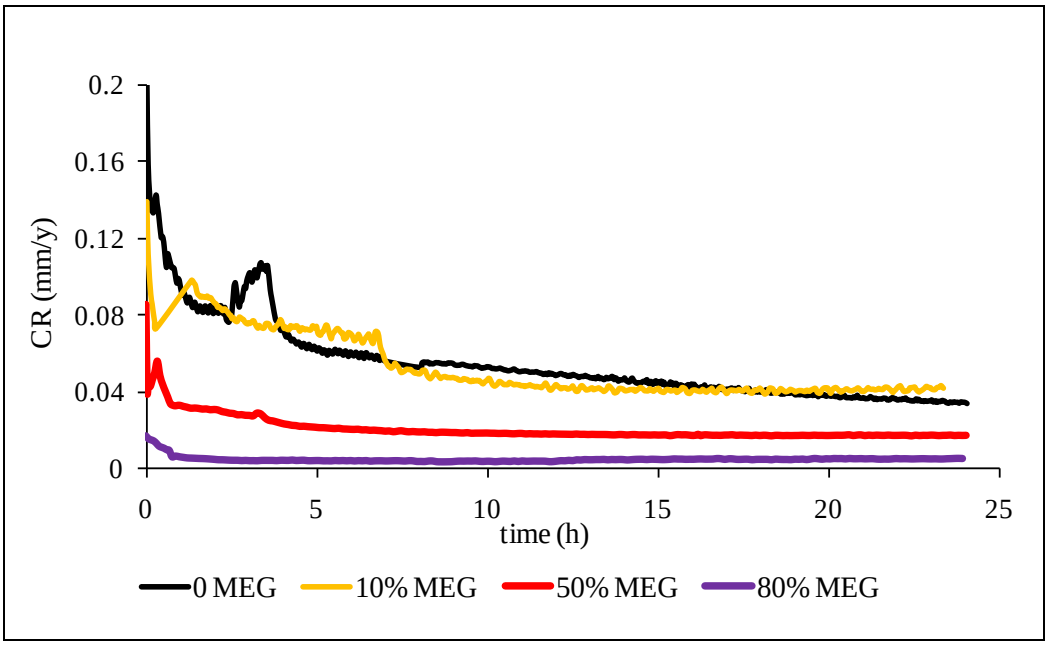

Figure 3.8: Corrosion rates of carbon steel in N_2 saturated 3% NaCl solution containing various concentrations of MEG after 24 hours immersion at 24°C.

Table 3.8: Corrosion rate values of N_2 saturated solutions with various MEG concentrations after 24 hours immersion measured by LPR at 24°C.

C_{MEG} (vol%)	0	10	50	80
CR (mm/y)	0.035±0.030	0.040±0.051	0.017±0.015	0.005±0.006

Polarization scans are conducted after 24 hours exposure of the sample to the corrosive media and the results are shown in Figure 3.8 and Table 3.9. It can be seen that with increasing MEG concentrations the potentials shift to more positive values. The anodic current density is inhibited with increasing MEG concentration in a comparable manner as is shown for a CO_2 saturated system (Figure 3.3), except for the 10% MEG solution were the anodic current increased at higher potentials. The cathodic part of the corrosion reaction is different from that in the CO_2 saturated solution (Figure 3.3). In the CO_2 environment, the addition of MEG increases the viscosity of the solution and lowers diffusivity of CO_2. This results in decrease of

the cathodic current densities in the potentiodynamic measurements. In the N_2 environment (absence of CO_2), the effect of MEG on the cathodic reaction is less pronounced due to the absence of CO_2. In this case, the reduction of water remains the dominant cathodic reaction, unaffected by the presence of MEG.

The reduction of the anodic polarization current in the presence of MEG in the N_2 saturated solution and decrease in the corrosion rate is an indication of spontaneous adsorption of MEG and the formation of a protective film on the metal surface. The same effect is shown in the CO_2 environment (Figure 3.3).

The positive shift in corrosion potential coupled with a large decrease in anodic current densities indicates that the main effect of MEG is on the anodic reaction.

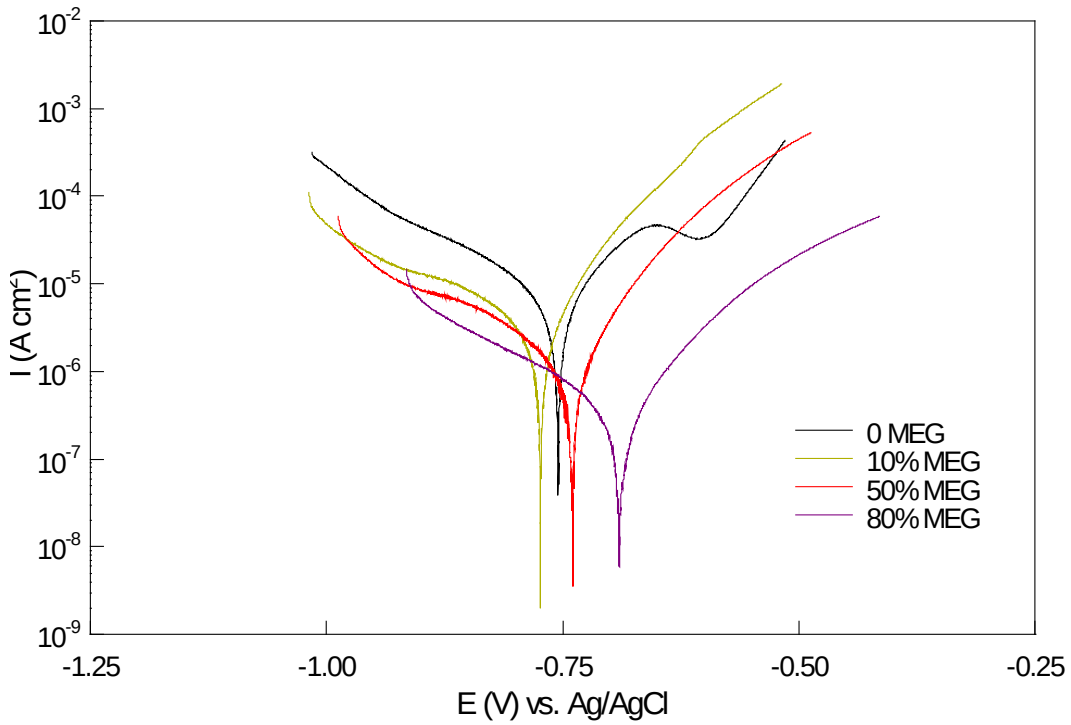

Figure 3.9: Representative potentiodynamic polarization plots of carbon steel in N_2 saturated 3% NaCl solution containing various concentrations of MEG after 24 hours immersion at 24°C.

Table 3.9: Electrochemical parameters of carbon steel in N_2 saturated 3% NaCl solutions containing various concentrations of MEG at 24°C.

C_{MEG} (vol%)	E_{corr} (mV)	i_{corr} (µA /cm^2)	b_a (mV)	$-b_c$ (mV)	R_p (Ωcm²)	CR (mm/y)
0	-762	7.8	130	177	417	0.089±0.78
10	-770	3.0	85	230	740	0.040±0.30
50	-740	1.65	85	213	1571	0.018±0.002
80	-691	0.4	100	180	6975	0.004±0.006

These observations are further supported by the measured pH and conductivity of the MEG solutions saturated in CO_2 and N_2 systems. After saturation with nitrogen, the pH value is 8.25 in absence of MEG which decrease to 7.21 in 80% MEG solution (Table 3.10a). On the other hand, the pH of the solution in the absence of MEG drops to 3.95 after saturation with CO_2 and does not change significantly with increasing MEG concentrations (Table 3.10b). This can be explained by keeping in mind that MEG is a weak acid and causes a decrease in the pH of the N_2 saturated solutions with increasing amounts of MEG, while in CO_2 saturated solutions the pH of the solution is determined by the partial pressure of CO_2.

Table 3.10: The values of conductivity and pH of the solutions in the absence and presence of various concentrations of MEG at 24°C. (a) N_2 saturated and (b) CO_2 saturated solutions.

(a)

C_{MEG}	0	10	50	80
Conductivity (mS/cm)	46.5	33.9	7.1	1.1
pH	8.25	8.11	7.86	7.21

(b)

C_{MEG}	0	10	50	80
Conductivity (mS/cm)	53	33.9	7.1	1.1
pH	3.95	3.98	4.06	4.06

In the case of the measured conductivity in different MEG solutions, it is expected to have a higher conductivity in a CO_2 saturated system in the presence of MEG, as the pH is lower in this system (higher ionic strength) compared to a N_2 saturated system. The results (Table 3.10a and b) indicate that at the same concentration of MEG, the conductivity of the solution is the same in both N_2 and CO_2 systems, while it is lower in the N_2 system for the blank solution. However, one would expect different conductivity values to be measured in CO_2 and N_2 saturated solutions. The same values measured for each MEG concentration in these two systems indicate that MEG adsorbs on to the platinum electrode of the conductivity probe and forms a surface film. This is in agreement with the results presented earlier in this chapter

(Figures 3.3 and 3.9) showing that the anodic reaction in both CO_2 and N_2 saturated solutions is inhibited in the presence of MEG.

3.4 Surface Morphology Observation

Scanning electron microscopy analysis (SEM) is performed to determine the extent of the corrosion in the absence and presence of MEG at different concentrations at 60°C. Energy-dispersive X-ray spectroscopy (EDS) is also carried out to qualitatively determine the elemental composition of the corrosion film on the surface. Figure 3.10 presents the SEM images from the test coupons after 24 hours of immersion in 0 to 50% MEG solutions at 60°C. The morphology of specimen surface exposed in the solution without MEG (Figure 3.10a) reveals that a general type of corrosion proceeded at the surface which confirms the corrosion rates obtained from polarization scans (Table 3.4). The surface is uniformly corroded.

However, in the presence of MEG the corrosion effect is less pronounced with less corroded areas observed in 10% MEG solutions. With further increasing MEG concentrations (Figure 3.10c and 3.10d), the surfaces become visually less corroded compared to that without any MEG. These observations correlate well with the electrochemical results presented in this chapter, where the increasing MEG concentration is shown to results in lower corrosion rates (Table 3.5 and Table 3.6).

The EDS analysis was qualitative and no elemental mass percentage was determined. The EDS spectra show the same results in absence and presence of MEG. The representative EDS spectrum from corroded steel surfaces is shown in Figure 3.11. In all conditions (with and without MEG) tested the EDS spectra revealed iron (Fe), oxygen (O) and carbon (C).

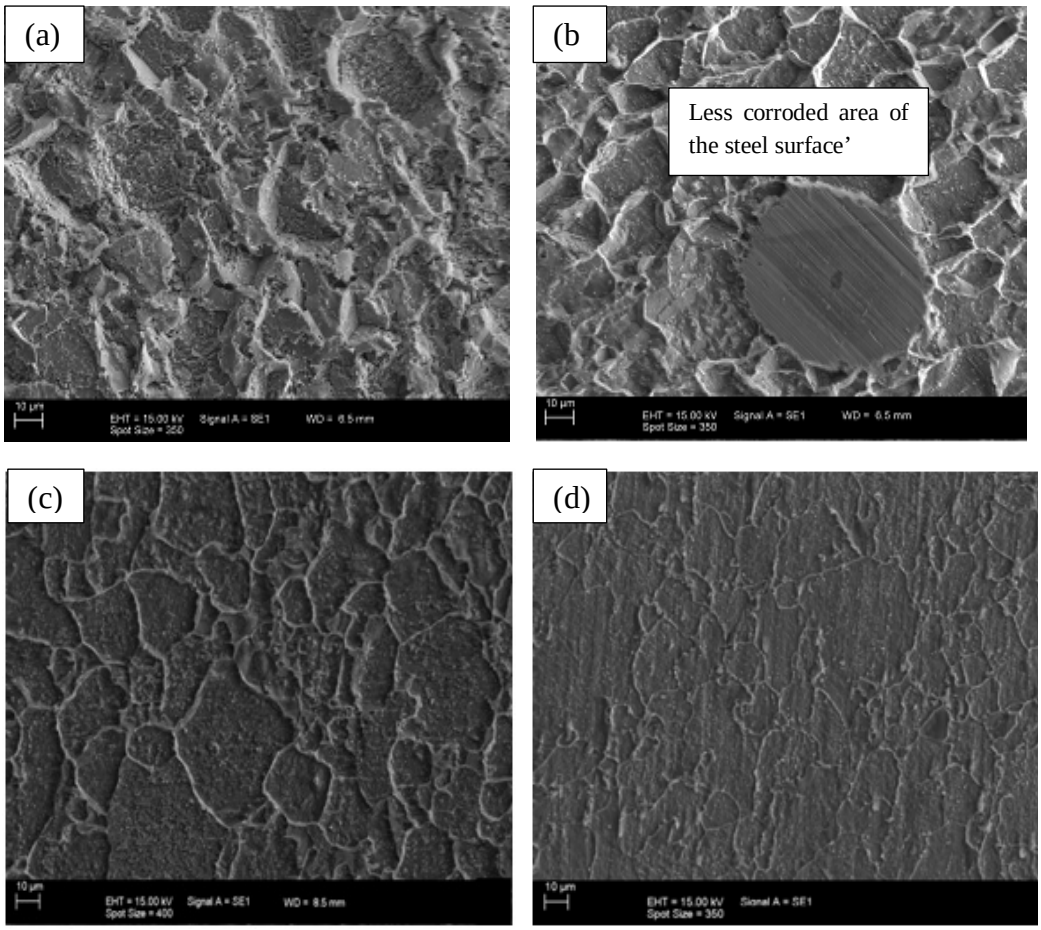

Figure 3.10: Representative SEM images of carbon steels after 24 hours immersion at 60°C (a) No MEG, (b) 10% MEG, (c) 33% MEG, (d) 50% MEG at 60°C, CO_2 saturated 3% NaCl solutions, stagnant conditions.

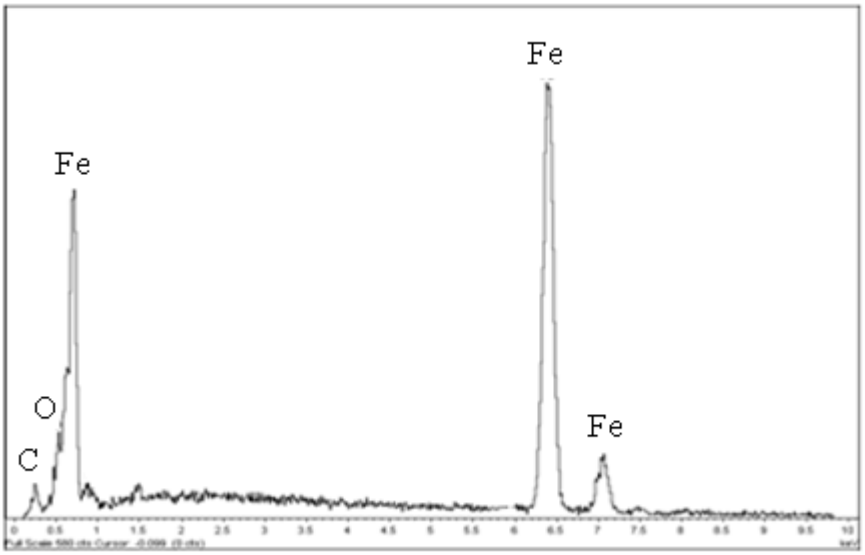

Figure 3.11: Representative EDS spectra of carbon steels after 24 hours immersion in absence and presence of 50% MEG at 60°C, CO_2 saturated 3% NaCl solutions, stagnant conditions.

3.5 Concluding Remarks

The comparisons of corrosion rates measured by LPR and potentiodynamic polarization at 24°C and 60°C in CO_2 are shown in Figure 3.12 and Figure 3.13. The corrosion rates estimated from these two techniques are in good agreement and confirm the general trend in the corrosion rates described in Sections 3.1 and 3.2.

Based on the results found, the corrosion rate of carbon steel in aqueous MEG solution depends on the concentration of MEG. An inverse exponential relationship between the MEG concentration and the resulting corrosion rates is established for both temperatures tested. The correlation coefficient (r^2) is 0.897 at 24°C and 0.981 at 60°C. This may suggest that the corrosion process in the presence of MEG is diffusion controlled and MEG molecules act as a barrier between the metal surface and corrosive species. The extent to which MEG can protect a steel surface at a given concentration is temperature dependent. EIS results indicate that the resistance and the thickness of the surface film on the metal surface increases with the amount of MEG in the solution. The corrosion rates at different concentrations of MEG measured by different techniques are in good agreement and SEM analysis further supports the above results.

It was also shown that MEG has a strong inhibition effect on both anodic and cathodic current densities of CO_2 corrosion at the conditions tested. The decrease in the cathodic current is found to be related to the decrease in solubility and diffusivity of CO_2 in the presence of MEG. This is evidenced by the evaluation of the effect of MEG in N_2 saturated solutions, which demonstrates that the cathodic reactions are not influenced by changing concentrations of MEG in such solutions.

The anodic reactions are effectively inhibited in both CO_2 and N_2 saturated systems by MEG, indicating that MEG may form a protective film on the metal surface which reduces the rate of the anodic dissolution of iron on the metal surface.

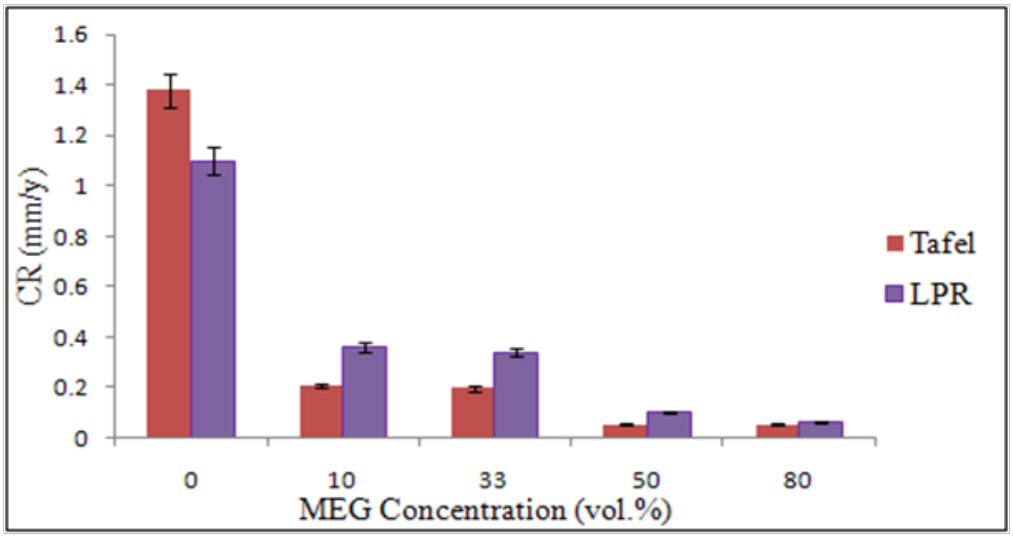

Figure 3.12: Corrosion rate vs. MEG concentration after 24 hours immersion at 24°C. Correlation between LPR measurements (Figure 3.1) and Tafel analysis of potentiodynamic curves (Figure 3.3).

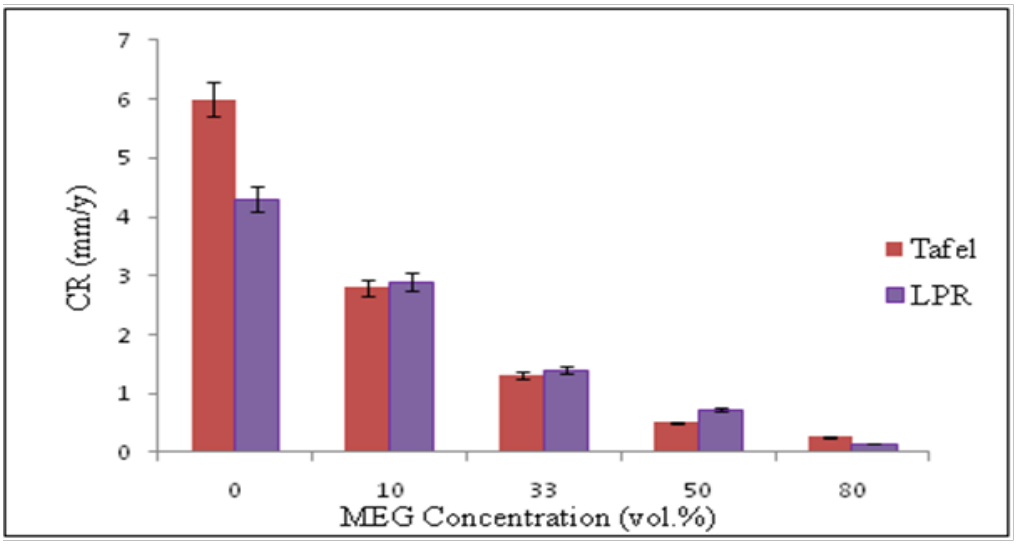

Figure 3.13: Corrosion rate vs. MEG concentration after 24 hour immersion at 60°C. Correlation between LPR measurements (Figure 3.2) and Tafel analysis of potentiodynamic curves (Figure 3.4).

CHAPTER 4. Synergic Effect of Acetic Acid and MEG on CO_2 Corrosion

It has been shown in Chapter 3 that MEG inhibits the CO_2 corrosion of carbon steel by influencing both the anodic and cathodic reactions. In this chapter, the efficiency of MEG to inhibit CO_2 corrosion is studied in a series of experiments with fixed concentrations of MEG or HAc. This approach allows for the determination of the role of each of these components in the corrosion process.

In the first part, the inhibition effect of MEG on the CO_2 corrosion of carbon steel in presence of HAc in the range of 0 to 5000 ppmv will be discussed (Section 4.1). In the second part (Section 4.2), the inhibition efficiency of MEG in the range of 0 to 80% in the presence of HAc will be determined. The temperature is 60°C in all experiments, CO_2 partial pressure is 1 bar. The last section in this chapter (Section 4.3) summarises and links the results.

4.1 The Effect of Variable Acetic Acid Concentration on CO_2 Corrosion in the Presence of MEG

The effect of HAc on the corrosion rate of carbon steel in CO_2 saturated brine in the absence and presence of MEG at 60°C is evaluated by LPR. LPR measurements are conducted over a period of 24 hours. HAc concentration varies between 0 and 5000 ppmv with 50% MEG concentration. No buffer is used in the HAc containing solutions. The experimental set-up is described in Chapter 2.

4.1.1 Evaluation of the Corrosion Rate

Figure 4.1a shows the results of the LPR measurements carried out over the period of 24 hours in 0 to 500 ppmv HAc solutions without MEG and Table 4.1a summarises the corrosion rates measured after 24 hours of immersion. The general trend of increasing corrosion rates with increasing HAc concentrations is observed. The corrosion rate stabilised around 4.3 mm/y after 24 hours of immersion for the blank solution (without HAc), which increases to 8.2 mm/y with the addition of 100

ppmv HAc. However, the corrosion rate does not change considerably by increasing the HAc concentration from 500 to 1000 ppmv. Increasing the HAc concentration to 5000 ppmv accelerated the corrosion rate to 20 mm/y after 24 hours. Increasing the corrosion rate with increasing HAc concentration has been reported by many authors.[8,34,90] A linear increase in corrosion current density with acetic acid concentration above 60 ppmv is reported by Garsany et al.[91] It is also accepted that the resultant corrosion failures for corrosion of steel in the presence of HAc (with a concentration higher than 60 ppmv) is due to the localized corrosion attack,[43,92] which will be discussed in detail in Section 4.1.3.

Figure 4.1b shows the changes of the corrosion rates with time from the LPR tests carried out in the presence of 50% MEG and Table 4.1b summarises the corrosion rate measurements after 24 hours of immersion. It is apparent that in 50% MEG media, similar observations are made compared to those from the experiments made in the absence of MEG (Figure 4.1a). It can be noticed that with increasing HAc concentration the corrosion rate increases.

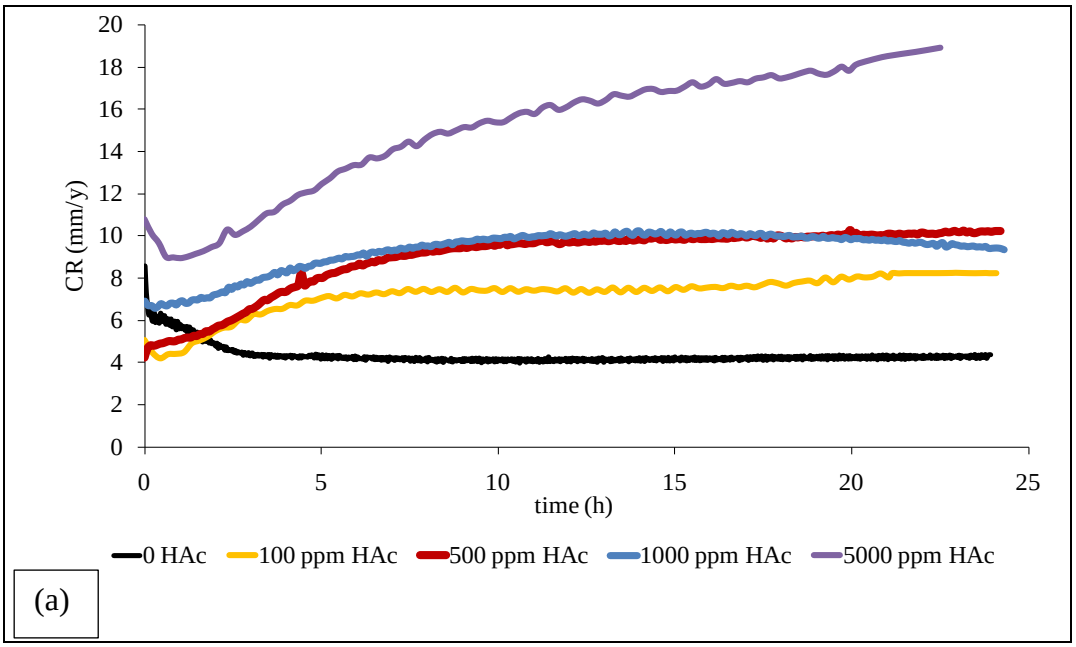

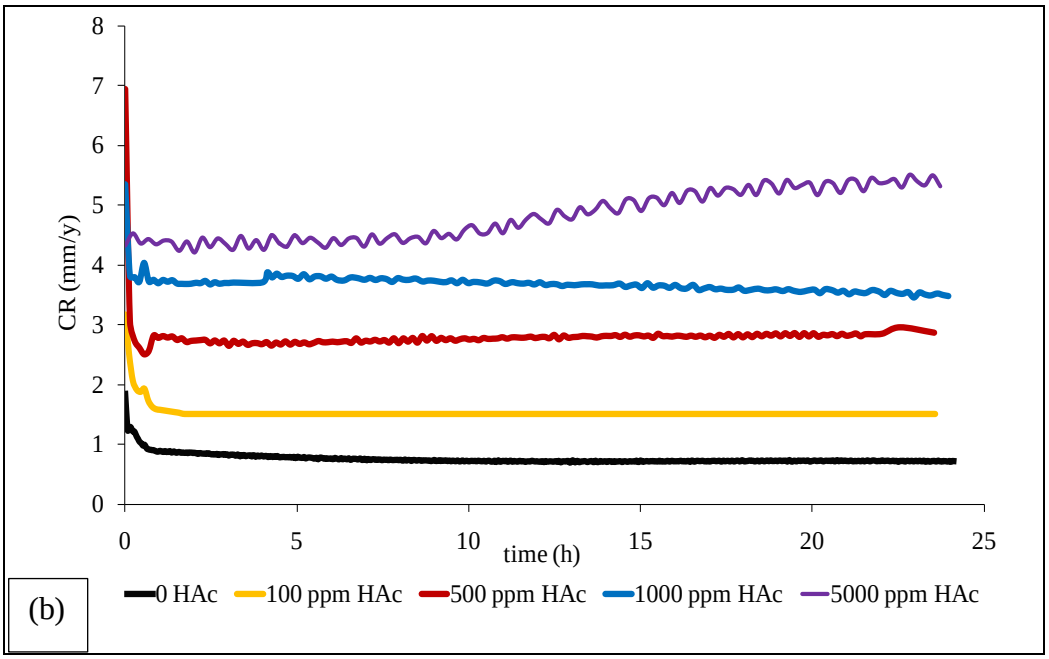

Figure 4.1: Corrosion rates of carbon steel in CO_2 saturated 3% NaCl solution containing various concentrations of HAc (a) in the absence and (b) in the presence of 50% MEG at 60°C for 24 hours immersion.

Table 4.1: Corrosion rate values at various concentrations of HAc after 24 hours at 60°C (a) in the absence and (b) in the presence of 50% MEG. Data from LPR measurements shown in Figure 4.1.

(a)

C_{HAc} (ppmv)	0	100	500	1000	5000
CR (mm/y)	4.37±0.26	8.20±0.95	10.0±0.15	9.50±0.21	20.0±0.75

(b)

C_{HAc} (ppmv)	0	100	500	1000	5000
CR (mm/y)	0.73±0.09	1.50±0.35	2.85±0.43	3.50±0.60	5.50±0.42

A comparison of Figure 4.1a and Figure 4.1b shows that the corrosion rates measured in HAc media decreased upon addition of MEG. The change in the pH values of the acidic solutions in the absence and the presence of MEG is shown in Table 4.2. It can be seen that when 50% MEG is presented in the unbuffered acetic acid systems with the concentration of 0 to 5000 ppm of HAc, the pH of the acid solutions increases slightly (refer to Table 4.2). However, the final pH values of the acidic solutions decreases in the presence of MEG compare to the final pH in the absence of MEG, which is an indication of the lower corrosion rates in acid solutions in the presence of MEG. Therefore, the corrosion rate reduced significantly at each concentration of HAc compared to the solutions without MEG (Table 4.1a

and b) and this reduction cannot be attributed to the pH effect. The general corrosion rate is 1.5 mm/y with 100 ppmv HAc and 5.5 mm/y in the presence of 5000 ppmv HAc. It is clear from the LPR measurement that MEG mitigates to a large extent the enhanced general corrosion rates caused by HAc.

Table 4.2: pH of the CO_2 saturated solutions before and after the tests at 60°C.

	0% MEG					50% MEG				
C_{HAc} (ppmv)	0	100	500	1000	5000	0	100	500	1000	5000
Initial pH	3.86	3.70	3.25	3.09	2.65	4.34	3.96	3.61	3.47	3.10
Final pH	4.10	5.10	4.20	3.80	3.50	5.01	4.62	4.03	3.86	3.41

4.1.2 Consideration of the Possible CO_2 Corrosion Mechanism

In order to determine the inhibition effect of MEG on the anodic and cathodic reactions of the corrosion process in the brine solution with different concentrations of HAc, potentiodynamic polarization measurements are performed after 24 hours immersion.

Figure 4.2 shows the polarization curves obtained in solutions of variable concentrations of HAc in the absence of MEG. The addition of HAc to the brine solution leads to a positive shift in the corrosion potential (E_{corr}) and enhancement of the corrosion current densities (i_{corr}). The most prominent effect of HAc occurs at potentials negative to the corrosion potential where the cathodic current density increases substantially with the addition of HAc in all concentrations. The anodic current densities do not follow a linear trend with increasing concentration of HAc and are relatively similar for all experiments with the HAc, especially in the higher potential range. The corrosion parameters derived from the polarization data shown in Figure 4.2 are presented in Table 4.3. The anodic Tafel slopes are found to increase with the addition of 100 ppmv HAc, but remain nearly constant in the concentration range of 100–1000 ppmv HAc and increase again after addition of 5000 ppmv of HAc. While, the cathodic Tafel slopes show the opposite, a decreasing trend with increasing HAc concentrations. The observed increasing anodic Tafel slope in the presence of HAc is an indication of the active dissolution of the steel surface compared with the surface exposed to the blank solution (without

HAc). There is a linear correlation between the corrosion rate of steel and increasing HAc concentration with the exception of 0 ppmv HAc. The correlation coefficient value determined from the linear least squares analysis is 0.996 indicating that the corrosion rate of the steel continues to increase at a constant linear rate with increasing acid concentration.

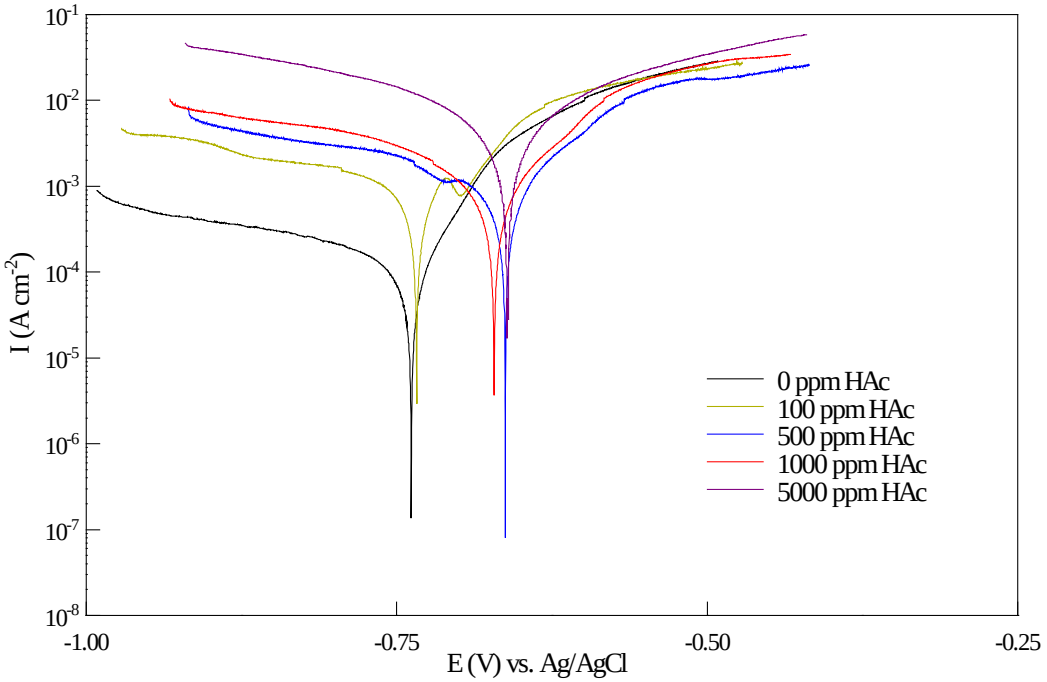

Figure 4.2: Representative potentiodynamic polarization plots of carbon steel in CO_2 saturated 3% NaCl solution containing various concentrations of HAc in the absence MEG after 24 hours immersion at 60°C.

Table 4.3: Corrosion parameters obtained from potentiodynamic polarization plots in 3% NaCl containing various concentrations of HAc in the absence of MEG at 60°C.

C_{HAc} (ppmv)	E_{corr} (mV)	i_{corr} (μA/cm²)	ba (mV/dec)	-bc (mV/dec)	R_p (Ω.cm²)	CR (mm/y)
0	-726	250	85	350	11.8	2.87±0.30
100	-735	900	130	345	4.5	10.3±0.09
500	-665	1000	120	325	3.6	11.4±0.76
1000	-668	1100	120	325	3.5	12.5±0.52
5000	-665	2500	160	255	2.1	28.6±0.85

When HAc is present in the system, it is the predominant source of acidity compared with carbonic acid.[42] Carbonic acid (pK_a = 6.35) is a much weaker acid compared to acetic acid (pK_a = 4.76)[36] and the conversion of carbon dioxide to carbonic acid is slow, so the contribution of carbonic acid reduction to the partial cathodic current density at the corrosion potential will be much lower compared with the contribution from the acetic acid reduction. Therefore, it could be suggested that the enhanced cathodic reaction in the presence of HAc is mainly caused by the direct reduction of undissociated HAc, which is supported by previous studies.[43]

The increase of the cathodic current density indicates that the overall corrosion attack increases with the introduction of HAc to the media. The increase in cathodic current density in presence of acetic acid has been previously reported[43,28] and has been related to direct reduction of adsorbed HAc on the metal surface.[43] The cathodic reductions in HAc solution have been shown by Guo et al.[93] are:

$$HAc_{aq} \leftrightarrow HAc_{ad} \quad (4.1)$$

$$HAc_{ad} + e \leftrightarrow Ac^{-} + \frac{1}{2} H_2 \quad (4.2)$$

Produced acetate (Ac^-) from the cathodic reaction is shown to suppress the anodic reaction by passivation of the corroding carbon steel.[30,38,78] Based on the above discussion, the presence of the adsorbed species at the steel surface and their effect on the corrosion reactions can explain the results observed in this work (Figure 4.2).

Potentiodynamic polarization experiments with variable concentrations of HAc are performed in the presence of MEG to evaluate the effect of MEG on the corrosion reactions in the presence of HAc. Figure 4.3 shows the polarization curves recorded at various concentrations of HAc in the presence of 50% MEG at 60°C after 24 hours immersion time. In the presence of HAc, in the MEG containing solution, the corrosion potential shifts in the positive direction and an increase of the corrosion current densities (i_{corr}) is observed. Also, the increasing amount of HAc in the MEG solution leads to cathodic reaction acceleration, whilst the anodic reactions of the corrosion process do not change with increasing amounts of HAc.

The corrosion parameters derived from the polarization data presented in Figure 4.3 are shown in Table 4.4. It can be seen that the corrosion current density increased

with the addition of 100 to 5000 ppm HAc to a 50% MEG solution from 80 μA/cm^2 to 520 μA/cm^2 indicating an enhanced corrosion attack of a MEG containing system with increasing HAc concentration. Even the relatively small amount of 100 ppm HAc more than doubles the corrosion rate.

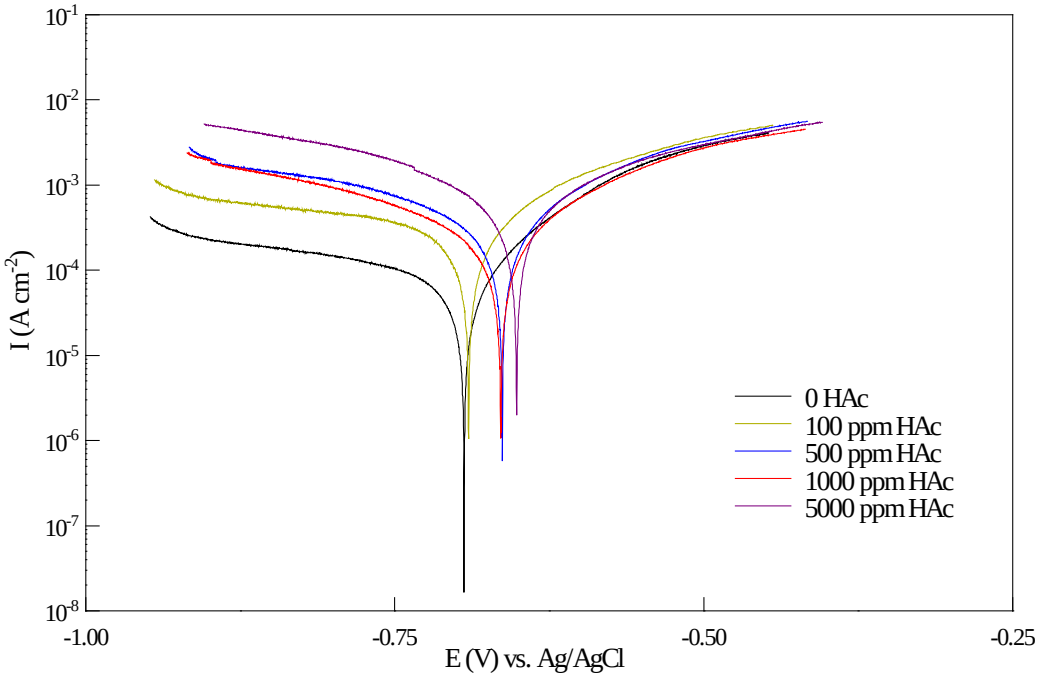

Figure 4.3: Representative potentiodynamic polarization plots of carbon steel in CO_2 saturated 3% NaCl solution containing various concentrations of HAc in the presence of 50% MEG after 24 hours immersion at 60°C.

Table 4.4: Corrosion parameters obtained from potentiodynamic polarization plots in 3% NaCl solution containing various concentrations of HAc in the presence of 50% MEG at 60°C.

C_{HAc} (ppmv)	E_{corr} (mV)	i_{corr} (μA/cm^2)	ba (mV/dec)	-bc (mV/dec)	R_p (Ω.cm^2)	CR (mm/y)
0	-690	38	118	60	45	0.43±0.43
100	-687	195	430	150	26	2.24±0.08
500	-660	260	315	170	18	2.99±0.54
1000	-661	390	250	180	12.3	4.48±0.20
5000	-610	520	195	203	8.3	5.98±0.61

It is shown in Chapter 3 that the presence of MEG reduces the CO_2 corrosion rates by reducing both anodic and cathodic current densities and the MEG acts as a mixed type inhibitor (refer to Figure 3.4). The results presented in this chapter clearly demonstrate that the addition of 50% MEG into HAc-containing CO_2 saturated

solutions also results in a decrease of corrosion rates (compared to HAc solutions without MEG), confirming the inhibition effect of MEG on carbon steel corrosion even in the presence of acetic acid.

The potentiodynamic results also suggest that the addition of MEG to the solutions with HAc affects both the anodic and cathodic reactions in a similar way at all HAc concentrations studied. To provide a better demonstration of the effect of MEG on the corrosion reactions in the acetic acid solutions, the potentiodynamic polarization curves recorded in the absence of MEG (Figure 4.2) and the presence of MEG (Figure 4.3) are compared at each individual HAc concentration in Figure 4.4. These results show that there is a similar trend among various HAc concentrations where the presence of MEG in HAc solutions results in a decrease in both the anodic and cathodic current densities in all HAc concentrations. This is a similar result to that obtained from potentiodynamic measurements in the presence and absence of MEG, where both reactions are suppressed upon addition of MEG to the test solution (see Chapter 3, Figure 3.4). Therefore, it can be concluded that the MEG acts as a mixed-type (anodic and cathodic type) inhibitor in the presence of HAc.

The concentration effect of HAc is apparent from the differences in the values of the cathodic and anodic current densities between the systems with and without MEG. The differences in current densities increase with increasing HAc concentrations from 500 to 5000 ppm. The positive shift of the corrosion potential obtained for the 100 ppm HAc may be due to the more pronounced effect of MEG on the anodic reaction in this system.

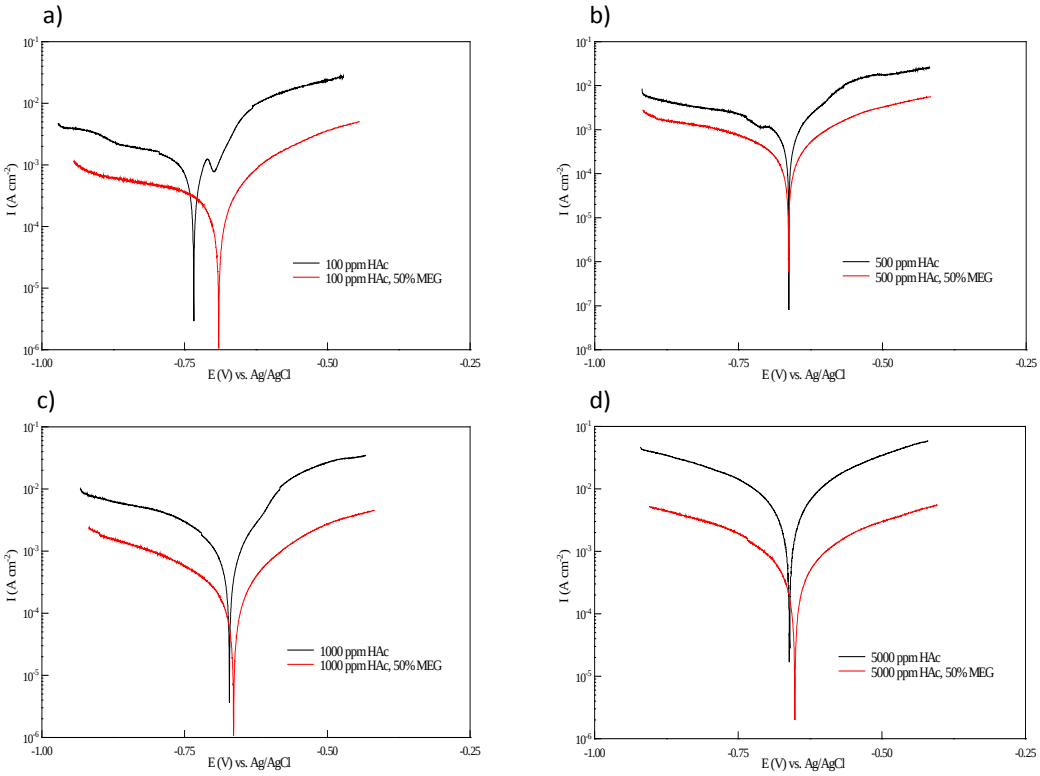

Figure 4.4: Representative comparison of the potentiodynamic polarization plots recorded in the absence of MEG (Figure 4.2) and the presence of MEG (Figure 4.3) at each individual HAc concentration at 60°C.

MEG clearly inhibits the accelerated cathodic reaction in the presence of acetic acid. In the presence of acetic acid (at pH 4 and below), the direct reduction of H^+ ions ($2H^+ + 2e^- \leftrightarrow H_2$) is important, particularly at lower partial pressure of CO_2,[47] to proceed with the corrosion process. Therefore, hindering this reduction process greatly inhibits the rate of the corrosion reaction. The depressed cathodic currents in the presence of MEG can be explained by the solution chemistry. With the addition of 50% MEG, pH increases of approximately 0.26–0.45 pH units depending on the MEG concentration (refer to Table 4.2). This rise in pH causes a drop in the hydrogen ion reduction reaction rate. Gulbrandsen and Bilkova[94] test the corrosion effect of different concentrations of NaCl in 200 ppm HAc solution. It is shown[94] from mass transfer calculations that a change from pH 3.7 to 3.5 causes a rise in the diffusion limited H^+ reduction current which in turn increase the corrosion rate by more than 10 mm/y.

Furthermore, the anodic current density on the metal surface in acetic acid media decreases strongly with the addition of MEG. The corrosion current density reduced

to lower values when introducing MEG and the decrease of the corrosion current density is directly related to the decrease of the corrosion rate. The decrease in the corrosion rate demonstrates the ability of MEG to partially inhibit the acetic acid corrosion in the CO_2 environment. The polarization curves indicate that the corrosion process in the presence of acetic acid and MEG is under both anodic and cathodic control. These results are consistent with the result published by Gulbransen and Morard.[16] The reduction in cathodic current densities in the presence of MEG in CO_2 systems (without HAc) is explained by accounting for the decrease in CO_2 solubility and decrease in H_2CO_3 diffusivity due to increasing solution viscosity.

A clearer insight into the influence of MEG on the corrosion processes in media containing acetic acid can be extracted from the electrochemical impedance spectroscopy (EIS). Figure 4.5 represents the Nyquist plot of the impedance response of mild steel in aqueous brine containing CO_2 with 0–1000 ppm HAc in the absence and the presence of MEG at 60°C, corresponding to the impedance parameters listed in Table 4.5. The equivalent circuit model shown in Figure 2.6 provides the best fit for the data and is therefore used to determine the impedance data. In general, there is only one capacitive loop at all frequencies in the absence and the presence of MEG. The addition of 500 ppm HAc to the brine solution does not change considerably the magnitude and diameter of the impedance. However, the addition of 1000 ppm HAc to the brine solution (in the absence of MEG) reduced the magnitude and diameter of the impedance. This indicates that at high enough concentrations, HAc accelerates the corrosion reactions by increasing the charge transfer rate of corrosive species. As mentioned in Chapter 2.1.3 the capacitance is an indication of the adsorption of organic molecules on the metal surface.[26] The decrease in the interface capacitance upon addition of HAc to the brine solution, confirms the change at the metal/solution interface due to adsorption of HAc on the metal surface (Equation 4.1). The adsorption of HAc on the surface is followed by a direct reduction of HAc on the surface (Equation 4.2), which enhances the cathodic current density and corrosion process. With increasing HAc concentrations more HAc reduces on the surface and further increases the cathodic current. This result confirms the polarization results presented in Figure 4.2, where increasing HAc concentrations resulted in an increase of the cathodic current density and thus an increase in the corrosion rate.

In the presence of MEG the magnitude and diameter of the impedance loop increases significantly. This indicates the inhibition effect of MEG by reducing the accelerated corrosion in the presence of HAc. From Table 4.5, it can be seen that both solution resistance and charge transfer resistance increases when 50% MEG is present in the acidic solution. EIS results confirm that the accelerated corrosion rate of carbon steel in various concentrations of HAc containing solutions decreases significantly with the addition of MEG.

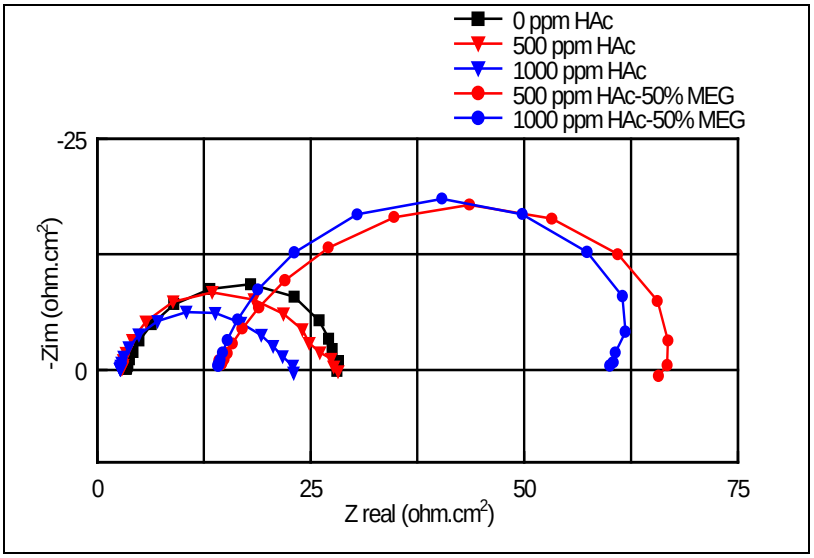

Figure 4.5: Representative Nyquist plots for carbon steel in CO_2 saturated 3% NaCl solution containing 0 and 1000 ppm HAc in the absence and presence of 50% MEG after 24 hours immersion at 60°C.

Table 4.5: Comparative analysis of equivalent circuit parameters obtained from 0 and 1000 ppm HAc in the absence and presence of MEG after 24 hours of immersion at 60°C.

C_{MEG} (vol%)	C_{HAc} (ppmv)	R_s ($\Omega.cm^2$)	R_{ct} ($\Omega.cm^2$)	C (F/cm^2)	i_{corr} ($\mu A/cm^2$)	CR (mm/y)
0	0	3.0	25.5	0.85	480	5.57±0.34
0	500	2.6	24	0.80	790	9.5±1.01
0	1000	2.6	19.5	0.80	970	11.3±0.08
50	500	14	55	0.71	321	3.7±0.42
50	1000	14	49	0.80	371	4.4±0.35

4.1.3 Surface Morphology Observation

Figure 4.6 shows the SEM images of the carbon steel surfaces treated in CO_2 saturated 3% NaCl solution with 1000 ppm HAc in the absence and the presence of 50% MEG at 60°C. It can be seen that the structure of the surfaces corroded in the absence and the presence of MEG are completely different. Localized corrosion (pitting) is found on the steel surface in HAc solution without MEG (Figure 4.6a and b) whilst in the presence of 50% MEG the corrosion was uniform (Figure 4.6c and d).

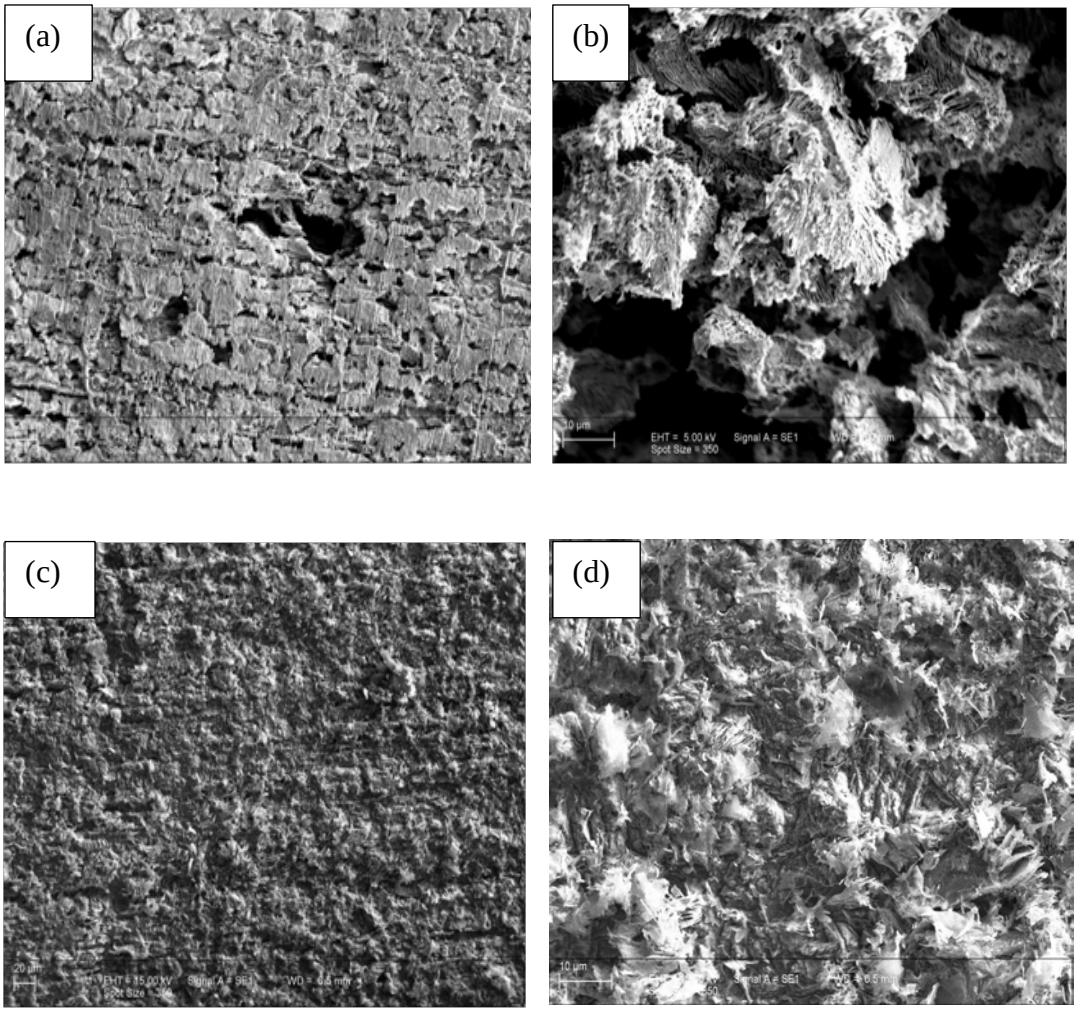

Figure 4.6: SEM images of carbon steels after 24 hours immersion in the acidic solutions at 60°C. (a) and (b) 1000 ppm HAc without MEG, (c) and (d) 1000 ppmv HAc, in the presence of 50% MEG (a and c 200X, b and d 800X).

EDS spectra of carbon steels in HAc media in the absence and the presence of MEG are shown in Figure 4.7a and b. It is observed that in acidic media and the absence of MEG the elements presented on the surface are iron (Fe) and carbon (C), whilst in the presence of MEG the elements are iron (Fe) and carbon (C) with small amounts of oxygen (O) hidden by the Fe peak, indicating the formation of a protective film at the surface.

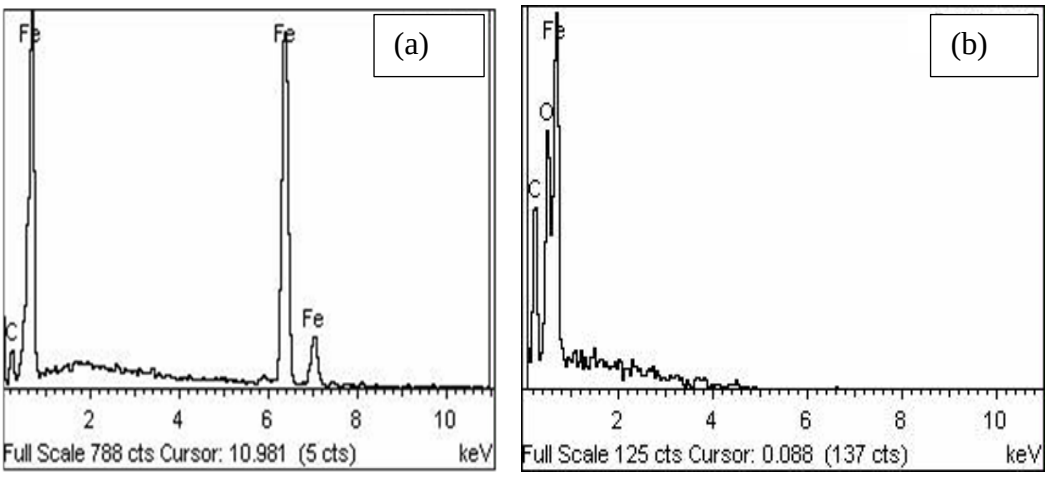

Figure 4.7: EDS spectra of carbon steels after 24 hours immersion in the acidic solutions at 60°C. (a) 1000 ppm HAc, without MEG (b) 1000 ppmv HAc, in the presence of 50% MEG.

The SEM and EDS results indicate that the presence of HAc in the brine solution causes an increase in the dissolution of iron. HAc is a weak acid which means it not only increases the cathodic reaction, but also acidifies the solution by reducing the pH. Therefore, in the presence of undissociated HAc, the carbonate species content (HCO_3^- and CO_3^{2-}) reduces in a constant pH and CO_2 partial pressure.[43,95] From the EDS spectra it is clear that acetic acid prevents the formation of an iron carbonate layer on the steel surface.

However, in the presence of MEG, although a rough surface is visible, the surface is less corroded and more compacted than in the absence of MEG. The presence of oxygen in the EDS spectra can be an indication of the formation of a protective film in the presence of MEG on the steel surface which inhibits the enhanced corrosion in the presence of HAc. The formation of iron carbonate is not observed from the SEM images. It should be noted that the oxygen level in the test solutions was kept below 20 ppb.

4.1.4 Summary of Section 4.1

It has been demonstrated that MEG acts as a corrosion inhibitor, even in the presence of HAc. A comparison of the corrosion rate of mild steel determined by Tafel extrapolation and LPR measurements at different concentration of HAc in absence and presence of MEG is presented in Figure 4.8. It can be seen that corrosion rates measured by these two techniques are relatively in agreement, both in the absence and the presence of MEG. The corrosion rates in HAc solutions in the absence and the presence of MEG do not follow the same trend in the conditions tested. With increasing HAc concentrations (in the absence of MEG) the corrosion rate follows an increasing exponential trend whereas in the solutions containing 50% MEG, the corrosion rate follows a linear trend with increasing HAc concentrations.

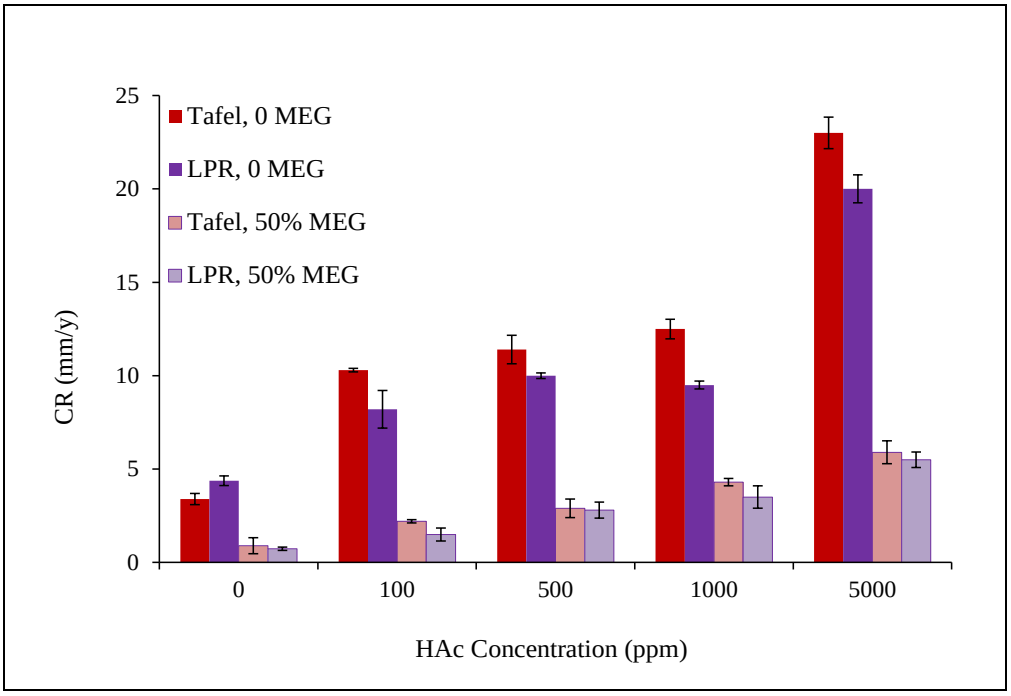

Figure 4.8: Corrosion rate vs. HAc concentration, correlation between LPR measurements and Tafel analysis of potentiodynamic curves in various concentration of HAc in the absence and presence of MEG at 60°C.

4.2 Effect of MEG Concentration on CO_2 Corrosion in the Presence of Acetic Acid

It is shown in Section 4.1 that MEG inhibits acetic acid corrosion and the extent of inhibition depends on the acetic acid concentration. The addition of MEG is found to suppress both the anodic and cathodic reactions at all concentrations of HAc studied. The aim in this section is to further investigate the effect of the MEG concentration on the corrosion reactions in the presence of acetic acid. The concentration of 5000 ppm HAc is selected to ensure a well pronounced effect of HAc in the tests.

4.2.1 Evaluation of the Corrosion Rate

The corrosion behaviour of carbon steel during 24 hours of immersion is shown in Figure 4.9 and the final corrosion rate values are presented in Table 4.6. In the absence of MEG, HAc (5000 ppmv) results in a very high corrosion rate (19 mm/y) to the steel (see also Table 4.1a for the effect to HAc concentration on the CO_2 corrosion rates). The corrosion rate nearly doubles during the 24 hours of exposure. A corrosion rate of 22.31 mm/y is reported earlier for carbon steel in 5000 ppm HAc at 90°C.[30] In the presence of 10% MEG, although the corrosion rate is nearly the same as in the solution without MEG, the results show that the corrosion rate is stabilized after 7 hours of the immersion in the corrosive media and does not change considerably after that. In the presence of 33% MEG, the high rate of acetic acid corrosion decreases significantly, although there is still a slight increase in the corrosion rate with time and the stabilization is not fully achieved. As expected, the presence of 50% and 80% MEG decreases the corrosion rate further to 3.4 and 1.1 mm/y, respectively. Furthermore, the corrosion rate is stabilized immediately after immersion.

The results indicate that reduction of acetic acid corrosion in the presence of MEG depends on both acetic acid (refer to Section 4.1) and MEG concentrations. Further analysis of data shows that there is an exponential trend between the MEG concentrations and related corrosion rates in the presence of HAc with a regression

coefficient (r^2) value of 0.995. This shows that each concentration of MEG gives a certain level of protection to the steel surface in the presence of HAc.

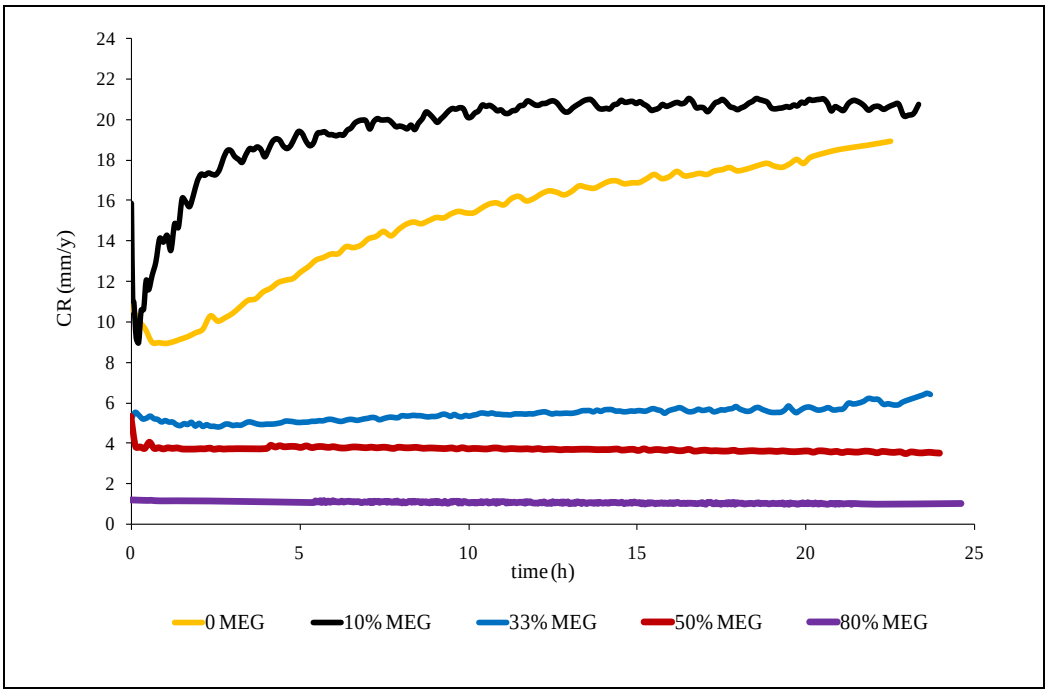

Figure 4.9: Corrosion rates of carbon steel in CO_2 saturated 3% NaCl solution containing various concentrations of MEG in the presence of 5000 ppmv HAc at 60°C.

Table 4.6: Corrosion rate values of carbon steel in CO_2 saturated 3% NaCl solution at various concentrations of MEG in the presence of 5000 ppm HAc after 24 hours of immersion at 60°C.

C_{MEG} (vol%)	0	10	33	50	80
CR (mm/y)	20.0±0.75	19.8±0.09	6.4±0.07	5.50±0.42	1.1±0.04

4.2.2 Consideration of the Possible CO_2 Corrosion Mechanism

The concentration effect of MEG on the CO_2 corrosion in the presence of HAc is further studied with potentiodynamic polarization experiments. The concentration of 5000 ppmv HAc is added to the CO_2 saturated 0 to 80% MEG solutions. The results are shown in Figure 4.10 and the polarization parameters obtained from the polarization curves are presented in Table 4.7. The curves show that the corrosion

current density decreases with increasing MEG concentration and both anodic and cathodic currents reduce. The corrosion potential (E_{corr}) oscillates between -660 and -604 mV as shown in Table 4.7. The E_{corr} does not change considerably at lower MEG concentrations (10% and 33%) with respect to the E_{corr} of the blank solution. However, it shifts in a positive direction at higher MEG concentrations (50% and 80%). The polarization scans show that at lower concentrations (below 50%) MEG affects both anodic and cathodic reactions to the same extent, while at higher concentrations (higher than 50%) the main effect of MEG is inhibiting the anodic dissolution of iron. It also can be seen from Figure 4.10 that the high corrosion current density of uninhibited acidic solution gradually decreases with increasing MEG concentration and reaches $12x10^{-5}$ A/cm^2 in the acidic solution containing 80% MEG. Cathodic Tafel slopes of acidic solutions slightly decrease upon introducing MEG to the acidic solution, whilst the anodic Tafel slopes do not change significantly. In summary, the inhibition efficiency of MEG increases with increasing concentrations of MEG and, as a consequence, the corrosion rate decreases.

As discussed in Section 4.1.2, both acetic acid and MEG can physically adsorb to the metal surface and retard the anodic dissolution of iron. This is confirmed by a positive shift in E_{corr} at all concentrations of MEG, which may be due to the formation of an unstable passive film/adsorbed layer. From LPR results (Figure 4.9) it is shown that the formation of such a passive film is very quick. The decrease in both anodic and cathodic current densities with increasing MEG concentration leads to a considerable decrease in the corrosion rate. The low change in the Tafel slope values indicates that the main reactions involved in the corrosion process remains unchanged in the MEG system compared to MEG free solutions.

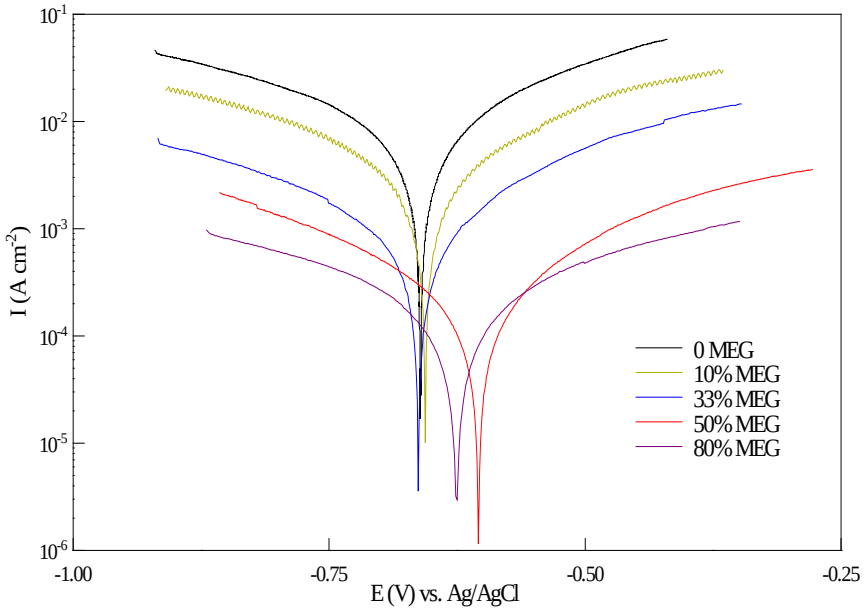

Figure 4.10: Representative potentiodynamic polarization plots of carbon steel in CO_2 saturated 3% NaCl containing various concentrations of MEG in the presence of 5000 ppmv HAc after 24 hours immersion at 60°C.

Table 4.7: Corrosion parameters obtained from potentiodynamic polarization plots in 3% NaCl solution containing various concentrations of MEG in the presence of 5000 ppmv HAc at 60°C.

C_{MEG} (vol%)	E_{corr} (mV)	i_{corr} (A/cm^2)	b_a (mV/dec)	$-b_c$ (mV/dec)	IE (%)	CR (mm/y)
0	-665	25 x10^{-4}	160	255	-	28.6±0.85
10	-650	23 x 10^{-4}	200	230	58	25±0.28
33	-655	65 x 10^{-5}	190	220	88	7.4±0.30
50	-610	52 x 10^{-5}	195	203	90	5.9±0.61
80	-620	12 x 10^{-5}	195	215	98	1.3±0.09

The concentration effect of MEG in the absence of HAc is discussed in Chapter 3. It is shown that both the cathodic and anodic current densities decrease with increasing MEG concentration (see Figure 3.4). The results in Figure 4.10 show that a similar trend is obtained from LPR data (Figure 4.9) in the presence of 5000 ppm HAc. It is also shown earlier in this chapter that the HAc has the predominant effect on the cathodic reaction in systems with and without MEG and does not significantly affect

the anodic reaction. This is best seen in Figure 4.2 (without MEG) and in Figure 4.3 (with MEG) showing a comparison of the potentiodynamic polarization curves recorded with 0 ppm HAc and 5000 ppm HAc.

In order to further demonstrate the concentration effect of MEG on the corrosion reactions in the presence of HAc (5000 ppm), the potentiodynamic polarization curves obtained in MEG-only solutions (without HAc, Figure 3.4) are compared with the measurements obtained from the same solutions with added 5000 ppm of HAc (Figure 4.10). The comparison is given in Figure 4.11. The results show that the addition of HAc to the solutions of variable concentration of MEG results in the increase of the cathodic current densities in all cases, whereas the anodic current density does not change. Figure 4.11 demonstrates that the increase in the cathodic current, caused by HAc, decreases with the amount of MEG in the solution from 10% to 80%. The shift in corrosion potential (E_{corr}) also depends on the MEG concentration. In 10% MEG solution, HAc has a greater increasing effect on the cathodic current. Conversely, in 80% MEG solution, HAc shows the lowest effect on the cathodic current density and corrosion potential positive shift. The lowest shift in corrosion potential in 80% MEG in the presence of acetic acid may indicate a more stable passive film formation in more concentrated MEG solutions.

Based on these results the inhibition efficiency of MEG in acidic solutions increases with increasing MEG concentration following an exponential trend with the regression coefficient of 0.978. Higher amount of MEG inhibits the sever corrosion attack caused by HAc more effectively, so that 80% MEG inhibits the corrosion rate in the presence of 5000 ppm HAc by 98%.

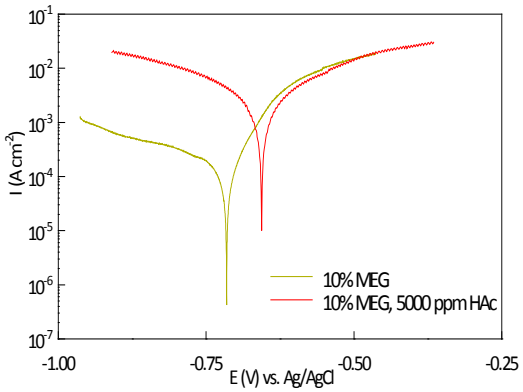

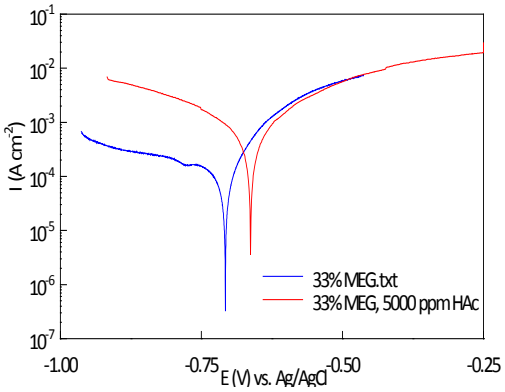

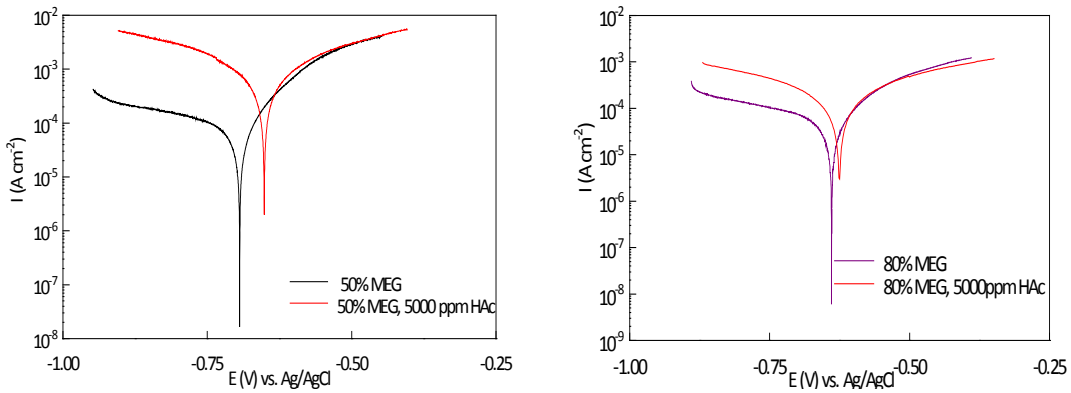

Figure 4.11: Comparison of the effect of 5000 ppmv HAc on the potentiodynamic polarization curves of various concentrations of MEG at 60°C.

Figure 4.12 shows a comparison of corrosion rates measured by LPR and Tafel analysis as a function of MEG concentration in the presence of 5000 ppmv MEG. The corrosion rates in the presence of MEG estimated from these two techniques are in good agreement and clearly show the exponential inhibition effect of each concentration of MEG on the acidic corrosion rate.

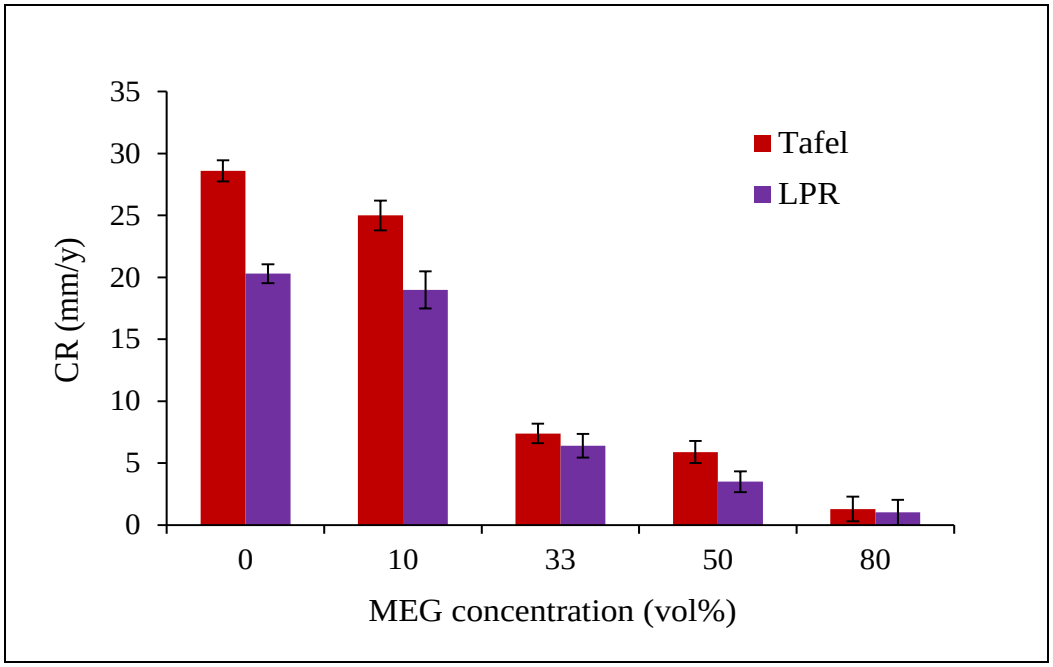

Figure 4.12: Corrosion rate vs. MEG concentration, correlation between LPR measurements and Tafel analysis of potentiodynamic curves in the presence of 5000 ppmv HAc at 60°C.

4.3 Concluding Remarks

In summary, the presence of MEG decreases the corrosion rate of carbon steel in CO_2 saturated brine solution in the presence of HAc. The polarization and impedance spectroscopy results confirm the effectiveness of MEG on the corrosion inhibition of carbon steel in the presence of acetic acid. The extent of inhibition depends on the concentrations of both the acetic acid and the MEG following a linear relationship for HAc concentrations (at concentrations larger 100 ppm) and an exponential relationship for MEG concentrations. The inhibition efficiency increases with increasing MEG concentration and decreases with increasing acetic acid concentration. The results show that the enhanced cathodic reaction of the corrosion process in HAc reduces in the presence of MEG by adsorption of MEG.

CHAPTER 5. Effect of Temperature and Immersion time

In this chapter, the effects of temperature and immersion time on the inhibition efficiency of MEG in CO_2 systems are investigated. The effect of temperature on the values of the electrochemical parameters is evaluated in detail. Potentiodynamic polarization measurements are performed with 50% and 80% MEG in 3% NaCl solution at 24°C, 40°C and 60°C. EIS measurements are performed in 80% MEG at 24°C to 80°C and the value of activation energy (E_a) in the presence of MEG is compared at different temperatures. Furthermore, the effect of immersion time on the values of electrochemical parameters is shown after 2, 24, 48 and 76 hours of immersion. The experimental set-up has been described in Section 2.2.1.

5.1 Effect of Temperature

The change of the corrosion rate with temperature in various MEG concentrations is summarized in Figure 5.1. It can be seen that the corrosion rate increases with increasing temperature both in the absence and presence of various concentrations of MEG. Analysis of the data in Figure 5.2 shows that increasing temperature has a linear increasing effect on the corrosion rate of the carbon steel at each MEG concentration. This indicates that at higher MEG concentrations the corrosion rate is less affected by temperature.

In general the electrochemical reaction rate increases with increasing temperature and this is the case in the absence of protective corrosion product scales.[28]

In MEG systems, in addition to the general increase in the corrosion rate at higher temperatures, the accelerated corrosion rate (at lower MEG concentration) with increasing temperature could be due to the changes of the solution properties that influence the corrosion rate. It has been shown that increasing temperature affects the conductivity and viscosity of MEG containing solutions[85] and thus, influences the corrosion rate. The conductivity of MEG solutions in the laboratory were measured at 24°C and 60°C. The results show that at the same concentration of MEG the conductivity is higher at higher temperatures (refer to Table 3.7). The increase in conductivity is an indication of the solution resistance reduction (this is

confirmed in Figure 5.6) and thus the corrosion rate increases. However, as it has been shown previously, the trend of conductivity vs. temperature becomes more linear as the MEG concentration increases.[96] This can explain the lower effect of temperature on the corrosion rates at higher MEG concentrations. In addition, increasing the temperature is known to reduce the viscosity of MEG solutions,[96] which increases the diffusivity of CO_2, and thus the corrosion rate.[24]

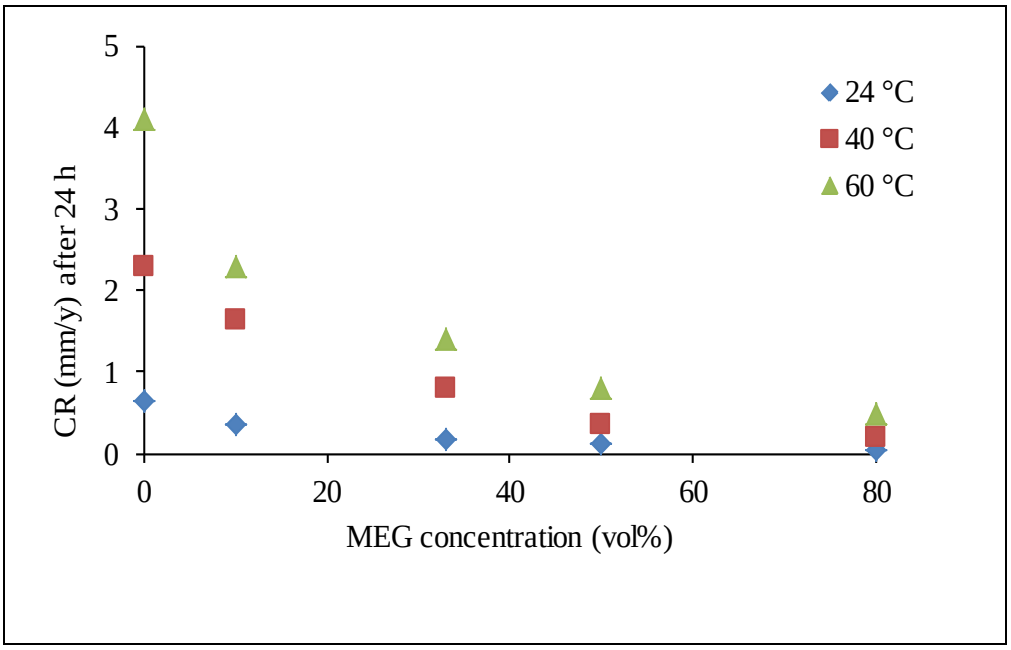

Figure 5.1: Temperature effect on carbon steel corrosion in CO_2 saturated solutions in the absence and presence of 10% to 80% MEG at 24°C, 40°C and 60°C. Results are obtained from the LPR technique.

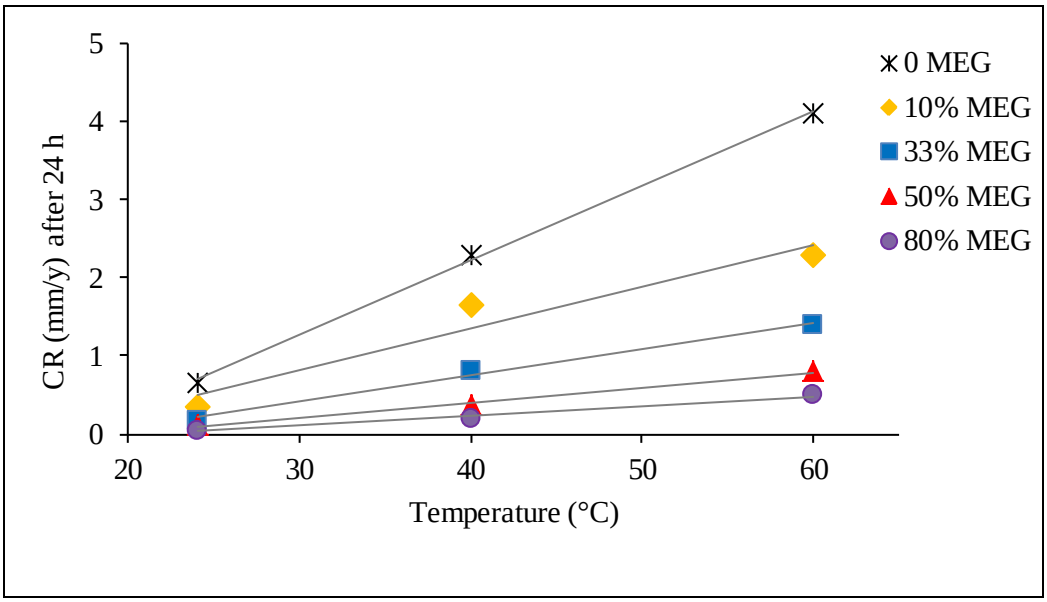

Figure 5.2: Corrosion rate vs. temperature in the absence and presence of 10% to 80% MEG. Results are obtained from the LPR technique.

The influence of the temperature on the anodic and cathodic reactions in 50% MEG solutions are presented in Figure 5.3. With an increase in temperature from 24°C to 60°C both anodic and cathodic current densities increase and the corrosion potential shifts to more negative potentials. The electrochemical parameters are listed in Table 5.1. It shows that the corrosion rate increases with temperature from 0.07 mm/y at 24°C to 0.43 mm/y at 60°C. Both anodic and cathodic Tafel slopes remains similar at all temperatures which indicates that increasing temperature does not change the mechanism of corrosion reaction in the presence of MEG.

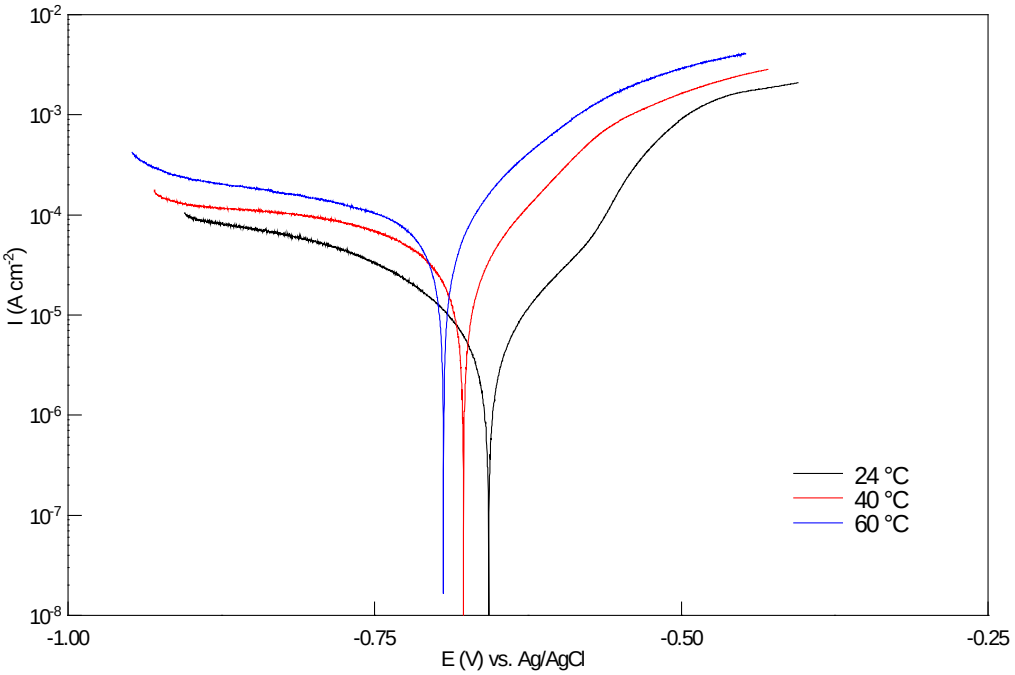

Figure 5.3: Effect of temperature on the potentiodynamic plots in CO_2 saturated 3% NaCl solution in the presence of 50% MEG after 24 hours of immersion.

Table 5.1: Electrochemical parameters of carbon steel in CO_2 saturated 3% NaCl solution in the presence of 50% MEG at various temperatures based on Figure 5.3.

Temperature (°C)	E_{corr} (mV)	i_{corr} (µA/cm²)	b_a (mV/dec)	$-b_c$ (mV/dec)	CR (mm/y)
24	-645	6.5	70	110	0.07±0.01
40	-669	35	65	115	0.39±0.00
60	-690	38	60	118	0.43±0.43

The influence of temperature on the anodic and cathodic reactions of polarization curves in 80% MEG/brine solutions are presented in Figure 5.4. There is a clear acceleration of both anodic and cathodic current densities with increase in temperature from 24°C to 80°C. Also, the corrosion potential shifts to more negative potentials. The electrochemical parameters are shown in Table 5.2. It can be seen that the corrosion rate increases with increasing temperature from 0.05 mm/y at 24°C to 2.35 mm/y at 80°C. There are no significant changes in anodic and cathodic Tafel slopes.

The results from polarization measurements confirm that the supersaturation of iron carbonate in the solution is not sufficiently high or the iron carbonate film is not adhering to the surface to reduce the corrosion rate, in the temperature range studied.[47] Thus, in the absence of a protective corrosion product layer, the corrosion

inhibition efficiency of MEG depends on the temperature. A negative shift in corrosion potential with increasing temperature shows that the main effect of temperature is on the cathodic reaction. This can be because of the change in conductivity and viscosity of the MEG solutions as temperature change (Table 3.7) which influences the cathodic hydrogen evolution reaction. It is known that the conductivity of the fluid increases with increasing temperature[96] resulting in an increase in the cathodic reaction.

Anodic and cathodic Tafel slopes do not change considerably with increasing temperature indicating that the corrosion mechanism does not change with increasing temperature in the presence of MEG.

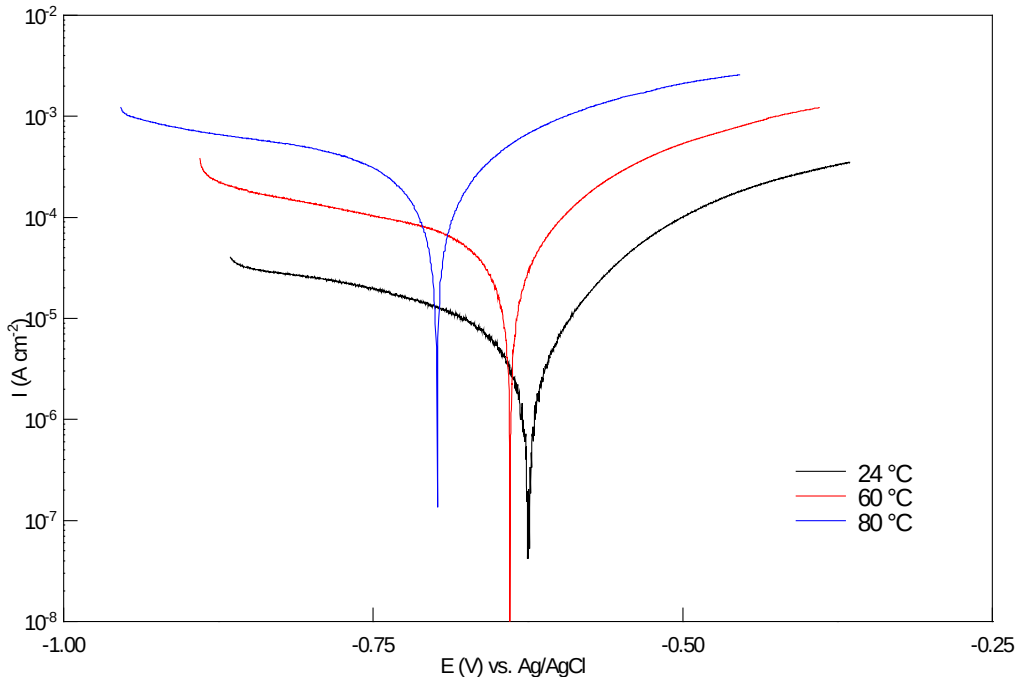

Figure 5.4: Effect of temperature on the potentiodynamic plots in CO_2 saturated 3% NaCl solution in the presence of 80% MEG after 24 hours of immersion.

Table 5.2: Electrochemical parameters of carbon steel in CO_2 saturated 3% NaCl solution in the presence of 80% MEG solution at various temperatures based on Figure 5.4.

Temperature (°C)	E_{corr} (mV)	i_{corr} (µA/cm²)	b_a (mV/dec)	$-b_c$ (mV/dec)	CR (mm/y)
24	-620	4.5	79	110	0.05±0.005
60	-634	24	70	116	0.27±0.27
80	-699	210	70	120	2.35±0.01

The temperature dependence of the inhibitor efficiency (IE) and the comparison of the values of effective activation energy (E_a) for the corrosion process both in the absence and in the presence of an inhibitor gives information about the mechanism of the inhibiting action[48] including the adsorption process of an inhibitor on the metal surface. For this reason the variation of the corrosion rate with temperature is utilized to calculate the parameters such as the inhibition efficiency (IE) and activation energy (E_a). Table 5.3 shows the inhibition efficiencies of MEG (10% to 80%) in CO_2 saturated solutions at 24°C and 60°C calculated using Equation 2.13.

It is clear that at each concentration of MEG, the changes in the solution properties with increased temperature leads to a decrease in the inhibition efficiency. In general, there is an exponential increase in the corrosion rate shown in all concentrations of MEG as the temperature increases. It is also observed that the effect of temperature on the inhibition efficiency becomes less at higher MEG concentration compared with lower concentration. In 10% MEG containing solution, the inhibition efficiency decreases from 80% to 63% with increasing temperature from 24°C to 60°C and from 95% to 90% with 80% MEG at the same temperature difference.

Activation energies (E_a) of the corrosion process in the absence and presence of the MEG are calculated using the Arrhenius law equation as follows:

$$\log\frac{\mathrm{icorr}_{(2)}}{\mathrm{icorr}_{(1)}} = \frac{\mathrm{E_a}}{2.303\ \mathrm{R}}\left(\frac{1}{\mathrm{T_1}} - \frac{1}{\mathrm{T_2}}\right) \tag{5.1}$$

Where R is the universal gas constant (8.3145 J/molK), $i_{corr(1)}$ and $i_{corr(2)}$ are the corrosion current densities in $\mu A/cm^2$ at temperatures T_1 (297.15 K) and T_2 (333.15 K), respectively. The calculated E_a values are given in Table 5.3. Analysis of the E_a values vs. MEG concentration shows that E_a values follow an increasing linear trend with increasing MEG concentration with the regression coefficient value of 0.989.

Table 5.3: The calculated inhibition efficiencies and activation energies in the absence and presence of 10% to 80% MEG containing solutions at 24°C and 60°C.

C_{MEG} (vol%)	IE (%)		E_a (J/mol)
	24°C	60°C	
0	-	-	612.60
10	80	63	626.23
33	81	72	682.29
50	94	84	699.13
80	95	90	752.84

Therefore, in addition to a reduction in the IE%, increasing temperature leads to an increase in E_a (compared to the MEG's absence) at all MEG concentrations. The increase in E_a can be interpreted as physical adsorption.[44,48] This means that a higher energy barrier for the corrosion process in MEG solution compared to an aqueous solution is associated with physical adsorption between the MEG molecules and the steel surface.[48] Physical (or electrostatic) adsorption is related to the electrostatic attraction between inhibiting organic ions or dipoles and the electrically charged surface of the metal.[97]

In order to further investigate the adsorption of MEG on the carbon steel surface, EIS measurements are carried out in 3% NaCl solution saturated with CO_2 in the absence and the presence of MEG at temperatures ranging from 24°C to 80°C as described in Section 2.2.1. The measurements are performed an hour after immersion.

Figure 5.5 shows the Nyquist plots obtained at various temperatures in the absence of MEG and Table 5.4 shows corresponding circuit parameters obtained from the circuit model shown in Figure 2.6. It is observed that the diameter and magnitude of the semicircle decrease with increasing temperature, indicating an increase in the corrosion rate, as evidenced by the polarization technique results (Figure 5.1). All experimental plots show a depressed capacitance semicircle in the complex plane, with the centre below the real axis which shows the frequency dispersion of the impedance data due to inhomogeneous properties of the corroding surface of mild steel.[82] The impedance spectra exhibit a single capacitive loop at high frequency with a diffusive part at low frequency at 24°C. The diffusive part disappears gradually with increasing temperature. The values of charge transfer resistance (R_{ct})

in the absence of MEG (shown in Table 5.4) decreases with increasing temperature which indicates an increase in corrosion rates with increasing temperature. The values of solution resistance do not change considerably with increasing temperature.

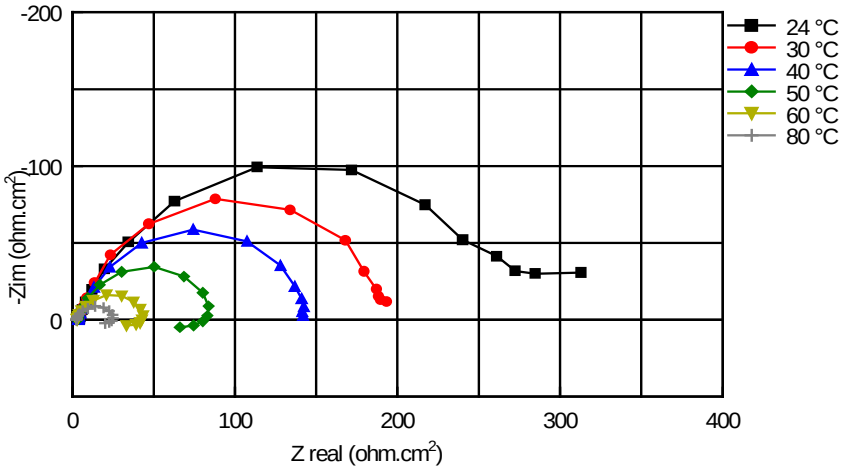

Figure 5.5: Representative Nyquist plots of carbon steel in CO_2 saturated 3% NaCl solutions at different temperatures in the absence of MEG.

Table 5.4: Equivalent circuit parameters of carbon steel in 3% NaCl solution at different temperatures in the absence of MEG.

No MEG	Temperature (°C)					
	24	30	40	50	60	80
R_s	3.5	3.8	3.5	2.9	2.7	2.2
R_{ct}	276.9	191.8	143.7	85.2	42.2	23.5
CR (mm/y)	0.67±0.31	0.78±0.43	1.15±0.58	2.05±0.40	3.45±0.13	4.60±0.61

In the presence of 80% MEG (shown in Figure 5.6), with increasing temperature the diameter and magnitude of the impedance spectra decrease indicating an acceleration of the corrosion process at higher temperatures in the presence of MEG, which confirms the results obtained by the polarization technique (Figure 5.1 and Figure 5.3).

The equivalent circuit parameters calculated from the circuit model in Figure 2.6 are shown in Table 5.5 indicating the charge transfer resistance (R_{ct}) of MEG solution decreases with an increase in temperature. The values of the solution resistance (R_s) in the presence of MEG decrease with an increase in temperature. This is different

from the effect of temperature observed in the absence of MEG (Figure 5.5), which shows similar R_s values with increasing temperature. The reduction in solution resistance in the presence of MEG is an indication of a change in solution properties with increasing temperature, which confirms the result of the conductivity measurement (Table 3.7). The increase in corrosion rates of MEG containing solutions with increasing temperature is consistent with the behaviour observed in potentiodynamic polarization curves (Figure 5.3 and Figure 5.4).

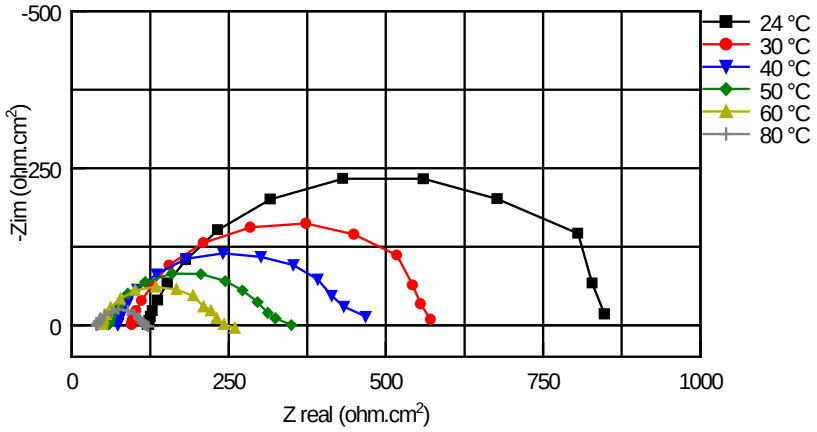

Figure 5.6: Representative Nyquist plots of carbon steel in CO_2 saturated 3% NaCl solution at different temperatures in the presence of 80% MEG.

Table 5.5: Equivalent circuit parameters of carbon steel in 3% NaCl solution at different temperatures in the presence of 80% MEG.

80% MEG	Temperature (°C)					
	24	30	40	50	60	80
R_s	120	92	70	56	46	39
R_{ct}	752	490	371	263	185	75
CR (mm/y)	0.07±0.24	0.15±0.08	0.23±0.18	0.53±0.18	0.75±0.10	2.06±0.13

A comparison of the impedance data in the absence and presence of MEG (Table 5.4 and Table 5.5) indicates that introducing 80% MEG increases the magnitude and diameter of the impedance spectra at all temperatures due to the inhibition of the corrosion process. The capacitance is observed to decrease in MEG solutions compared with the non-MEG solutions at the same temperature. The decrease in capacitance may be interpreted as a decrease in the dielectric constant and/or an

increase of the double electric layer thickness as a result of the physical adsorption of MEG on the metal surface.[48]

5.2 Summary of Section 5.1

The results indicate that increasing temperature has a linear increasing effect on the corrosion rate of carbon steel in the presence of MEG. Furthermore, at higher MEG concentrations the corrosion rate is less affected by increasing temperature. In MEG systems, in the absence of a protective corrosion product scale, in addition to the general increase in corrosion rate at higher temperatures, the accelerated corrosion rate (at lower MEG concentration) with increasing temperature could be due to the changes of the solution properties that influence the corrosion rate. At each concentration of MEG, the change in the solution properties with increasing temperature leads to a decrease in the inhibition efficiency. In addition to a reduction in the IE%, increasing temperature leads to an increase in E_a (compared with the MEG's absence) at all MEG concentrations. The increase in E_a can be interpreted as physical adsorption of the MEG molecules at the steel surface. Decreasing the capacitance of the impedance spectra is an indication of a decrease in dielectric constant and/or an increase in the double electric layer thickness as a result of MEG physical adsorption on the metal surface. This indicates that at each temperature, the presence of MEG promotes the formation of an inhibition layer on the steel surface.

5.3 The Effect of Immersion Time

Some aspects of the effect of immersion time have already been discussed in Section 3.3. The results presented in Figure 3.5 showed the fast inhibition effect of MEG on the anodic reaction immediately after immersion of the sample in the solution. To further examine the effect of immersion time on the inhibition efficiency of MEG, electrochemical tests are run at different immersion times of up to 72 hours.

Figure 5.7 shows the influence of the immersion time on the polarization plots of a carbon steel electrode in the absence of MEG at 24°C. Increasing exposure time is

observed to have effects on both anodic and cathodic current densities in the absence of MEG. Both cathodic and anodic reactions are increased and the corrosion potential shifted to more negative potentials with increasing immersion time from 2 hours to 76 hours of immersion. The corrosion rates increase from 0.96 mm/y after 2 hours to 4.21 mm/y after 76 hours of immersion. Increasing corrosion rates with increasing time in the absence of MEG is consistent with the results observed in Chapter 3 (Figure 3.5a and b) which shows an increase in the corrosion rate at 60°C between 2 hours and 24 hours of immersion. This is attributed to the acceleration of the corrosion current with increasing time due to the uniform CO_2 corrosion of carbon steel in aqueous solution (Section 1.1).

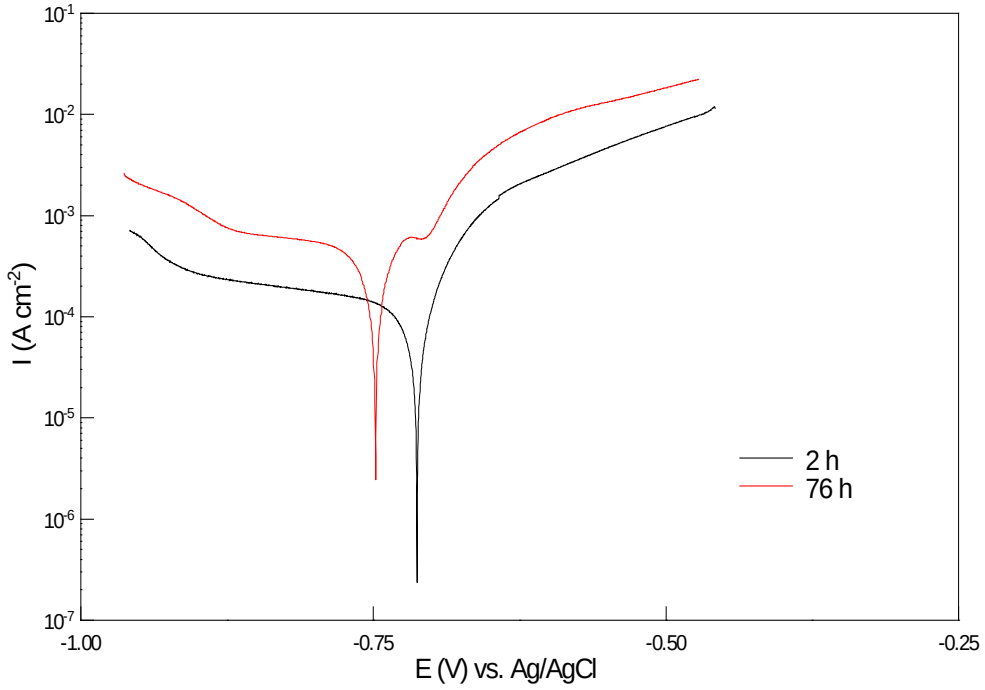

Figure 5.7: Representative potentiodynamic polarization plotsof carbon steel in CO_2 saturated solution at different immersion times in the absence of MEG at 24°C.

In the presence of 80% MEG (Figure 5.8) the anodic and cathodic reactions do not change considerably with longer immersion time from 2 hours to 76 hours and the corrosion rate is around 0.05 mm/y. This observation indicates that in the presence of 80% MEG (Figure 5.8) the increasing trend of corrosion rates with time, which was shown in the absence of MEG (Figure 5.7), has vanished and the corrosion process stabilised (proceeds at a constant rate) after 2 hours of immersion.

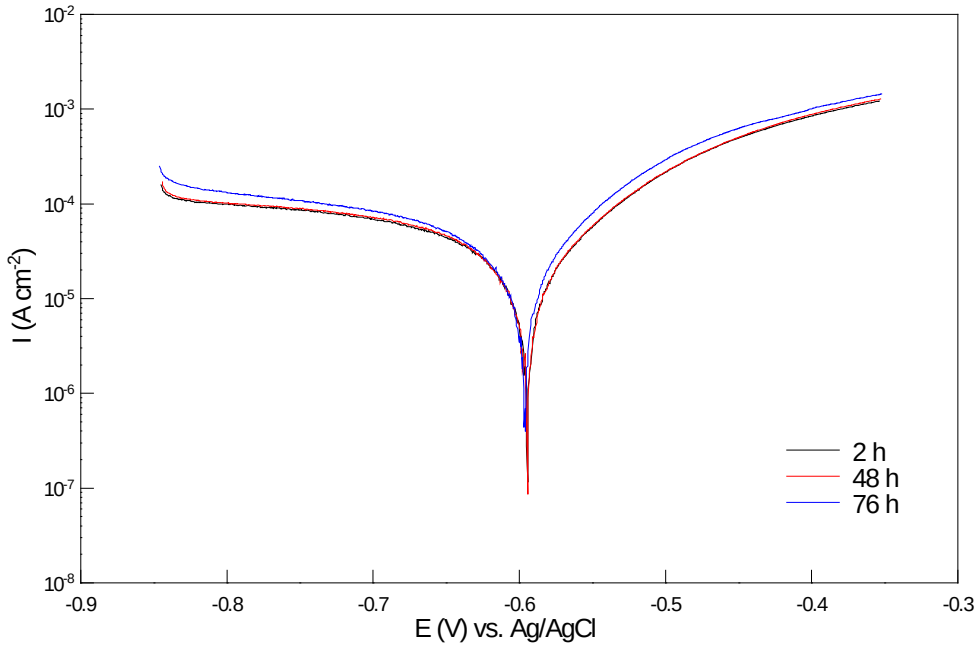

Figure 5.8: Representative potentiodynamic polarization plots of carbon steel in CO_2 saturated solution at different immersion times in the presence of 80% MEG at 24°C.

The influence of the immersion time on the electrochemical behaviour of carbon steel in the presence of MEG is further evaluated by EIS. The impedance diagrams obtained after 2 to 76 hours of immersion in the absence of MEG at 24°C are shown in Figure 5.9 and Figure 5.10 and the relative corrosion rates are shown in Table 5.6. As can be seen from the Nyquist plot of the electrode in absence of MEG (Figure 5.9), a single depressed semicircle equivalent to charge transfer resistance (R_{ct}) is observed indicating that the corrosion reactions are charge transferred at all immersion times. The magnitude and diameter of the impedance decreases with time for up to 76 hours and the values do not stabilize after this time. A decrease in diameter of the impedance loop corresponds to a charge transfer resistance reduction due to the increase in the corrosion rate. This is supported by the potentiodynamic results, which show an increase in both anodic and cathodic current densities with longer exposure time (Figure 5.7). From the frequency vs. phase angel plot of the Bode curve (Figure 5.10) the shift in the curve's peak from high frequencies to the lower frequencies is related to the reduction of charge transfer resistance between 2^{nd} and 76^{th} hours. The frequency vs. log |Z| mode plot of the Bode plot (Figure 5.10) shows the shift in the curves with longer immersion times, indicating the active change on the metal surface as a result of the accelerated corrosion

process. The calculated corrosion rate of the carbon steel electrode in the absence of MEG (Table 5.6) is observed to increase from 0.86 mm/y after 2 hours of immersion to 1.50 mm/y after 24 hours and 3.68 mm/y after 76 hours of immersion, which are in good agreement with the corrosion rates obtained from the potentiodynamic polarization scans.

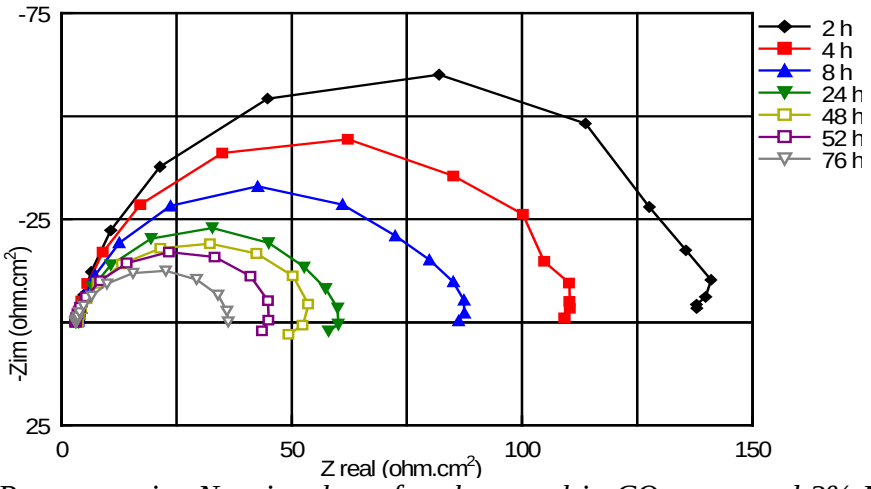

Figure 5.9: Representative Nyquist plots of carbon steel in CO_2 saturated 3% NaCl solution at different immersion times in the absence of MEG at 24°C.

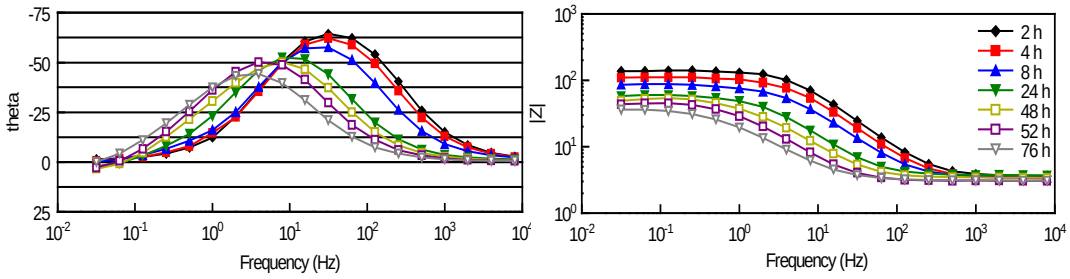

Figure 5.10: Representative Bode plots of carbon steel in CO_2 saturated 3% NaCl solution at different immersion times in the absence of MEG at 24°C.

Table 5.6: Corrosion rate values of carbon steel in CO_2 saturated 3% NaCl solution at different immersion times in the absence of MEG at 24°C.

Immersion time (h)	2	4	8	24	48	52	76
CR (mm/y)	0.86±0.04	1.12±0.08	1.30±0.01	1.50±0.05	2.23±0.35	2.85±0.51	3.68±0.32

The impedance diagrams obtained after 2 hours to 76 hours of immersion in the presence of 80% MEG at 24°C are shown in Figure 5.11 and Figure 5.12 and the relative corrosion rates are shown in Table 5.7. The Nyquist plot of the electrode in the presence of MEG (Figure 5.11) also shows a single depressed semicircle. The magnitude and diameter of the impedance plot increase between 2 hours and 52 hours after immersion in the presence of MEG. After this time, the impedance plot does not change considerably for the rest of the time to 76 hours .

The increase in magnitude and diameter of the impedance shows an increase in the charge transfer resistance and inhibition effect of MEG on the metal corrosion with increasing time. This is probably due to continuous replacement of water molecules and chlorine (Cl^-) with MEG molecules on the metal surface from a short time after immersion, which causes a decrease in the corrosion rate from 0.22 mm/y to 0.09 mm/y after 2 hours to 52 hours. This result confirms the result from Figure 3.1 where the corrosion rate trend recorded for 80% MEG solution suggests that MEG gradually adsorbs on the metal surface from a short time after immersion and keeps water and CO_2 molecules away from the surface. However, longer exposure time (up to 52 hours) does not have a significant effect on the impedance response. This shows that with longer exposure time the replacement of water and MEG molecules on the metal surface is in equilibrium. Thus, the resistance of the film does not change with longer immersion times.

From the frequency vs. phase angle plot of the Bode curve (Figure 5.12) a peak in the mid frequency region is noted after 2 h immersion which splits into two peaks after 4 h immersion. The second time constatant in the Bode plot shows formation of a protective film on the metal surface.[98] At 24°C, this film is more likely a thin layer of MEG molecules on the metal surface as the conditions are not favourable to the formation of a protective corrosion products layer.[99] However, this is not observed in the impedance plots obtained at other exposure times. The reason may be that the thin layer of MEG has a resistance much lower than the charge transfer resisistance and the impedance loop corresponding to the MEG's film merges with the charge transfer resistance and represents a single semicircle for the rest of the time. This film can protect the metal surface from corrosion by restraining the mass transfer of the reactants involved in the corrosion process between the metal surafce and the bulk solution.

The frequency vs. log |Z| mod plot of the bode curve (Figure 5.12) indicates that the impedance spectra just oscillate in a narrow range between 2 and 76 hours of exposure and does not shift with increasing immersion time. This indicates that during the initial time of immersion a stable film of MEG molecules forms on the surface, which does not change with a longer time of exposure. The calculated corrosion rates from the EIS measurements (Table 5.7) at different immersion times confirm the LPR (Figure 3.1) and potentiodynamic polarization results (Figure 5.8), which show the corrosion rate decreases from the initial time of exposure in the presence of 80% MEG and then proceeds with an almost constant rate over the first 24 hours.

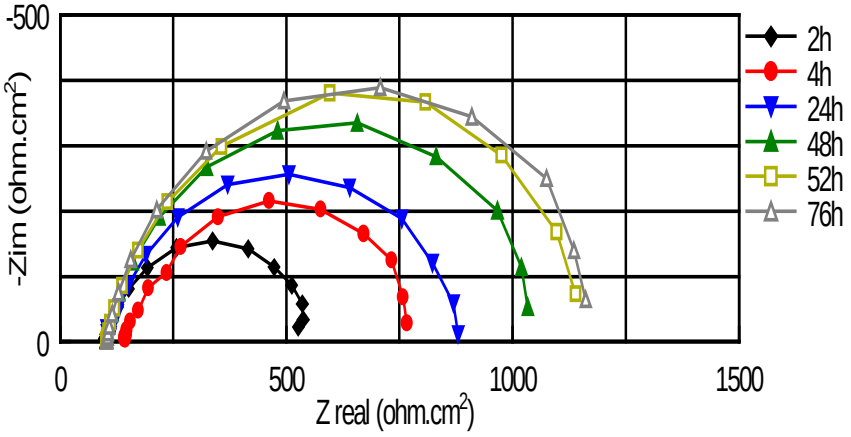

Figure 5.11: Representative Nyquist plots of carbon steel in CO_2 saturated 3% NaCl solutions at different immersion times in presence of 80% MEG at 24°C.

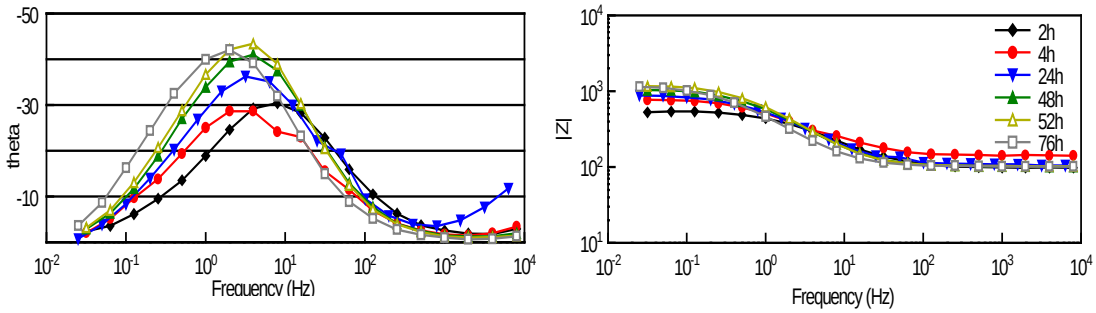

Figure 5.12: Representative Bode plots of carbon steel in CO_2 saturated 3% NaCl solutions at different immersion times in presence of 80% MEG at 24°C.

Table 5.7: Corrosion rates of carbon steel in 3% NaCl brine solution at different immersion times in presence of 80% MEG at 24°C.

Immersion time (h)	2	4	8	24	48	52	76
CR (mm/y)	0.22±0.08	0.17±0.23	0.13±0.09	0.11±0.03	0.10±0.07	0.09±0.06	0.09±0.09

5.4 Concluding Remarks

The effects of temperature and immersion time on the corrosion behaviour of a carbon steel electrode in CO_2 saturated solution in the presence of MEG, give complementary information about the inhibition effect of MEG on carbon steel.

The results reveal that temperature has an increasing effect on the corrosion behaviour of carbon steel in the absence and the presence of MEG in the conditions tested. Corrosion rates in MEG solutions are enhanced with increasing temperature. The decrease in the inhibition efficiency and increase in the activation energy of MEG containing systems with increase in temperature indicates a decrease in adsorption of the MEG molecules on the metal surface, which is supported by EIS measurements.

While the increasing immersion time in the absence of MEG shows increases in both anodic and cathodic current densities (Figure 5.7) and, hence, increase in the corrosion rate (Table 5.6), increasing the immersion time in a MEG system does not change the polarization scan of the working electrode (Figure 5.8). EIS results show increased R_{ct} in time 2 to 52 h, indicating continuous adsorption of MEG on the metal surface (Figure 5.11). This results in decrease of the corrosion rates as shown in Table 5.7. The results confirm the findings shown in Chapter 3 (Figure 3.5), which reveal increase in the inhibition efficiency of MEG on the anodic reaction with increasing concentration of MEG and the development of a layer of MEG on the metal surface.

CHAPTER 6. The Effect of MEG on the Condensation Rate

This chapter discusses the possibility of transportation of MEG from the bulk liquid phase to the gas phase and its condensation at the top of the line. It aims to determine the amount of MEG present at the top of the line and the role of temperature on its transfer from the liquid phase. In order to follow this chapter some terminology is introduced. The term 'bulk liquid' refers to the test solution at the bottom of the autoclave and consists of a 50 or 90 vol% MEG/water ratio. Autoclave temperature (T_a) is the temperature of the bulk liquid. The T_a values are 60°C, 90°C and 120°C. Cooling temperature (T_c) is the temperature of the inhibited cooling water solution which is pumped through the U–tube sample to stimulate condensation on the outside of the sample, simulating top of the line conditions. The temperature difference between the autoclave and the cooling water ($\Delta T = T_a - T_c$) varies between 20°C and 60°C. Condensation volumes are measured after an 18 hour test period. The experimental set-up is described in details in Section 2.2.2.

6.1 Condensation Rate Measurements

As a first step to determine the possible inhibition effect of MEG on the top of the line corrosion rate of carbon steel, series of tests are run from an uninhibited (non-MEG) system at various bulk liquid and cooling temperatures. Calculation of the condensation rates as a function of ΔT ($T_a - T_c$) (Equation 2.15) shows that at each bulk temperature, the condensation rate increases with increasing ΔT both in the absence and the presence of MEG (Figure 6.1). From the test without MEG at 120°C bulk liquid temperature and ΔT = 60°C, a maximum condensation rate of 1.31 g/m^{2}s is measured. In comparison with 50% MEG in the bulk liquid at the same testing temperatures, the condensation rate decreased to 0.71 g/m^{2}s and decreased more than three times to 0.2 g/m^{2}s with 90% MEG/water in the bulk liquid phase, which is just below the threshold for initiating top of the line corrosion in the absence of acetic acid.[58] When the cooling temperature increased to 90°C (ΔT = 30°C), the condensation rate drops to 0.091 g/m^{2}s in a non-MEG system (Figure 6.1a). The condensation rate further decreases to values of 0.027 g/m^{2}s and 0.018 g/m^{2}s with 50% MEG and 90% MEG/water bulk liquid, respectively, which is at the reported

threshold for top of the line corrosion in the presence of acetic acid.[58] However, when the bulk liquid temperature decreases to 90°C (Figure 6.1b), the general water condensation rate decreases sharply compared with that at 120°C.

At bulk liquid temperature of 60°C (Figure 6.1c), the general water condensation rate decreases once more compared to the water condensation rates measured at 90°C. In this case (60°C) the water condensation rate drops to values of 0.1 g/m^2s at all three cooling temperatures in non MEG systems, which is still high enough to initiate top of the line corrosion if acetic acid is present.[58] In a 50% MEG/water aqueous phase system the water condensation rate is almost half compared with an uninhibited system with a value of 0.05 g/m^2s with ΔT of 50°C which decreases to 0.025 g/m^2s in a 90% MEG bulk liquid. At the same bulk liquid temperature of 60°C, when the temperature difference between the bulk liquid and cooling temperature (ΔT) decreases the water condensation rate follows a decreasing trend as with the other two bulk liquid temperatures (Figure 6.1a, b and c).

These results indicate that the water condensation rate depends on the MEG concentration in the liquid phase and temperature (both bulk liquid temperature and cooling temperature). At constant temperatures (T_a and T_c), the condensation rate decreases with increasing MEG concentration (Figure 6.1). The reducing effect of MEG on the condensation rate is related to its water binding function. At the same bulk liquid temperature, increasing MEG concentration reduces the partial pressure of water vapour, [23] which results in a lower dewpoint of the gas.[29] In other words, at the same temperature, the water content in the saturated gas will be lower in the presence of MEG. For this reason, it is expected to reduce the condensation rate with increasing MEG concentrations. Top of the line corrosion rate measurements by Nyborg et al.[55] indicate that the addition of 50% glycol in the liquid phase decreased the corrosion rate in the top of the line to very low values. The reduction in the condensation rate and the dew point are introduced as the cause of the reduced corrosion rate when glycol is present. The lower condensation rate (or higher glycol concentration) reduces the iron carbonate solubility[55] and facilitates the formation of a protective film.

Another factor influencing the condensation rate in the absence and the presence of MEG is temperature. The water condensation rate reduces sharply when the

temperature of the bulk liquid decreases. This is due to the reduction of the MEG/water mixture vapour pressure at lower temperatures. According to Ullmann's Encyclopedia of Industrial Chemistry[96] vapour pressure of pure water decreases more than two times with reducing temperature from 90°C to 65°C (Figure 6.2). This can explain the sharp decrease in condensation rate at lower temperatures. On the other hand, increasing ΔT leads to an increase in condensation rate.

In Nyborg et al.[55] the condensation rate of 0 to 50% glycol/water mixture in a three-phase loop at 40°C with two temperature differences between the gas and the pipe wall at a 3 m/s gas flow rate is determined. Measurements of condensation rates in their work show that at a 1 K temperature difference between the gas and pipe wall, the condensation rate is 0.39 g/m^{2}s and increases to 0.69 g/m^{2}s when the temperature difference is increased to 4 K.

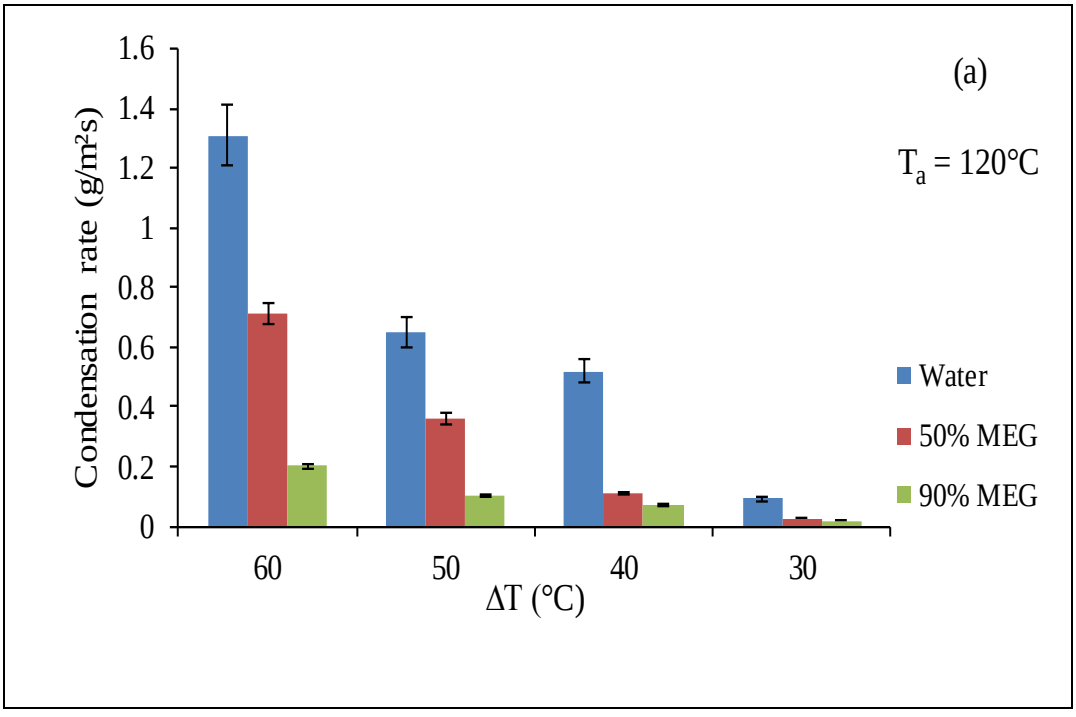

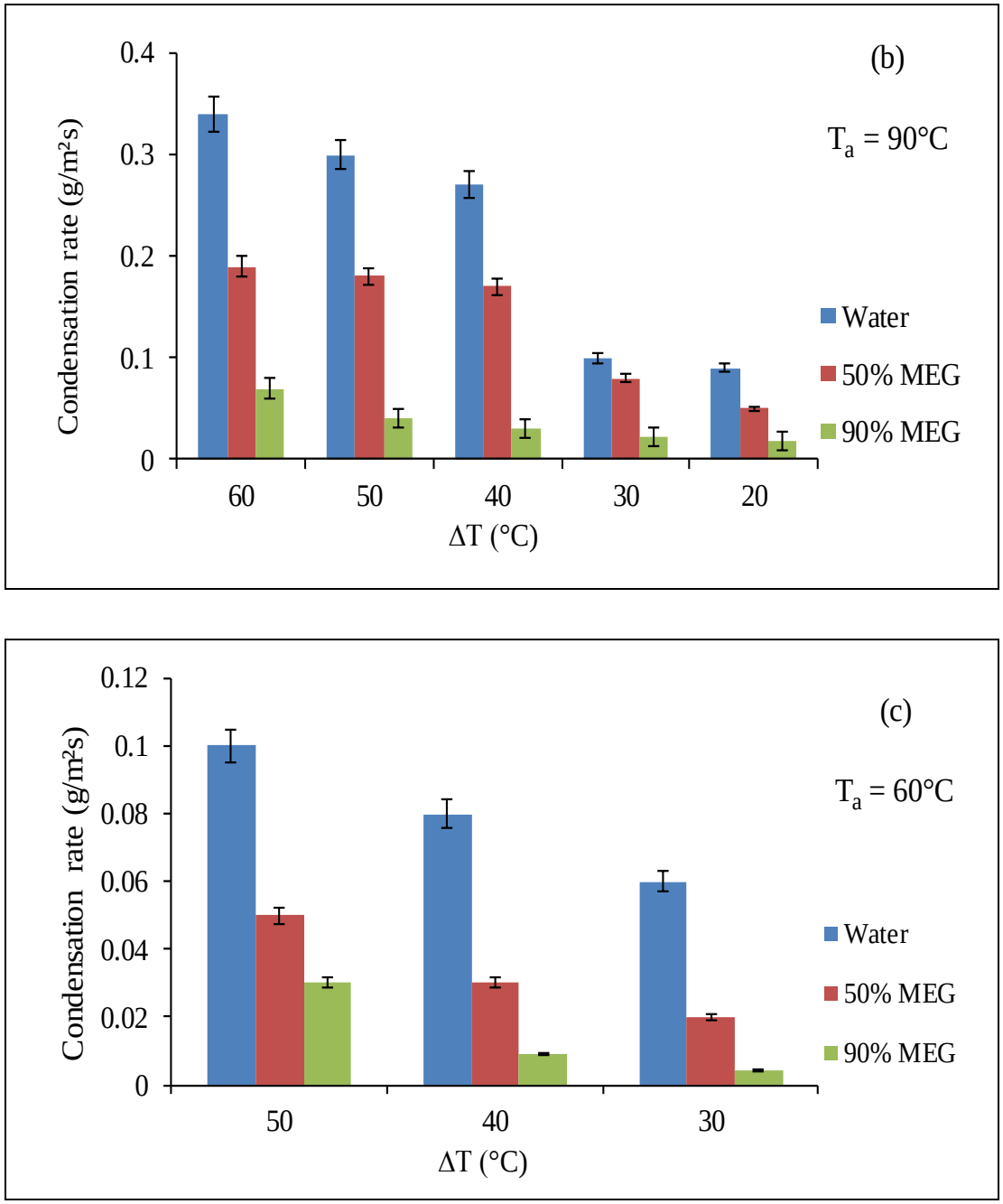

Figure 6.1: Condensation rate as a function of cooling temperature at different MEG/water mixtures at (a) 120°C, (b) 90°C and (c) 60°C bulk liquid temperatures, 20 bar CO_2.

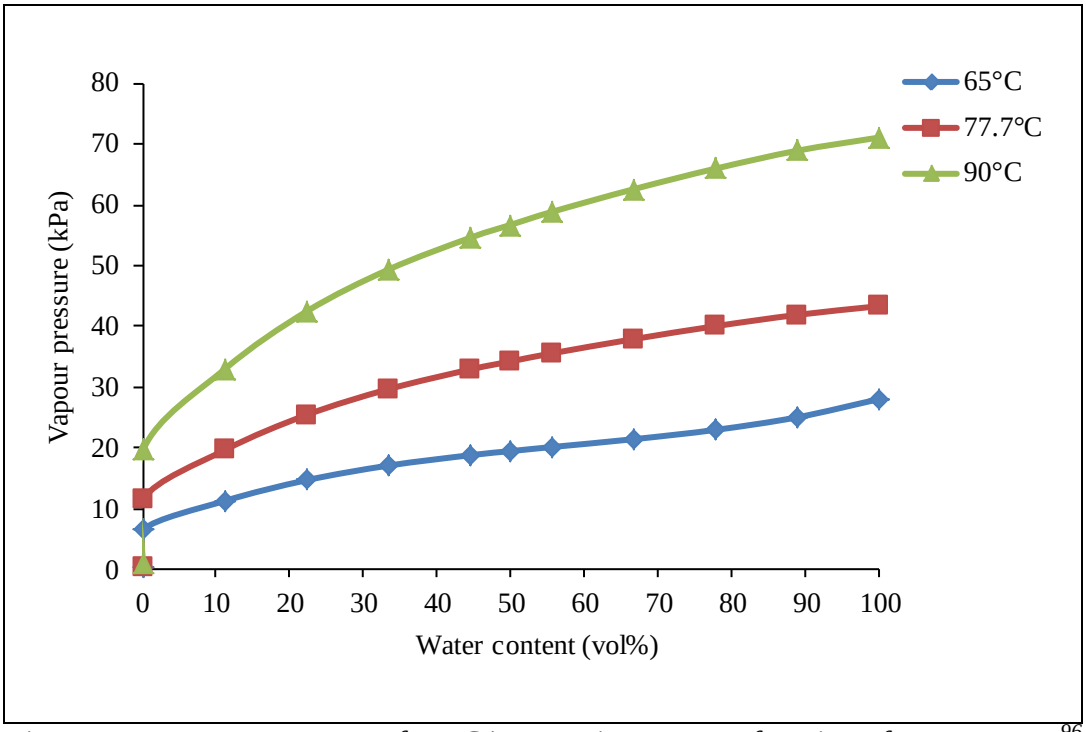

Figure 6.2: Vapour pressure of MEG/water mixtures as a function of temperature.[96]

6.2 Determination of MEG Content in the Condensing Liquid

MEG can affect the corrosion rate at the top of the line, only if it is transported from the liquid MEG/water mixture phase to the above gas phase, and then condenses from gas to the condensing liquid film on the sample surface.[100] The calibration method of the absorbance of the standard MEG/water mixtures is explained in Chapter 2 (Section 2.2.2.4).

Representative FTIR spectra from the condensing and bulk liquids are shown in Figure 6.3 and Figure 6.4. In both figures, spectrum (a) belongs to the bulk liquid phase in 50% and 90% MEG solutions, respectively. While (b), (c) and (d) are spectra from condensing liquid when the autoclave temperatures is (a) 120°C, (b) 90°C and (c) 60°C. At both concentrations of MEG (50% and 90% MEG) a comparison between these spectra and the condensing liquid spectra at different temperatures shows that the absorbance decreases as the bulk liquid temperature reduces from 120°C to 60°C. It also shows that the adsorption peaks are stronger when the bulk liquid consists of the higher concentration of MEG (90%).

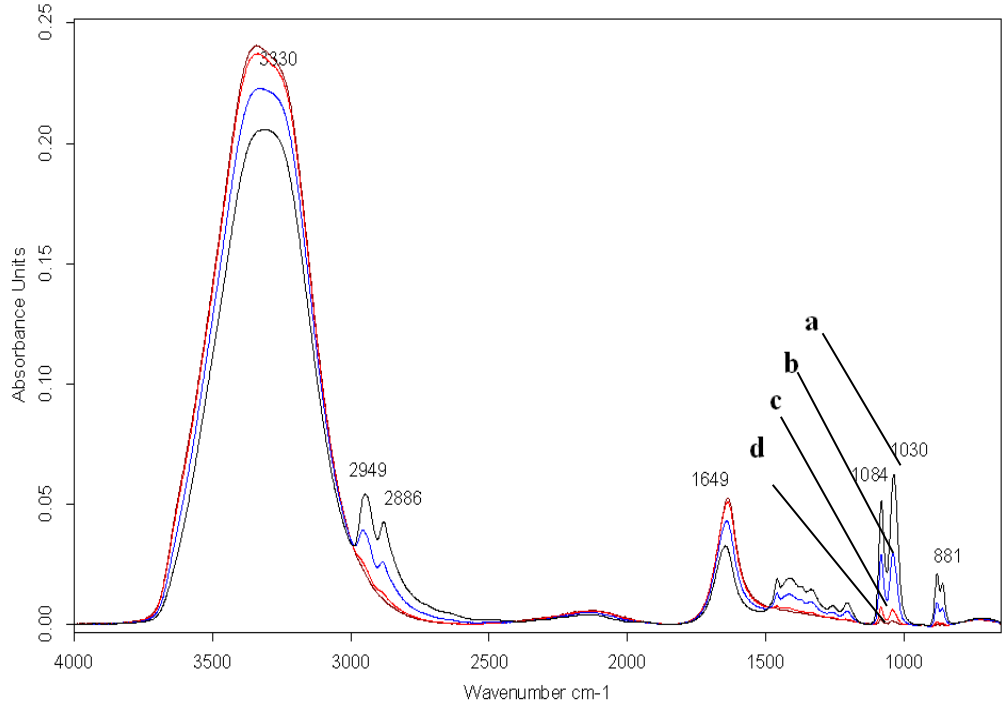

Figure 6.3: Representative FTIR spectra of the condensing liquid with 50% MEG/water mixture in the bulk liquid; Liquid bulk solution containing 50% MEG/water at temperature 120°C (a); and condensing liquid with bulk liquid temperature of (b) 120°C,(c) 90°C and (d) 60°C, ΔT = 30°C.

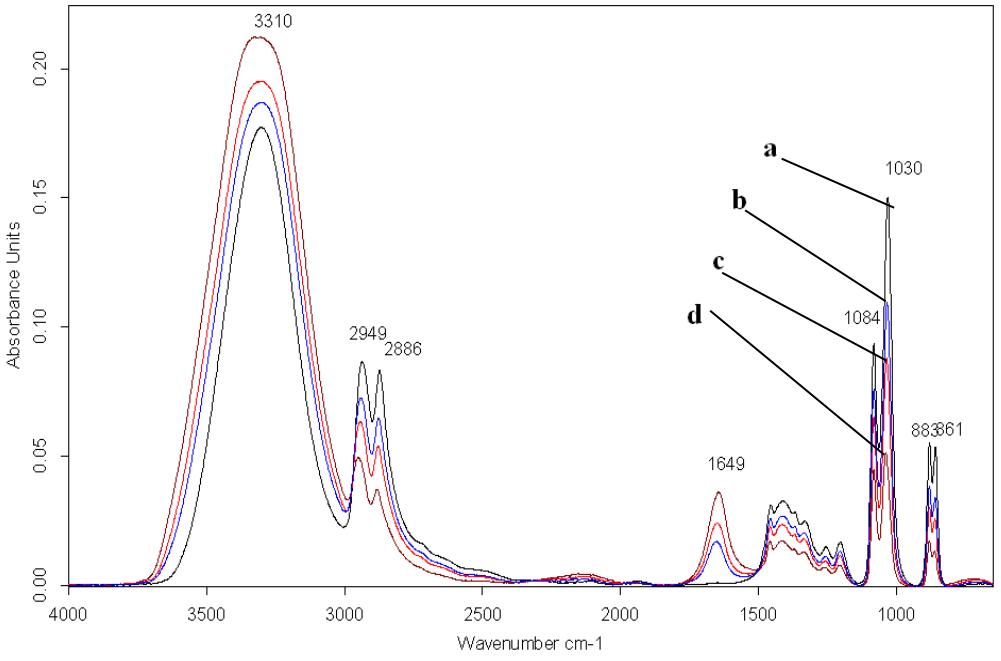

Figure 6.4: Representative FTIR spectra of the condensing liquid with 90% MEG/water mixture in the bulk liquid; Liquid bulk solution containing 50% MEG/water at temperature 120°C (a); and condensing liquid with bulk liquid temperature of (b) 120°C, (c) 90°C and (d) 60°C, ΔT = 30°C.

The results of the measurements of MEG concentration in the condensing liquid from each test conditions are shown in Table 6.1. It can be seen that when the bulk liquid phase contains 50% MEG/water at 120°C, a significant amount of MEG is presented in the condensing liquid at all different cooling temperatures. At a lower bulk liquid temperature of 90°C the amount of MEG in the condensing liquid reduces and at a T_a of 60°C less than 3 vol% MEG is transported to the condensate. The results from experiments conducted using 90% MEG in the bulk liquid show a similar trend: the MEG content in the condensate decreases with decreasing bulk liquid temperature. However, at each bulk liquid temperature, the amount of MEG in the condensate decreases with increasing temperature difference between bulk liquid and cooling temperature (ΔT).

When the MEG/water ratio in the bulk liquid phase increases to 90 vol%, more MEG is present in the condensing liquid compared to a 50 vol% MEG bulk liquid solution. With 90 vol% MEG in the bulk liquid, at 120°C, more than 70 vol% MEG is condensing at the sample surface at all cooling temperatures. In comparison a 50 vol% MEG bulk solution, at the same temperature, reduces the content of MEG in the condensate to between 35 and 44.5 vol%.

The results of the measurements of the MEG content in the condensing liquid at the top of the line show that MEG transports from the bulk liquid to the gas phase and condenses at the top of the line. The amount of transported MEG depends on the MEG concentration, the bulk liquid temperature and the temperature difference between the bulk liquid and the cooling temperature (ΔT). The concentration of MEG in the condensing liquid increases markedly with increasing MEG concentration in the bulk liquid. The temperature of the bulk liquid has, furthermore, a significant effect on the condensation rate and consequently on the amount of MEG present in the condensing liquid. The concentration of MEG in the condensing liquid increases significantly with increases in both bulk liquid and cooling temperatures. The lower condensation rate and the pronounced amount of MEG at lower ΔT may be due to re-evaporation of water from the metal surface or due to the increased water vapour pressure at higher temperatures.

A comparison of the results in Figure 6.1 and Table 6.1, indicates that at each bulk liquid temperature, with increasing temperature difference between the bulk liquid and the cooling temperature, the condensation rate increases and, in contrast, the

amount of MEG in the condensing liquid decreases. In a study concerning the amount of the glycol available for condensation with water Hinkson et al. study the transport of glycol from a bulk liquid in a three-phase flow loop at 40°C. They show that the glycol added for hydrate prevention most probably reaches to the top of the line even when a hydrocarbon layer covers the glycol/water phase in the bottom of the line.[57]

The relationship between ΔT and resulting MEG concentration in the condensate as a function of T_a and vol% of MEG in the bulk solution is shown in Figure 6.5. The results are given as vol% of MEG in the condensing liquid. It can be seen that there is a linear trend between ΔT and the resulting MEG concentration in the condensate in all cases studied.

Table 6.1: MEG content (vol%) in the condensing liquid at various temperatures with 50% and 90% MEG/water bulk liquid phase.

C_{MEG} (vol%) in the bulk liquid	Ta(°C)	ΔT(°C)				
		20	30	40	50	60
50	120	_	44.5	43.0	41.5	35.0
	90	_	25.0	17.5	16.0	11.0
	60	_	2.5	2.0	0.5	_
90	120	_	76.5	76.5	75.0	72.5
	90	71.0	65.0	63.5	63.0	58.0
	60	_	44.0	34.0	27.0	_

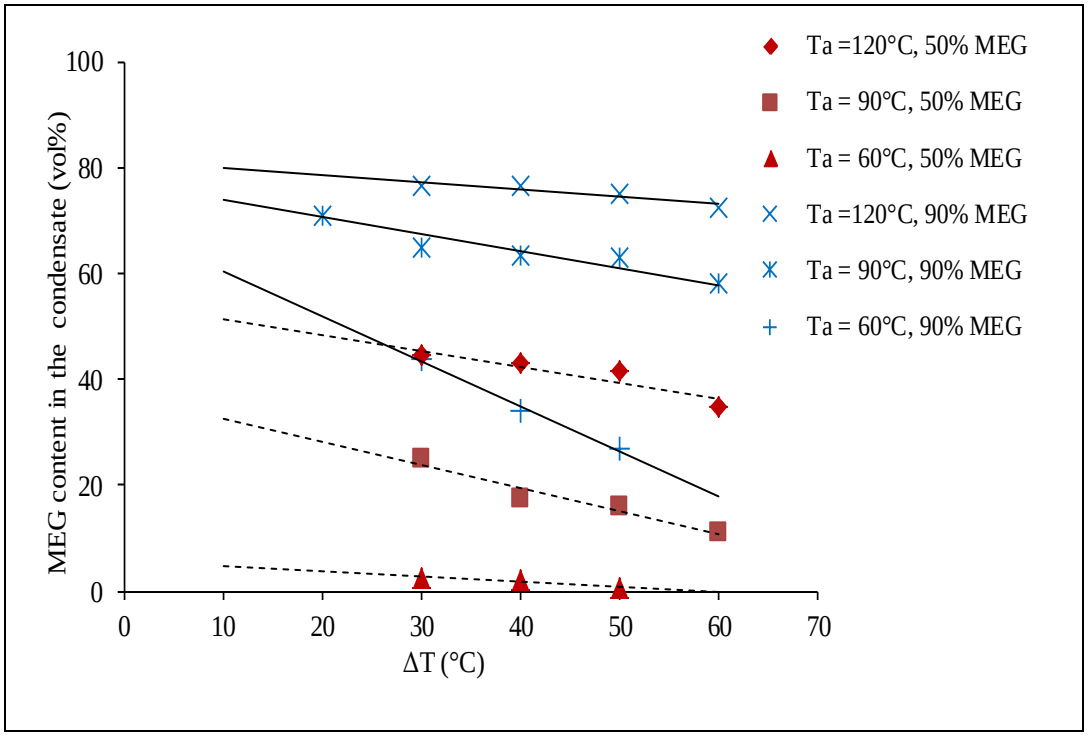

Figure 6.5: MEG content (vol%) in the condensing liquid vs. ΔT (°C) as a function of MEG concentration in the bulk liquid (50 and 90 vol%) at different bulk liquid temperatures (T_a). The lines are the trend lines.

The presence of MEG in the condensing liquid is an indication of the contribution of MEG to the vapour pressure of the system, which is more pronounced at higher temperatures. The concentration of MEG in the condensate is correlated to the partial pressure of MEG in the gas phase. For the system studied the total vapour pressure of the system (p_t) can be simplified as the sum of the partial pressures from H_2O and MEG:

$$p_t = p_{H_2O} + p_{MEG} \qquad (6.1)$$

With increasing temperature, as the vapour pressure of the system increased, the contribution of the MEG partial pressure in the gas phase increases, which results in a higher amount of MEG present in the condensing liquid. For example, from Figure 6.2, at 90°C, the vapour pressure of the system in the presence of 50 vol% MEG/water is 56.7 kPa.[96] From Table 6.1, at the same bulk liquid temperature and concentration (with ΔT = 30°C) 25 vol% MEG enters the condensing liquid. Thus, the contribution of MEG in the total vapour pressure of the system is approximately

14.1 kPa (56.7 x 0.25 = 14.1 kPa). While with the same concentration of MEG in the bulk solution, at 65°C, as the vapour pressure of the system decreases, the partial pressure of MEG in the system reduces to 0.5 kPa showing that at lower temperatures the contribution of MEG in the gas phase, and consequently in the condensing liquid, is low. At higher temperatures the contribution of MEG in the vapour phase and the amount of MEG in the condensate is higher.

From the above discussion, it can be suggested that the corrosion rate at the top of the line will decrease in the presence of MEG in the bulk solution, as a result of the reduction in the condensation rate and co-condensation of MEG with water at the top of the line.

6.3 Concluding Remarks

The results presented in this chapter indicate that under the conditions tested, the water condensation rate depends on the MEG concentration in the bulk liquid, and temperature (both bulk liquid temperature and cooling temperature). Under the same test conditions, the condensation rate decreases with increasing amounts of MEG in the bulk liquid following an exponential trend. The likelihood of MEG transportation from the bulk liquid to the condensing liquid on the sample surface is also investigated. The results reveal that the amount of MEG in the condensing liquid depends on the concentration of MEG in the bulk liquid, bulk liquid temperature and cooling temperature.

The results in this chapter suggest that MEG present in the condensing liquid may lower the corrosion rate at the top of the line. As top of the line corrosion (in a HAc free system) can be initiated at a condensation rate above 0.25 g/m^2s,[101] the results from this chapter can be used to estimate the conditions to avoid top of the line corrosion.

The results of condensation rate measurements show that the presence of 90% MEG is sufficient to reduce the condensation rate below the critical rate of 0.25 g/m^2s and avoid top of the line corrosion. Presenting 50% MEG in the bulk liquid can only avoid top of the line corrosion at $\Delta T = 40$ and 30°C.

CHAPTER 7. Conclusions and Future Work

7.1 Conclusions

This work presents a study of the effect of monoethylene glycol (MEG) on CO_2 corrosion of carbon steel. The study addresses the corrosiveness of the field conditions in oil and gas pipelines and provides laboratory approach to evaluate the performance of MEG to mitigate CO_2 corrosion. Corrosion rates are determined by linear polarization resistance, potentiodynamic polarization and EIS techniques. Concerning bottom of the line corrosion, tests are performed to study the effect of MEG in solutions de-oxygenated using both carbon dioxide and nitrogen. The range of MEG concentrations is expanded to study the effect of the concentration of MEG on the cathodic and anodic reactions in carbon dioxide solutions. Furthermore, the effect of MEG concentration is investigated in the presence of acetic acid (HAc). Also, the effect of temperature and immersion time is studied. To address condensing water corrosion, the efficiency of MEG in reducing the condensation rate on the steel surface is studied as well as the likelihood of transportation of MEG from the bulk liquid to the gas phase and its condensation on the metal surface.

Results from this study provide clear evidence that all concentrations of MEG (10–80 vol%) have a pronounced inhibiting effect on the CO_2 corrosion rate of carbon steel. MEG has inhibiting properties on both the anodic and cathodic parts of the corrosion process, at both 24°C and 60°C. A decrease in cathodic current is found to be related to the decrease in solubility and diffusivity of CO_2 in the presence of MEG. The impedance measurements show that both solution and charge transfer resistance of the system increases with increasing MEG concentration as it decreases the conductivity of the solution and retards the transport process of the corrosive species. A decrease in anodic current is related to the adsorption of MEG on the steel and formation of a surface film. The morphology of a specimen surface exposed in MEG solution shows that a general type of corrosion proceeds at the surface and the surface is uniformly corroded. With increasing MEG concentration the corrosion effect is less pronounced with less corroded areas observed at the surface.

The presence of MEG reduces the enhanced corrosion rate of carbon steel in a CO_2 saturated brine solution in the presence of HAc. The polarization and impedance spectroscopy results confirm the effectiveness of MEG in the corrosion inhibition of carbon steel in acetic acid. The extent of inhibition depends on the MEG and acetic acid concentrations. The inhibition efficiency increases with MEG concentration in an inverse exponential manner and decreases linearly with acetic acid concentration. The results show that MEG reduces the enhanced cathodic reaction of the corrosion process in HAc by increasing the charge transfer resistance of the species involved in the corrosion process and inhibition of the enhanced corrosion film dissolution caused by HAc. Furthermore, all concentrations of MEG tested (except for 10% MEG) had a well pronounced inhibiting effect on the corrosion of carbon steel in the presence of acetic acid. Morphology observation of the corroded steel surfaces reveals that localized corrosion (pitting) of carbon steel in the presence of HAc is suppressed in the presence of MEG.

MEG has inhibiting properties at all temperatures studied. With temperature increases, the inhibition efficiency decreases. Also, an adequate change of the activation energy compared with the absence of MEG suggests that it is most probable that the inhibiting property of MEG is determined by the adsorption of MEG on the metal surface. Increasing the immersion time of steel in a MEG solution does not result in changes in the polarization scans. However, EIS results showed continuous adsorption of MEG on the metal surface between 2 hours and 52 hours of immersion which remains unchanged to 76 hours. The effect of temperature on the inhibition efficiency of MEG is less pronounced at higher MEG concentration.

Condensation rate measurements are used to evaluate the inhibition effect of MEG on the top of the line corrosion. It is found that the water condensation rate depends on the MEG concentration in the bulk liquid and temperature (both bulk liquid temperature and cooling temperature). Under the same test conditions, the condensation rate decreases with the amount of MEG in the bulk liquid. Moreover, when the temperature of the bulk liquid is decreased, the water condensation rate reduces sharply due to the reduction of the MEG/water mixtures vapour pressure at

lower temperatures. The likelihood of transportation of MEG from the bulk liquid to the condensing liquid on the sample surface is also investigated. The results reveal that the amount of MEG in the condensing liquid depends on the concentration of MEG in the bulk liquid, the bulk liquid temperature and the cooling temperature.

7.2 Future Work

- Further studies should be conducted under scale formation conditions to evaluate the influence of MEG on the formation of a protective corrosion film. For example, experiments above 60°C and longer exposure times, where the rate of corrosion and scale formation are enhanced, should be performed. The inhibition effect of MEG in the presence of corrosion scales can also be examined. This will enhance the knowledge on the corrosion behaviour of steel in the presence of MEG.

- A detailed study on the role of the pH on the synergic effect of MEG and HAc is required in order to gain a better understanding of the extent of inhibition efficiency of MEG in a HAc system.

- This study defines the amounts of MEG transported into the condensing liquid at different temperatures and MEG concentration in the bulk solution. Further investigation on the effect of MEG at the top of the line corrosion is required. The study should be extended to define the effect of MEG on HAc-induced corrosion at the top of the line. Furthermore, effects of the condensate pH, surface roughening and film formation on the condensation and corrosion rates need to be studied.

References

1 Dugstad A, Lunde L, Nesic S. Control of Internal Corrosion in Multiphase Oil and Gas Pipelines. Prevention of Pipeline Corrosion Conference; Houston, Texas: Pipeline Industry and Pipes & Pipelines International; 17–20 October 1994.

2 Cragnolino G, Sridhar N. Application of Accelerated Corrosion Tests to Service Life Prediction Materials. Issue 1194, ASTM Committee G-1 on Corrosion of Metals. ASTM International, 1994, American Society for Testing and Materials. Philadelphia, PA. p. 274.

3 Nabhani F, Jasim AM, Graham SW. Electrochemical Behaviour of Low Carbon Steel in Aqueous Solutions. Proceedings of the World Congress on Engineering; London, U.K: 2–4 July 2007.

4 Ekawati D. Effect of Temperature, Bicarbonate, and MEG Concentration on Pre-Corroded Carbon Steels. Master's Thesis: University of Stavanger, Norway; 2011.

5 Vedapuri D, Kang C, Dhanabalan D, Gopal M. Inhibition of Multiphase Wet Gas Corrosion. Corrosion 2000 Conference and Expo; Houston, TX, USA: NACE International; 2000; paper no. 0043.

6 Fosbøl Pl. Carbon Dioxide Corrosion: Modelling and Experimental Work Applied to Natural Gas Pipelines. PhD Thesis: Technical University of Denmark; 2008.

7 Revie RW, editor. Uhlig's Corrosion Handbook. 3rd ed. Hobart, NJ: John Wiley & Sons; 2011.

8 Roberts BE, Tremaine PR. Vapor Liquid Equilibrium Calculations for Dilute Aqueous Solutions of CO_2, H_2S, NH_3, and NaOH to 300°C. Journal of Chemical Engineering. 1985; 63: p. 294–300.

9 Zhu SD, Fu AQ, Miao J, Yin ZF, Zhou GS, Wei JF. Corrosion of N80 Carbon Steel in Oil Field Formation Water Containing CO_2 in the Absence and Presence of Acetic Acid. Corrosion Science. 2011; 53(10): p. 3156-3165.

10 Nordsveen M, Nesic S, Nyborg R, Stangeland A. A Mechanistic Model for Carbon Dioxide Corrosion of Mild Steel in the Presence of Protective Iron Carbonate Films–Part 1: Theory and Verification. Corrosion. 2003; 59(05): p. 443–456.

11 DeWaard C, Milliams DE. Carbonic Acid Corrosion of Steel. Corrosion. 1975; 31(05): p. 177–181.

12 Kelly RG. Electrochemical Techniques in Corrosion Science and Engineering. 2003. NY: Marcel Dekker. p. 2.

13 Fosbøl Pl, Thomsen K, Stenby EH. Improving Mechanistic CO_2 Corrosion Models. Corrosion 2009 Conference and Expo; Atlanta, GA: NACE International; 22–26 March 2009, paper no. 09561.

14 Dugstad A, Seiersten M, Nyberg R. Flow Assurance of pH Stabilized Wet Gas Pipelines. Corrosion 2003 Conference and Expo; San Diego, CA: NACE International; March 2003, paper no. 03314.

15 Stefi BA, Bosen SF. Buffering and Inhibition of Glycol in Gas Dehydration Applications: An Alternative to Amines. Corrosion. 1997; 53(02).

16 Gulbrandsen E, Morard J. Why Does Glycol Inhibit CO_2 Corrosion? Corrosion 98 Conference and Expo; Houston, TX: NACE International; 1998, paper no. 98221.

17 Gregg MR, Sharp A, Bartrip K. Corrosion Inhibitor Developments for Offshore Gas Gathering Systems on Canada's Atlantic Coast. Corrosion 2003, paper no. 03332.

18 Halversen AMK, Andersen TR. pH Stabilization for Internal Corrosion Protection of Pipeline Carrying Wet Gas with CO2 and Acetic Acid. Corrosion 2003 Conference and Expo; San Diego, CA, NACE International; March, 2003. paper no. 03329.

19 Olsen S, Dugstad A. pH-Stabilization in the Troll Gas-Condensate Pipelines, Corrosion 1999 Conference and Expo; NACE International; San Antonio, TX: April 25 - 30, 1999, paper no. 99019.

20 Hagerup O, Olsen S. Corrosion Control by pH Stabilizer, Materials and Corrosion Monitoring in 160 km Multiphase Offshore Pipeline. Corrosion 2003 Conference and Expo; NACE International; Huston, TX: paper no. 03328.

21 Ramachandran S, Mancuso S, Bartrip K, Hammonds P. Inhibition of Acid Gas Corrosion in Pipelines Using Glycol for Hydrate Control. Materials Performance. 2006; 45(08): p. 44–47.

22 Bogedom VL, Gelder VKJ, Spaninks AM, Simon Thomas MJJ. Control of CO_2 Corrosion in Wet Gas Lines by Injection of Glycol. Corrosion 1988 Conference and Expo; NACE International; Huston, TX: paper no. 187.

23 De Ward C, Lotz U. Prediction of CO_2 Corrosion of Carbon Steel, Corrosion 1993 Conference and Expo; NACE International; Houston, TX: paper no. 9369.

24 Oyevaar MH, Morssinkhof RWJ, Westerterp KR. Density, Viscosity, Solubility, and Diffusivity of CO_2 and N_2O in Solutions of Diethanolamine in Aqueous Ethylene Glycol at 298 K. Journal of Chemical and Engineering Data. 1989; 34(01): p. 77–82.

25 Douheret G.; Pal A. Dielectric Constants and Densities of Aqueous Mixtures of 2-Alkoxyethanols at 25°C. Journal of Chemical and Engineering Data. 1988; 33(01): p. 40–43.

26 Song G, StJohn D. Corrosion Behaviour of Magnesium in Ethylene Glycol. Corrosion Science. 2004; 46(06): p. 1381–1399.

27 Fekry AM, Fatayerji MZ. Electrochemical Corrosion Behaviour of AZ91D Alloy in Ethylene Glycol. Electrochemica Acta. 2009; 54(26): p. 6522–6528.

28 Okafor PC, Brown B, Nesic S. CO_2 Corrosion of Carbon Steel in the Presence of Acetic Acid at Higher Temperatures. Journal of Applied Electrochemistry. 2009; 39(06): p. 873–877.

29 Méndez C , Joosten M, Gunaltun Y, Singer M, Nesic S, Camacho A, Sun Y, Hernández S. Effect of Acetic Acid, pH and MEG on the CO_2 Top of the Line Corrosion. Corrosion 2005 Conference and Expo; NACE International; Houston, TX, USA: paper no. 05278.

30 Sun Y, George K, Nesic S. The Effect of $C1^-$ and Acetic Acid on Localized CO_2 Corrosion in Wet Gas Flow, Corrosion 2003 Conference and Expo; NACE International; Houston, TX, USA: paper no. 03327.

31 Nafday O, Nesic S, Iron Carbonate Scale Formation and CO_2 Corrosion in the Presence of Acetic Acid. Corrosion 2005 Conference and Expo; NACE International; Houston, TX; USA: 3–7 April. 2005.

32 Crolet JL, Bonis M. The Role of Acetate Ions in CO_2 Corrosion. Corrosion 1983 Conference and Expo; NACE International; Anaheim, CA: paper no. 160.

33 Hinkson DC. A Study of the Chemical Composition and Corrosivity of the Condensate for Top of the Line CO_2 Corrosion. Master of Science Thesis. Ohio University. 2007. p. 25.

34 Keith G. Electrochemical Investigation of Carbon Dioxide Corrosion of Mild Steel in the Presence of Acetic Acid. Master of Science Thesis. Ohio University. 2003. p. 15.

35 George K, Wang S, Nesic S, deWaard C. Modelling of CO_2 Corrosion of Mild Steel at High Partial Pressures of CO_2 and in the Presence of Acetic Acid. Corrosion 2004 Conference and Expo; NACE International; Houston, TX: paper no. 04623.

36 Garsany Y, Pletcher D, Hedges B. The Role of Acetate in CO_2 Corrosion of Carbon Steel: Has The Chemistry Been Forgotten? Corrosion 2002 Conference and Expo; paper no. 02273.

37 Veloz MA, Gonzalez I. Electrochemical Study of Carbon Steel Corrosion in Buffered Acetic Acid Solutions with Chlorides and H_2S. Electrochemica Acta. 2002; 48(02): p. 135–144.

38 De Marco, Jiang RZT, John D, Sercombe M, Kinsella B. An Insitu Electrochemical Impedance Spectroscopy/Synchrotron Radiation Grazing Incidence X-Ray Diffraction Study of The Influence of Acetate on The Carbon Dioxide Corrosion of Mild Steel. Electrochemica Acta. 2007; 52(11): p. 3746–3750.

39 Sercombe M. Honours Thesis. Curtin University of Technology. 2004. p. 63.

40 George KS, Nesic S. Investigation of Carbon Dioxide Corrosion of Mild Steel in the Presence of Acetic Acid-Part 1: Basic Mechanisms. Corrosion. 2007; 63(02): p. 178–186.

41 Zhang GA, Cheng YF. On the Fundamentals of Electrochemical Corrosion of X65 Steel in CO_2-Containing Formation Water in the Presence of Acetic Acid in Petroleum Production. Corrosion Science 2009; (51): p. 87–94.

42 George KS, Nesic S, de Waard C. Electrochemical Investigation and Modelling Of Carbon Dioxide Corrosion of Carbon Steel in the Presence of Acetic Acid. Corrosion 2004 Conference and Expo; paper no. 04379.

43 Zhang GA, Cheng YF. Corrosion of X65 Steel in CO_2-Saturated Oilfield Formation Water in the Absence and Presence of Acetic Acid. Corrosion Science. 2009; 51(08): p. 1589–1595.

44 Garsany Y, Pletcher D, Hedges B. Speciation and Electrochemistry of Brines Containing Acetate Ion And Carbon Dioxide. Journal of Electroanalytical Chemistry. 2002; 538(539): p. 285–297.

45 Liu D, Chen ZY, Guo XP. Effect of Acetic Acid and Acetate on CO_2 Corrosion of Carbon Steel. Anti-Corrosion Methods and Materials. 2008; 55 (03): p. 130–134.

46 Andersen TR, Halvorsen AMK, Valle A, Kojen GP, Dudstad A. The Influence of Condensation Rate and Acetic Acid Concentration on Top of the Line Corrosion in Multiphase Pipelines. Corrosion 2007 Conference and Expo; NACE International; Nashville, Tennessee: March 11–15, paper no. 07312.

47 Nesic S. Key issues related to modelling of internal corrosion of oil and gas pipelines-A review. Corrosion Science. 2007; 49(12): 4308–4338.

48 Popova A, Sokolova E, Raicheva S, Christov M. AC and DC Study of The Temperature Effect on Mild Steel Corrosion in Acid Median the Presence of Benzimidazole Derivatives. Corrosion Science. 2003; 45(01): 33–58.

49 Kermani MB, Smith LM. CO_2 Corrosion Control in Oil and Gas Production. Published for the European Federation of Corrosion by Institute of Materials. Number 23, 1997. Maney Publishing.

50 Connors KA. Chemical Kinetics: The Study of Reaction Rates in Solution. 1990. VCH Publisher: NY.

51 Hinkson D, Singer M, Zhang Z, Nesic S. A Study of the Chemical Composition and Corrosivity of the Condensate in Top of the Line Corrosion. Corrosion 2008 Conference and Expo; NACE International; New Orleans, LA: March 16–20, paper no. 0466.

52 Kvarekval J, Dugstad A. Pitting Corrosion Mechanisms on Carbon Steel in Sour Glycol Water Mixtures. Corrosion 2004 Conference and Expo; NACE International; New Orleans, LA: March 28–April 1, paper no. 04737.

53 Gunaltun YM, Supriyatman D, Achmad J. Top-of-Line Corrosion in Gas Lines Confirmed by Condensation Analysis. Oil and Gas Journal. 1999; 97(28).

54 Erickson DD, Mai MC. Application of Transient Multiphase-Flow Technology. Journal of Petroleum Technology. 1999; 51(04): p. 84–87.

55 Nyborg R, Dugstad A, Lunde L. Corrosion and Glycol Distribution in a Large Wet-Gas Pipeline. Materials Performance. 1993; 32(9): p. 57–61.

56 Gunaltun YM, Larrey D. Correlation of Cases of Top of Line Corrosion with Calculated Water Condensation Rates . Corrosion 2000 Conference and Expo; NACE International; Houston, TX; paper no. 00071.

57 Hinkson D, Zhang Z, Singer M, Nesic S. Chemical Composition and Corrosiveness of the Condensate in Top of the Line Corrosion. Corrosion. 2010, 66(4); p. 045002.1–045002.8.

58 Singer M, Nesic S, Gunaltun YM. Top of Line Corrosion in Presence of Acetic Acid and Carbon Dioxide. Corrosion 2004 Conference & Expo; NACE International; New Orleans, Louisiana, USA: April 2004, paper no. 04377.

59 Pots B.F.M, Hendriksen E.L.J.A. CO_2 Corrosion under Scaling Conditions-The Special Case of Top of Line Corrosion in Wet Gas Pipelines. Corrosion 2000 Conference and Expo; NACE International; March 26–31, 2000, Orlando, Fl: paper no. 00031.

60 Gellings PJ. Introduction to Corrosion Prevention and Control. Netherlands: Delft University Press, 1985.

61 Baboian R. Corrosion Tests and Standards-Application & Interpretation. ASTM International, 2005.

62 Linear Polarization Resistance (LPR) General Information. Available from: http://www.caproco.com/catalog/pdf/Probes-Instruments/Linear-Polarization-Resistance/LPR-General-Information.pdf

63 Roberge PR. Handbook of Corrosion Engineering. New York: McGraw-Hill, 2000.

64 Hilbert L.R. Monitoring Corrosion Rates and Localised Corrosion in Low Conductivity Water. Corrosion Science. 2006; 48: 3907–3923.

65 ASTM International. Standard Practice for Calculation of Corrosion Rates and Related Information from Electrochemical Measurements. G102-89. West Conshohocken, USA: ASTM International; 2010.

66 Gerald S. Frankel1. Electrochemical Techniques in Corrosion: Status, Limitations and Needs. Journal of ASTM International, 2008; 5(2), paper ID JAI101241. Available online at www.astm.org.

67 ASTM International. Standard Practice for Conducting Potentiodynamic Polarization Resistance Measurement. G 59–97. West Conshohocken, USA: ASTM International; 2010.

68 Yang L. Techniques for Corrosion Monitoring: Woodhead Publishing Limited; 2008.

69 Rieger PH. Electrochemistry. New York: NY: Chapman & Hall, Inc. 1994.

70 Conrad MB. Electrochemical Surface Potential and Mass Loss Corrosion Investigation of Improved Corrosion Resistant Steels for Highway Bridge Construction. Master of Science Thesis. Lehigh University. May 2009.

71 Marcus PH, Mansfeld F, editors. Analytical Methods in Corrosion Science and Engineering, Boca Raton, FL: CRC Press, 2006.

72 Steinmetz CP. Lectures on electrical engineering, Volume 1, edited by Alger PL. New York: Dover Publications; 1971.

73 Barsoukov E, Macdonald JR. Impedance Spectroscopy Theory, Experiment, and Applications. Hoboken, NJ: John Wiley & Sons, Inc. 2005.

74 Macdonald JR, Johnson WB. Fundamental of Impedance Spectroscopy: Impedance Spectroscopy Theory, Experiment, and Application. Hoboken, NJ: John Wiley & Sons, Inc.; 2005. p. 1–20.

75 John DA. Mechanism of Carbon Dioxide Corrosion and Inhibition under High Flow–A Jet Impingement Study. PhD Thesis, Curtin University of Technology. 2006.

76 Gamry Application Note: Basic of Electrochemical Impedance Spectroscopy: Gamry Instrument; 2010. Available from: http://www.gamry.com/App_Notes/EIS_Primer/Basics_Of_%20EIS.pdf

77 ASTM International. Standard Practice for Conventions Applicable to Electrochemical Measurements in Corrosion Testing. G3-89. West Conshohocken, USA: ASTM International; 2010.

78 Ashassi-Sorkhabi H, Ghalebsaz-Jeddi N. Inhibition Effect of Polyethylene Glycol on the Corrosion of Carbon Steel in Sulphuric Acid. Materials Chemistry and Physics. 2005; 92(2-3): p. 480–486.

79 Trethewey KR, Chamberlain J. Corrosion for Science and Engineering. 2nd ed. Singapore: Logman Group Limited, Second edition, 1995; p. 124-127.

80 Taylor SR, Cahen GL and Stoner GE. Ion Beam Assisted Deposition of Thin Carbonaceous Films. III Barrier properties. Journal of the Electrochemical Society. 1989; 136(04): p. 929–35.

81 Randles JEB. Kinetics of Rapid Electrode Reactions. Disc. Farad. Soc. 1947. p. 11.

82 Friesen G, Özsar ME. Dunlop ED. Impedance Model for CdTe Solar Cells Exhibiting Constant Phase Element Behaviour. Thin Solid Films 361–2000; 362(21): p. 303-308.

83 Seiersten M, Dugstad A, Gulbrandsen E. Conditions for Scaling in Pipelines-pH in Glycol Solutions. Oilfield Scaling, SPE International, Aberdeen: Society of Petroleum Engineers, January 2003; paper no. 80393.

84 Sandengen K, Kaasa B, Østvold T. pH Measurement in Monoethylene Glycol (MEG) + Water Solutions. Ind. Eng. Chem. Res. 2007, 46; p. 4734–4739.

85 ASTM International. Standard Practice for Seamless Cold-Drawn Low-Carbon Steel Heat-Exchanger and Condenser Tubes1. A 179/A 179M-90a. West Conshohocken, USA: ASTM International; 2010.

86 Socrates G. Infrared Characteristic Group Frequencies: Tables and Charts. 2nd ed. New York, NY; John Wiley & Sons; 1994.

87 Fosbøl pl, Thomsen K, Stenby EH. Modelling of the Mixed Solvent Electrolyte System CO_2-$NaCO_3$-$NaHCO_3$-Monoethylene Glycol-Water. Ind. Eng. Chem. Res. 2009, 48: p. 4565–4578.

88 Cao C. On Electrochemical Techniques for Interface Inhibitor Research. Corrosion Science. 1996; 38(12): p. 2073–2082.

89 Zhang GA, Xu LY, Cheng YF. Mechanistic Aspects of Electrochemical Corrosion of Aluminium Alloy in Ethylene Glycol-Water Solution. Electrochimica Acta. 2008; 53(28): p. 8245–8252.

90 Amri J, Gulbrandsen E, Nogueira RP. Propagation and Arrest of Localized Attacks in Carbon Dioxide Corrosion of Carbon Steel in the Presence of Acetic Acid. Corrosion. 2010; 66(3): p. 35001–35007.

91 Garsany Y, Pletcher D, Hedges B. The Role Of Acetate in CO_2 Corrosion of Carbon Steel: Studies Related to Oilfield Conditions. Corrosion 2003 Conference and Expo; NACE International; paper no. 03324.

92 Gulbrandsen E. Acetic Acid and Carbon Dioxide Corrosion of Mild steel Covered with Iron Carbonate. Corrosion 2007 Conference and Expo; NACE International; Houston, TX, USA: paper no. 07322.

93 Guo XP, Chen Z.Y, Lio D, Bando K, Tomoe Y. The Effect of Acetic Acid and Acetate on CO_2 Corrosion of Carbon Steel. Corrosion 2005 Conference and Expo; NACE International; Houston, TX, USA: 3-5 April, paper no. 05306.

94 Gulbrandsen E, Bilkova K. Solution Chemistry effects on Corrosion of Carbon Steels in Presence of CO_2 and Acetic Acid. Corrosion 2006 Conference & Expo; NACE International; San Diego, CA, USA: 12-16 March, paper no 06364.

95 Yin ZF, Zhao WZ, Lai WY, Yin CX, Zhu SD. Film Characteristics of Carbon Steel in Simulant Solution with the Effect of Acetic Acid and CO_2. Materials Engineering and Performance. 2010; 19(5): p. 693–699.

96 Ullmann F. Ethylene Glycol. In: Ullmann's Encyclopedia of Industrial Chemistry. 7th ed.; Weinheim, Germany: Wiley-VCH, 2009.

97 Chawla SL, Gupta RK. Materials Selection for Corrosion Control. Material Park, OH; ASM International). 1993; 75–84.

98 Lopez DA, Simison SN, de Sanchez SR. The Influence of Steel Microstructure on CO_2 Corrosion. EIS Studies on the Inhibition Efficiency of Benzimidazole. Electrochimica Acta. 2003, 48,(7): p. 845–854.

99 Illa Biidznihi WF. Effect of Precorrosion by Galvanostatic Anodic Polarization and Temperature on the Formation Rate of Iron (II) Carbonate Film. Master's Thesis, University of Stavanger. December, 2011.

100 Kvarekval J, Dugstad A. Pitting Corrosion Mechanisms on Carbon Steel in Sour Glycol Water Mixtures. Corrosion 2004 Conference & Expo; NACE International; New Orleans, LA; March 28–April 1, paper no. 04737.

101 Singer M, Hinkson D, Zhang Z, Wang H, Nesic S. CO_2 Top of the Line Corrosion in Presence of Acetic Acid: A Parametric Study. Corrosion. 2013; 69(7): p. 719–735.